NATIONAL ADVISORY COMMITTEE FOR AERONAUTICS

TECHNICAL NOTE 2121

STUDY OF EFFECTS OF SWEEP ON THE FLUTTER OF CANTILEVER WINGS

By J. G. Barmby, H. J. Cunningham, and I. E. Garrick

Langley Aeronautical Laboratory
Langley Air Force Base, Va.

Washington
June 1950

NATIONAL ADVISORY COMMITTEE FOR AERONAUTICS

TECHNICAL NOTE 2121

STUDY OF EFFECTS OF SWEEP ON THE FLUTTER OF CANTILEVER WINGS

By J. G. Barmby, H. J. Cunningham, and I. E. Garrick

SUMMARY

An experimental and analytical investigation of the flutter of sweptback cantilever wings is reported. The experiments employed groups of wings swept back by rotating and by shearing. The angle of sweep ranged from 0° to 60° and Mach numbers extended to approximately 0.85. A theoretical analysis of the air forces on an oscillating swept wing of high length-to-chord ratio is developed, and the approximations inherent in the assumptions are discussed. Comparison with experiment indicates that the analysis developed in the present paper is satisfactory for giving the main effects of sweep, at least for nearly uniform cantilever wings of high and moderate length-to-chord ratios. A separation of the effects of finite span and compressibility in their relation to sweep has not been made experimentally but some combined effects are given. A discussion of some of the experimental and theoretical trends is given with the aid of several tables and figures.

INTRODUCTION

The present paper is an outgrowth of the trend toward the use of swept wings for high-speed flight and reports the results of an analysis and of an accompanying exploratory program of research in the Langley 4.5-foot flutter research tunnel on swept cantilever wings. The material was assembled in a memorandum form with a similar title in 1948. The chief purposes of the present paper are to provide a more detailed exposition of the analysis and to make the main material more generally available.

Mention of some previous experimental and analytical work on swept wings follows. A preliminary experimental investigation of the effect of sweep on flutter has been made (reference 1) with a single, simple rigid wing mounted flexibly at one end of a base which could be rotated to various desired sweep angles. This investigation was made at low

Mach numbers for two bending–torsion frequency ratios and at several angles of sweepback. Another investigation (data unpublished) in which the density of the test medium was a variable was conducted by D. Benun on the same type of rigid, flexibly mounted wing at higher Mach numbers and at sweep angles of 0° and 45°. Other unpublished work on swept wings exists, but a search of the available information indicates a need for further systematic study.

The experimental work reported herein dealt with models mounted as cantilevers at their roots. These cantilever models differed from the rigid, flexibly mounted wings, which had all bending and torsion flexibility concentrated at the root, and thus were subject to different root effects. In order to facilitate analysis the cantilever models were uniform and untapered. The intent of the experimental program was to establish trends and to indicate orders of magnitude of the various effects of sweep on flutter, rather than to isolate precisely the separate effects.

The models were swept back in two basic manners – shearing and rotating. For the case in which the wings which were swept back by shearing the cross sections parallel to the air stream, the span and aspect ratio remained constant. For the other case, a series of rectangular-plan-form wings were mounted on a special base which could be rotated to provide any desired angle of sweepback. This rotatory base was also used to examine the critical speed of sweptforward wings.

Tests were conducted also on special models that were of the "rotated" type (sections normal to the leading edge were the same at all sweep angles) with the difference that the bases were alined parallel to the air stream. Two series of such rotated models having different lengths were tested.

Inasmuch as the location of the center of gravity, the mass-density ratio, and the Mach number have important effects on the flutter characteristics of unswept wings, these parameters were varied for swept wings. In order to investigate possible changes in flutter characteristics which might be due to different flow over the tips, various tip shapes were included in the experiments.

In an analysis of flutter, vibrational characteristics are very significant; accordingly, vibration tests were made on each model. A special study of the change in frequency and mode shape with angle of sweep was made for a simple aluminum-alloy beam and is reported in appendix A.

Theoretical analyses of the effect of sweep on flutter exist only in brief or preliminary forms. In England in 1942 W. J. Duncan estimated by certain dimensional considerations the effect of sweep on the flutter

speed of certain specialized wing types. Among other British workers whose names are mentioned in connection with problems of flutter involving sweep are R. McKinnon Wood, A. R. Collar, and I. T. Minhinnick. An account of Minhinnick's work was given by Broadbent in reference 2. In reference 3 a preliminary analysis for the flutter of swept wings in incompressible flow is developed on the basis of a "strip theory" (with the strips taken in the stream direction) and is applied to the experimental results of reference 1. Examination of the limiting case of infinite span discloses that the aerodynamic assumptions employed in reference 3 are not well-grounded. Reference 4 adapts this "strip theory" to flexible wings and also presents an alternative "velocity component" treatment employing other aerodynamic assumptions which in their end result appear more akin to those employed in the analysis of the present paper. No definite choice is made in reference 4 between the two methods although the "strip theory" method is favored.

In the present paper a theoretical analysis is developed anew and given a general presentation. Application of the analysis has been limited at this time chiefly to those calculations needed for comparison with experimental results. A wider examination of the effect of various parameters and of additional degrees of freedom on the flutter characteristics is desirable.

SYMBOLS

b	half-chord of wing measured perpendicular to elastic axis, feet
b_r	half-chord perpendicular to elastic axis at reference station, feet
l'	effective length of wing, measured along elastic axis, feet
c	wing chord measured perpendicular to elastic axis, inches
l	length of wing measured along midchord line, inches
Λ	angle of sweep, positive for sweepback, degrees
A_g	geometric aspect ratio $\left(\frac{(l \cos \Lambda)^2}{lc}\right)$
x'	coordinate perpendicular to elastic axis in plane of wing, feet
y'	coordinate along elastic axis, feet

z'	coordinate in direction perpendicular to $x'y'$ plane, feet
Z	coordinate of wing surface in z' direction, feet
η	nondimensional coordinate along elastic axis (y'/l')
ξ	coordinate in wind-stream direction
h	bending deflection of elastic axis, positive downward
θ	torsional deflection of elastic axis, positive with leading edge up
σ	local bending slope of elastic axis $\left(\frac{\partial h}{\partial y'}\right)$
τ	local rate of change of twist $\left(\frac{\partial \theta}{\partial y'}\right)$
$f_h(y')$, $F_h(\eta)$	deflection function of wing in bending
$f_\theta(y')$, $F_\theta(\eta)$	deflection function of wing in torsion
t	time
ω	angular frequency of vibration, radians per second
ω_h	angular uncoupled bending frequency, radians per second
ω_α	angular uncoupled torsional frequency about elastic axis, radians per second
f_{h_1}	first bending natural frequency, cycles per second
f_{h_2}	second bending natural frequency, cycles per second
f_t	first torsion natural frequency, cycles per second

f_α uncoupled first torsion frequency relative to elastic axis, cycles per second $\left(f_t\left[1-\frac{\left(\frac{x_\alpha}{r_\alpha}\right)^2}{1-\left(\frac{f_{h_1}}{f_t}\right)^2}\right]^{\frac{1}{2}}\right)$

f_e experimental flutter frequency, cycles per second

f_R reference flutter frequency, cycles per second

f_Λ flutter frequency determined by analysis of present report, cycles per second

v free-stream velocity, feet per second

v_e experimental flutter speed, feet per second

v_n component of air-stream velocity perpendicular to elastic axis, feet per second ($v \cos \Lambda$)

V_e experimental flutter speed taken parallel to air stream, miles per hour

V_R reference flutter speed, miles per hour

V_R' reference flutter speed based on wing elastic axis, miles per hour (defined in appendix B)

V_Λ flutter speed determined by theory of present report, miles per hour

V_D theoretical divergence speed, miles per hour

k_n reduced frequency employing velocity component perpendicular to elastic axis $\left(\frac{\omega b}{v_n}\right)$

φ phase difference between wing bending and wing torsion strains, degrees

ρ density of testing medium at flutter, slugs per cubic foot

q	dynamic pressure at flutter, pounds per square foot
M	Mach number at flutter
M_{cr}	critical Mach number
x_{cg}	distance of center of gravity behind leading edge taken perpendicular to elastic axis, percent chord
x_{ea}	distance of elastic center of wing cross section behind leading edge taken perpendicular to elastic axis, percent chord
x_{ea}'	distance of elastic axis of wing behind leading edge taken perpendicular to elastic axis, percent chord
a	nondimensional elastic-axis position $\left(\frac{2x_{ea}}{100} - 1\right)$
$a + x_\alpha$	nondimensional center-of-gravity position $\left(\frac{2x_{cg}}{100} - 1\right)$
m	mass of wing per unit length, slugs per foot
κ	wing mass-density ratio at flutter $\left(\frac{\pi\rho b^2}{m}\right)$
I_α	mass moment of inertia of wing per unit length about elastic axis, slug-feet^2 per foot
r_α	nondimensional radius of gyration of wing about elastic axis $\left(\sqrt{\frac{I_\alpha}{mb^2}}\right)$
EI	bending stiffness, pound-inches^2 in tables, pound-feet^2 in analysis
GJ	torsional stiffness, pound-inches^2 in tables, pound-feet^2 in analysis
g_h	structural damping coefficient for bending vibration

g_α structural damping coefficient for torsional vibration

$[\,]$ a special bracket used to identify terms which are due solely to inclusion of the last term in equation (5a)

Note: In order to preserve continuity and to facilitate comparison with previous work on the unswept wing, the subscript α rather than θ is retained with certain quantities to refer to the torsional degree of freedom.

EXPERIMENTAL INVESTIGATION

Apparatus

Wind tunnel.- The tests were conducted in the Langley 4.5-foot flutter research tunnel which is of the closed-throat, single-return type employing either air or Freon-12 as a testing medium at pressures varying from 4 inches of mercury to 30 inches of mercury. In Freon-12, the speed of sound is 324 miles per hour and the density is 0.0106 slug per cubic foot at standard pressure and temperature. The maximum choking Mach number for these tests was approximately 0.92. The Reynolds number range was from 0.26×10^6 to 2.6×10^6 with most of the tests at Reynolds numbers of the order of 1.0×10^6.

Models.- In order to obtain structural parameters required for the flutter studies, different types of construction were used for the models. Some models were solid spruce, others were solid balsa, and many were combinations of balsa with various aluminum-alloy inserts. Seven series of models were investigated, for which the cross sections and plan forms are shown in figure 1.

Figure 1(a) shows the series of models which were swept back by shearing the cross sections parallel to the air stream. In order to obtain flutter with these low-aspect-ratio models, thin sections and relatively light and weak wood construction were employed.

The series of rectangular-plan-form models shown in figure 1(b) were swept back by using a base mount that could be rotated to give the desired sweep angle. The same base mount was used for testing models at forward sweep angles. It is known that for forward sweep angles divergence is critical. In an attempt to separate the divergence and flutter speeds in the sweepforward tests, a D-spar cross-sectional construction was used to get the elastic axis relatively far forward (fig. 1(c)).

Two series of wings (figs. 1(d) and 1(e)) were swept back with the length-to-chord ratios kept constant. In these series of models, the chord perpendicular to the leading edge was kept constant and the bases were alined parallel to the air stream. The wings of length-to-chord ratio 8.5 (fig. 1(d)) were cut down to get the wings of length-to-chord ratio 6.5 (fig. 1(e)).

Another series of models obtained by using this same manner of sweep (fig. 1(f)) was used for investigating some effects of tip shape.

Spanwise strips of lead were fastened to the models shown in figure 1(e) and a series of tests were conducted with these weighted models to determine the effect of center-of-gravity shift on the flutter speed of swept wings. The method of varying the center of gravity is shown in figure 1(g). In order to obtain data at zero sweep angle it was necessary, because of the proximity of flutter speed to wing-divergence speed, to use three different wings. These zero-sweep-angle wings, of 8-inch chord and 48-inch length, had an internal weight system.

The models were mounted from the top of the tunnel as cantilever beams with rigid bases (fig. 2). Near the root of each model two sets of strain gages were fastened, one set for recording principally bending deformations and the other set for recording principally torsional deflections.

Methods

Determination of model parameters.- Pertinent geometric and structural properties of the model are given in tables I to VII. Some parameters of interest are discussed in the following paragraphs.

As an indication of the nearness to sonic-flow conditions, the critical Mach number is listed. This Mach number is determined by the Kármán-Tsien method for a wing section normal to the leading edge at zero lift.

The geometric aspect ratio of a wing is here defined as

$$A_g = \frac{\text{Semispan}^2}{\text{Plan-form area}} = \frac{(l \cos \Lambda)^2}{lc} = \frac{l}{c} \cos^2 \Lambda = \frac{A}{2}$$

The geometric aspect ratio A_g is used in place of the conventional aspect ratio A because the models were only semispan wings. For sheared swept wings, obtained from a given unswept wing, the geometric

aspect ratio is constant, whereas for the wings of constant length-to-chord ratio the geometric aspect ratio decreases with $\cos^2\Lambda$ as the angle of sweep is increased.

The weight, center-of-gravity position, and polar moment of inertia of the models were determined by usual means. The models were statically loaded at the tip to obtain the rigidities in torsion and bending, GJ and EI.

A parameter occurring in the methods of analysis of this paper is the position of the elastic axis. A "section" elastic axis located at x_{ea} was obtained for wings from each series of models as follows: The wings were clamped at the root normal to the leading edge and at a chosen spanwise station were loaded at points lying in the chordwise direction. The point for which pure bending deflection occurred, with no twist in the plane normal to the leading edge, was determined. The same procedure was used for those wings which were clamped at the root, not normal, but at an angle to the leading edge. A different elastic axis designated the "wing" elastic axis and located at x_{ea}' was thus determined.

For these uniform, swept wings with fairly large length-to-chord ratios, the "wing" elastic axis was reasonably straight and remained essentially parallel to the "section" elastic axis, although it was found to move farther behind the "section" elastic axis as the angle of sweep was increased. It is realized that in general for nonuniform wings, for example, wings with cut-outs or skewed clamping, a certain degree of cross stiffness exists and the concept of an elastic axis is an oversimplification. More general concepts such as those involving influence coefficients may be required. These more strict considerations, however, are not required here since the elastic-axis parameter is of fairly secondary importance.

The wing mass-density ratio κ is the ratio of the mass of a cylinder of testing medium, of a diameter equal to the chord of the wing, to the mass of the wing, both taken for unit length along the wing. The density of the testing medium when flutter occurred was used in the evaluation of κ.

Determination of the reference flutter speed.- It is convenient in presenting and comparing data of swept and unswept wings to employ a certain reference flutter speed. This reference flutter speed will serve to reduce variations in flutter characteristics which arise from changes in the various model parameters such as density and section properties not pertinent to the investigation. It thus aids in systematizing the data and emphasizing the desired effects of sweep including effects of aspect ratio and Mach number.

This reference flutter speed V_R may be obtained in the following way. Suppose the wing to be rotated about the intersection of the elastic axis with the root to a position of zero sweep. In this position the reference flutter speed is calculated by the method of reference 5, which assumes an idealized, uniform, infinite wing mounted on springs in an incompressible medium. For nonuniform wings, a reference section taken at a representative spanwise position, or some integrated value, may be used. Since the wings used were uniform, any reference section will serve. The reference flutter speed may thus be considered a "section" reference flutter speed and parameters of a section normal to the leading edge are used in its calculation. This calculation also employs the uncoupled first bending and torsion frequencies of the wing (obtained from the measured frequencies) and the measured density of the testing medium at time of flutter. The calculation yields a corresponding reference flutter frequency which is useful in comparing the frequency data. For the sake of completeness a further discussion of the reference flutter speed is given in appendix B.

Test procedure and records.- Since flutter is often a sudden and destructive phenomenon, coordinated test procedures were required. During each test, the tunnel speed was slowly raised until a speed was reached for which the amplitudes of oscillation of the model in bending and torsion increased rapidly while the frequencies in bending and torsion, as observed on the screen of the recording oscillograph, merged to the same value. At this instant, the tunnel conditions were recorded and an oscillograph record of the model deflections was taken. The tunnel speed was immediately reduced in an effort to prevent destruction of the model.

From the tunnel data, the experimental flutter speed V_e, the density of the testing medium ρ, and the Mach number M were determined. No blocking or wake corrections to the measured tunnel velocity were applied.

From the oscillogram the experimental flutter frequency f_e and the phase difference φ (or the phase difference $\pm 180^\circ$) between the bending and torsion deflections near the root were read. A reproduction of a typical oscillograph flutter record, which indicated the flutter to be a coupling of the wing bending and torsion degrees of freedom, is shown as figure 3. Since semispan wings mounted rigidly at the base were used, the flutter mode may be considered to correspond to the flutter of a complete wing having a very heavy fuselage at midspan, that is, to the symmetrical type.

The natural frequencies of the models in bending and torsion at zero airspeed were recorded before and after each test in order to ascertain possible changes in structural characteristics. In most cases there were no appreciable changes in frequencies but there were some

reductions in stiffnesses for models which had been weakened by fluttering violently. Analysis of the decay records of the natural frequencies indicated that the wing damping coefficients g_h and g_α (reference 5) were about 0.02 in the first bending mode and 0.03 in the torsion mode.

ANALYTICAL INVESTIGATION

General

Assumptions.— An attempt is first made to point out the main assumptions which seem to be applicable for swept wings of moderate taper and of high or moderate length-to-chord ratios.

(a) The assumptions, such as small disturbances and potential flow, commonly employed in linearized treatment of unswept wings in an ideal incompressible fluid are made.

(b) The structural behavior is such that over the main part of the wing the elastic axis may be considered straight. The wing is also considered sufficiently stiff at the root so that it behaves as if it were clamped normal to the elastic axis. An effective length l' needed for integration reasons may be defined (for example, as in fig. 4). The angle of sweepback is measured in the plane of the wing from the direction normal to the air stream to the elastic axis. All section parameters such as semichord, locations of elastic axis and center of gravity, radius of gyration, and so forth, are based on sections normal to the elastic axis.

(c) The aerodynamic behavior is such that any section dy' of the wing normal to the elastic axis, taken in the direction of the component $v \cos \Lambda$ of the main-stream velocity, generates a velocity potential associated with a uniform infinite swept wing having the same instantaneous distribution over the chord of velocity normal to the wing surface as does the actual section.

Additional remarks on these assumptions are appropriate. With regard to assumption (a), in accordance with linearization of the problem, the boundary conditions are stated and treated with respect to a reference surface, in this case a plane, containing the mean equilibrium position of the wing and the main-stream velocity. Furthermore, incompressible flow is assumed in order to avoid complexity of the analysis, although modifications due to Mach number effects can be added. Such modifications may be based, for example, for wings having large length-to-chord ratios, on existing theoretical calculations of aerodynamic

coefficients for subsonic or supersonic two-dimensional flow appropriate to the component $v \cos \Lambda$. On the other hand the modifications may be partly empirical, especially for "transonic" conditions and for small length-to-chord ratios. The transonic conditions and the general aerodynamic behavior of swept wings may depend, for large length-to-chord ratios, on the component $v \cos \Lambda$, but the dependence may shift to the stream velocity v for small length-to-chord ratios.

With respect to assumption (b), results of analyses of and experiment on unswept wings having low ratios of bending frequency to torsion frequency show that small variations of position of the elastic axis are not important. The assumption of a straight elastic axis over the main part of a swept wing, similarly, is not critical for many cases. This assumption is made for convenience, however, and modifications for a curved elastic axis can be made when necessary, for example, for plate-like wings. Small differences in the angle of sweepback of the leading edge, quarter-chord line, elastic axis, and so forth, are neglected. The analysis could be further modified to take into account variation of the angle of sweepback along the length of the wing.

Assumption (c) implies that associated with the action of the wing in pushing air downward there is a noncirculatory potential-type flow similar to that around sections of an infinite flat-plate wing. Furthermore, as in the case of the unswept airfoil, a circulatory potential-type flow is generated in which for the swept airfoil the component $v \cos \Lambda$ is decisive in fixing the circulation. (This assumption differs from that made in the "strip theory" of references 3 and 4 which employs the main-stream velocity together with sections of the wings parallel to the stream direction.) Effects of the floating of the wake in the stream direction rather than in the direction of $v \cos \Lambda$ and induced effects of variation of the strength of the wake in the wing-length direction are neglected, as are three-dimensional tip effects. For large values of the reduced frequency k_n a given segment of the wing might be influenced chiefly by the nearby wake and the correction would be small. On the other hand, for small values of k_n a given segment might be influenced by a more widespread portion of the wake; corrections for this condition may possibly be based on knowledge of the static case (for example, slope of the lift curve). As the angle of sweep approaches 90°, obviously the mechanism for the generation of lift is different from the one postulated here; for example, a tip condition may replace the trailing-edge condition, and considerations of very small aspect ratio arise.

Basic considerations.- Consider the configuration shown in figure 4 where the vertical coordinate of the wing surface is denoted by $z' = Z(x',y',t)$ (positive downward). The effect of the position and motion of the wing may be given by the disturbance-velocity distribution

to be superposed on the uniform stream in order to represent the condition of tangential flow at the wing surface. This velocity distribution normal to the surface (positive upward) is, for small disturbances,

$$w(x',y',t) = \frac{\partial Z}{\partial t} + v \frac{\partial Z}{\partial \xi} \tag{1}$$

where ξ is the coordinate in the wind-stream direction. With the use of the relation

$$\frac{\partial Z}{\partial \xi} = \frac{\partial Z}{\partial x'} \frac{\partial x'}{\partial \xi} + \frac{\partial Z}{\partial y'} \frac{\partial y'}{\partial \xi}$$

$$= \frac{\partial Z}{\partial x'} \cos \Lambda + \frac{\partial Z}{\partial y'} \sin \Lambda$$

the vertical velocity at any point is

$$w(x',y',t) = \frac{\partial Z}{\partial t} + v \frac{\partial Z}{\partial x'} \cos \Lambda + v \frac{\partial Z}{\partial y'} \sin \Lambda \tag{1a}$$

Let the wing be bending so that a segment dy' (see fig. 4) is displaced from its equilibrium position by an incremental distance h (positive down) and also let the wing segment be twisting about the elastic axis through an incremental angle θ (positive leading edge up). The position of each point of the segment may be defined, for small deflections, by

$$Z = h + x'\theta \tag{2}$$

The velocity distribution normal to the surface, equation (1a), consequently becomes

$$w = \dot{h} + x'\dot{\theta} + v\theta \cos \Lambda + v(\sigma + x'\tau)\sin \Lambda \tag{3}$$

where $\sigma = \frac{\partial h}{\partial y'}$ is the local bending slope of the elastic axis, and is thus analogous to dihedral, and where $\tau = \frac{\partial \theta}{\partial y'}$ is the local change of twist of the elastic axis.

In accordance with assumption (c) the noncirculatory-flow velocity potentials associated with the vertical-velocity distribution are first needed. In equation (3) the terms involving $\dot{h}$, θ, and σ are constant across the chord, whereas those involving $\dot{\theta}$ and τ vary in a linear

manner. The noncirculatory velocity potentials as in reference 6 and the new potentials associated with σ and τ are

$$\left.\begin{aligned}
\phi_{\dot{h}} &= \dot{h}b\sqrt{1-x^2} \\
\phi_{\theta} &= v_n\theta b\sqrt{1-x^2} \\
\phi_{\sigma} &= v_n\sigma \tan\Lambda\, b\sqrt{1-x^2} \\
\phi_{\dot{\theta}} &= \dot{\theta}b^2\left(\frac{x}{2}-a\right)\sqrt{1-x^2} \\
\phi_{\tau} &= v_n\tau \tan\Lambda\, b^2\left(\frac{x}{2}-a\right)\sqrt{1-x^2}
\end{aligned}\right\} \qquad (4)$$

where $v_n = v\cos\Lambda$ and x is the nondimensional chordwise coordinate measured from the midchord as in reference 6, related to the coordinate x' in the manner

$$x = \frac{x'}{b} + a$$

The velocity potential for the circulatory flow associated with the wake may be developed on the basis of assumption (c) and the concepts for the infinite unswept wing introduced in reference 6. (Thus the circulatory-flow pattern for a section dy' of the finite swept wing is to be obtained from the corresponding flow pattern for an infinite uniform yawed wing. This infinite wing is assumed to have undergone harmonic oscillations for a long time; the full wake is established, remains where formed, and consequently is harmonically distributed in space. For the infinite uniform yawed wing results for the circulatory flow are like those of reference 6 with v replaced by the component v_n and with the addition of terms to take care of σ and τ.) In particular, the strength of the wake acting on each section is determined by the condition of smooth flow (the velocity remaining finite) at the trailing edge. This condition is utilized in the form $\frac{\partial}{\partial x}(\phi_\Gamma + \phi_N)$ is equal to a finite quantity at the trailing edge; (where ϕ_Γ is the velocity potential due to the vorticity in the wake, and ϕ_N is the total noncirculatory velocity potential) and leads to a relation analogous to equation (VII) of reference 6 involving the basic quantity $Q = \dot{h} + v_n\theta + v_n\sigma\tan\Lambda + b\left(\frac{1}{2}-a\right)(\dot{\theta} + v_n\tau\tan\Lambda)$ which occurs in the terms associated with the wake. The net result of these considerations is that the circulatory-flow velocity potential may be regarded as determined.

The pressure difference between upper and lower surfaces of the wing at a point x is

$$p = -2\rho\left(\frac{\partial \phi}{\partial t} + v\,\frac{\partial \phi}{\partial \xi}\right)$$

$$= -2\rho\left(\frac{\partial \phi}{\partial t} + v\,\frac{\partial \phi}{\partial x'}\cos\Lambda + v\,\frac{\partial \phi}{\partial y'}\sin\Lambda\right) \qquad (5)$$

where ϕ is in general the total potential, the sum of circulatory- and noncirculatory-flow potentials. The last term in equation (5) is the product of the component of main-stream velocity taken along the wing and the lengthwise change in the velocity potential, and is often neglected even in steady-flow work. The question of the retention or neglect of this last term seems partly dependent on the order in which the approximations are introduced; specifically, whether velocity potentials for the whole flow pattern are found and then the integrated forces are determined or whether section forces are first determined and then integrated. It seems appropriate to retain at least the noncirculatory part ϕ_N of ϕ in the last term of equation (5). In view, however, of the nature of the approximate treatment of the circulatory potential and of the inherent shortcomings of a strip analysis, in particular the neglect of lengthwise variations in wake vortex strength, complicating the results by also including ϕ_Γ in this term does not appear worth while. (This neglect of ϕ_Γ and retention of ϕ_N is realized to involve some inconsistencies in that account may not be taken of other higher order terms associated with lengthwise variation of the wing wake, which may be of the same order as terms retained.) Thus equation (5) becomes

$$p = -2\rho\left(\frac{\partial \phi}{\partial t} + v\,\frac{\partial \phi}{\partial x'}\cos\Lambda + v\,\frac{\partial \phi_N}{\partial y'}\sin\Lambda\right) \qquad (5a)$$

For harmonic motion in each degree of freedom, relations for the pressure may be integrated over the chord to yield expressions for the air forces and moments. For the sake of separating and identifying the terms in force and moment expressions which are due solely to the inclusion of the last term in equation (5a) a special bracket $\left\{\ \right\}$ is employed. Thus these terms may be readily omitted. Numerical checks among the calculations made for the present paper showed the effect of inclusion of the last term in (5a) on the calculated results to be quite small, even for 60° of sweepback within the range of other parameters investigated.

The expressions for the aerodynamic lift (positive down) and for the moment about the elastic axis (positive leading edge up), each per unit length of the wing, are:

$$P = -2\pi\rho v_n bC\left[\dot{h} + v_n\theta + v_n\sigma \tan\Lambda + b\left(\frac{1}{2} - a\right)\left(\dot{\theta} + v_n\tau \tan\Lambda\right)\right] -$$

$$\pi\rho b^2\left[\ddot{h} + v_n\dot{\theta} + v_n\dot{\sigma} \tan\Lambda + \left[v_n\dot{\sigma} \tan\Lambda + v_n{}^2\tau \tan\Lambda + \right.\right.$$

$$\left.\left. v_n{}^2 \frac{\partial\sigma}{\partial y'} \tan^2\Lambda\right]\right] + \pi\rho b^3 a\left[\ddot{\theta} + v_n\dot{\tau} \tan\Lambda + \left[v_n\dot{\tau} \tan\Lambda + v_n{}^2 \frac{\partial\tau}{\partial y'} \tan^2\Lambda\right]\right] \tag{6}$$

$$M_\alpha = 2\pi\rho v_n b^2\left(\frac{1}{2} + a\right) C\left[\dot{h} + v_n\theta + v_n\sigma \tan\Lambda + b\left(\frac{1}{2} - a\right)\left(\dot{\theta} + v_n\tau \tan\Lambda\right)\right] -$$

$$\pi\rho v_n b^3\left[\left(\frac{1}{2} - a\right)\dot{\theta} + \frac{1}{2} v_n\tau \tan\Lambda\right] + \pi\rho b^3 a\left[\ddot{h} + v_n\dot{\sigma} \tan\Lambda + \right.$$

$$\left.\left[v_n\dot{\sigma} \tan\Lambda + v_n{}^2\tau \tan\Lambda + v_n{}^2 \frac{\partial\sigma}{\partial y'} \tan^2\Lambda\right]\right] - \pi\rho b^4\left(\frac{1}{8} + a^2\right)\left[\ddot{\theta} + \right.$$

$$\left. v_n\dot{\tau} \tan\Lambda + \left[v_n\dot{\tau} \tan\Lambda + v_n{}^2 \frac{\partial\tau}{\partial y'} \tan^2\Lambda\right]\right] \tag{7}$$

where

$$C = C(k_n) = F(k_n) + iG(k_n)$$

is the function associated with the wake developed by Theodorsen in reference 6; the reduced frequency parameter k_n is defined by

$$k_n = \frac{\omega b}{v_n} = \frac{\omega b}{v \cos\Lambda} \tag{8}$$

As has already been stated, the foregoing expressions were developed and apply for steady sinusoidal oscillations,

$$\left.\begin{aligned} h &= h_1(y)e^{i\omega t} \\ \theta &= \theta_1(y)e^{i\omega t} \end{aligned}\right\} \tag{9}$$

The amplitude, velocity, and acceleration in each degree of freedom are related as in the h degree of freedom; that is,

$$\dot{h} = i\omega h$$

$$\ddot{h} = -\omega^2 h$$

Expressions for force and moment.— With the use of such relations equations (6) and (7) may be put into the form

$$P = -\pi\rho b^3\omega^2\left(hB_{ch} + \theta B_{c\theta}\right) \tag{10}$$

$$M_\alpha = -\pi\rho b^4\omega^2\left(hB_{ah} + \theta B_{a\theta}\right) \tag{11}$$

where

$$B_{ch} = \frac{1}{b}A_{ch} + \frac{\sigma}{h}\tan\Lambda\left(-i\frac{1}{k_n}\right)\left(\left[-1\right] + A_{ch}\right) + \left[\frac{b}{h}\frac{\partial\sigma}{\partial y'}\tan^2\Lambda\left(\frac{1}{k_n^2}\right)\right]$$

$$B_{c\theta} = A_{c\alpha} + \frac{\tau}{\theta}b\tan\Lambda(A_{c_\tau}) + \left[\frac{b^2}{\theta}\frac{\partial\tau}{\partial y'}\tan^2\Lambda\left(-\frac{a}{k_n^2}\right)\right]$$

$$B_{ah} = \frac{1}{b}A_{ah} + \frac{\sigma}{h}\tan\Lambda\left(-i\frac{1}{k_n}\right)\left(\left[a\right] + A_{ah}\right) + \left[\frac{b}{h}\frac{\partial\sigma}{\partial y'}\tan^2\Lambda\left(-\frac{a}{k_n^2}\right)\right]$$

$$B_{a\theta} = A_{a\alpha} + \frac{\tau}{\theta}b\tan\Lambda(A_{a_\tau}) + \left[\frac{b^2}{\theta}\frac{\partial\tau}{\partial y'}\tan^2\Lambda\left(\frac{1}{8} + a^2\right)\frac{1}{k_n^2}\right]$$

in which the four following coefficients:

$$A_{ch} = -1 - \frac{2G}{k_n} + i\frac{2F}{k_n}$$

$$A_{c\alpha} = a + \frac{2F}{k_n^2} - \left(\frac{1}{2} - a\right)\frac{2G}{k_n} + i\left[\frac{1}{k_n} + \frac{2G}{k_n^2} + \left(\frac{1}{2} - a\right)\frac{2F}{k_n}\right]$$

$$A_{ah} = a + \left(\frac{1}{2} + a\right)\frac{2G}{k_n} + i\left(\frac{1}{2} + a\right)\left(-\frac{2F}{k_n}\right)$$

$$= -\frac{1}{2} - \left(\frac{1}{2} + a\right)A_{ch}$$

$$A_{a\alpha} = -\frac{1}{8} - a^2 - \left(\frac{1}{2} + a\right)\frac{2F}{k_n^2} + \left(\frac{1}{4} - a^2\right)\frac{2G}{k_n} +$$

$$i\left[\left(\frac{1}{2} - a\right)\frac{1}{k_n} - \left(\frac{1}{4} - a^2\right)\frac{2F}{k_n} - \left(\frac{1}{2} + a\right)\frac{2G}{k_n^2}\right]$$

are identical with those used in the case of the unswept wing. Additionally,

$$A_{c\tau} = -\left[\frac{1}{k_n^2}\right]- - i\frac{1}{k_n}\left[\frac{1}{2} + \left[a\right]- + \left(\frac{1}{2} - a\right)A_{ch}\right]$$

$$A_{a\tau} = -i\frac{1}{k_n}\left[-\left(\frac{3}{8} + \left[\frac{1}{8} + a^2\right]-\right) + i\frac{1}{k_n}\left(\frac{1}{2} - \left[a\right]-\right) - \left(\frac{1}{4} - a^2\right)A_{ch}\right]$$

As was previously stated, the special bracket $-[\ ]-$ is used to identify terms originating in the last term of equation (5a).

It is of interest to note that equations (6) and (7) reduce, for the case of the wing in steady flow ($k_n = 0$), to

$$P = -2\pi\rho b v_n^2\left[\theta + \sigma\tan\Lambda + \tau b\tan\Lambda\left(\left[\frac{1}{2}\right]- + \frac{1}{2} - a\right) + \right.$$

$$\left.-\left[\frac{b}{2}\frac{\partial\sigma}{\partial y'}\tan^2\Lambda - \frac{a}{2}b^2\frac{\partial\tau}{\partial y'}\tan^2\Lambda\right]-\right] \tag{10a}$$

$$M_\alpha = 2\pi\rho b^2 v_n^2\left[(\theta + \sigma\tan\Lambda)\left(\frac{1}{2} + a\right) + \tau ab\tan\Lambda\left(\left[\frac{1}{2}\right]- - a\right) + \right.$$

$$\left.-\left[\frac{ab}{2}\frac{\partial\sigma}{\partial y'}\tan^2\Lambda - \frac{1}{2}b^2\left(\frac{1}{8} + a^2\right)\frac{\partial\tau}{\partial y'}\tan^2\Lambda\right]-\right] \tag{11a}$$

per unit length of wing.

Introduction of modes.- Equations (10) and (11) give the total aerodynamic force and moment on a segment of a sweptback wing oscillating in a simple harmonic manner. Relations for mechanical equilibrium applicable to a wing segment may be set up, but it is preferable to bring in directly the three-dimensional-mode considerations. (See for example, reference 7.) This end may be readily accomplished by the combined use of Rayleigh type approximations and the classical methods of Lagrange. The vibrations at flutter are assumed to consist of a combination of fixed mode shapes, each mode shape representing a degree of freedom associated with a generalized coordinate. The total mechanical energy, the potential energy, and the work done by applied forces, aerodynamic and structural, are then obtained by the integration of the section characteristics over the span. The Rayleigh type approximation enters in the representation of the potential energy in terms of the uncoupled frequencies.

As is customary, the modes are introduced into the problem as varying sinusoidally with time. For the purpose of simplicity of analysis, one bending degree of freedom and one torsion degree of freedom are carried through in the present development. Actually, any number of degrees of freedom may be added if desired, exactly as with an unswept wing. Let the mode shapes be represented by

$$\left.\begin{aligned} h &= \left[f_h(y')\right]\underline{h} \\ \theta &= \left[f_\theta(y')\right]\underline{\theta} \end{aligned}\right\} \tag{12}$$

where $\underline{h} = h_o e^{i\omega t}$ is the generalized coordinate in the bending degree of freedom, and $\underline{\theta} = \theta_o e^{i\omega t}$ is the generalized coordinate in the torsion degree of freedom. (In a more general treatment the mode shapes must be solved for, but in this procedure $f_h(y')$ and $f_\theta(y')$ are chosen, ordinarily as real functions of y'. Complex functions may be used to represent twisted modes.) The constants h_o and θ_o are in general complex and thus signify the phase difference between the two degrees of freedom.

For each degree of freedom an equation of equilibrium may be obtained from Lagrange's equation

$$\frac{d}{dt}\left(\frac{\partial T}{\partial \dot{q}_i}\right) - \frac{\partial T}{\partial q_i} + \frac{\partial U}{\partial q_i} = Q_i \tag{13}$$

where q_i is a generalized coordinate and Q_i is the corresponding generalized force. The kinetic energy of the mechanical system is

$$T = \frac{1}{2}\underline{\dot{h}}^2 \int_0^{l'} m\left[f_h(y')\right]^2 dy' + \frac{1}{2}\underline{\dot{\theta}}^2 \int_0^{l'} I_\alpha \left[f_\theta(y')\right]^2 dy' +$$

$$\underline{\dot{h}}\underline{\dot{\theta}} \int_0^{l'} mx_\alpha b \left[f_h(y')\right]\left[f_\theta(y')\right] dy' \qquad (14)$$

where

m mass of wing per unit length, slugs per foot

I_α mass moment of inertia of wing about its elastic axis per unit length, slug-feet^2 per foot

$x_\alpha b$ distance of sectional center of gravity from the elastic axis, positive rearward, feet

The potential energy of the mechanical system may be expressed in a form not involving bending-torsion cross-stiffness terms:

$$U = \frac{1}{2}\underline{h}^2 \int_0^{l'} EI\left(\frac{d^2 f_h}{dy'^2}\right)^2 dy' + \frac{1}{2}\underline{\theta}^2 \int_0^{l'} GJ\left(\frac{df_\theta}{dy'}\right)^2 dy' \qquad (15)$$

where

EI bending stiffness, pound-feet^2

GJ torsional stiffness, pound-feet^2

If Rayleigh type approximations are used to introduce frequency, the expression for the potential energy may be written in a more convenient form:

$$U = \frac{1}{2}\omega_h^2 \underline{h}^2 \int_0^{l'} mf_h^2 dy' + \frac{1}{2}\omega_\alpha^2 \underline{\theta}^2 \int_0^{l'} I_\alpha f_\theta^2 dy' \qquad (15a)$$

Another expression for the potential energy is

$$U = \frac{1}{2} \underline{h}^2 \int_0^{l'} C_h f_h^2 dy' + \frac{1}{2} \underline{\theta}^2 \int_0^{l'} C_\alpha f_\theta^2 dy' \tag{15b}$$

The effective spring constants C_h and C_α correspond to unit length of wing and thus conform to their use in references 5 to 7. The constants are effectively defined by

$$\omega_h^2 = \frac{\int_0^{l'} C_h f_h^2 dy'}{\int_0^{l'} m f_h^2 dy'}$$

$$\omega_\alpha^2 = \frac{\int_0^{l'} C_\alpha f_\theta^2 dy'}{\int_0^{l'} I_\alpha f_\theta^2 dy'}$$

These effective spring constants are related to the frequencies associated with the chosen modes. For so-called uncoupled modes the frequencies appropriate to pure modes (obtained by proper constraints) are often used. On the other hand, employment of the normal or natural modes and frequencies appropriate to them, which might be obtained by proper ground test or by calculation, may be preferred. In either case the convenience of not having cross-stiffness terms in the potential-energy expression is noted.

Application is now made to obtain the equation of equilibrium in the bending degree of freedom. Equation (13) becomes

$$\frac{d}{dt}\left(\frac{\partial T}{\partial \dot{h}}\right) - \frac{\partial T}{\partial \underline{h}} + \frac{\partial U}{\partial \underline{h}} = Q_h \tag{16}$$

The term Q_h represents all the bending forces not derivable from the potential-energy function and consists of the aerodynamic forces together with the structural damping forces. The virtual work δW done on the wing by these forces as the wing moves through the virtual displacements δh and $\delta\theta$ is:

$$\delta W = \int_0^{l'} \left[\left(P - C_h \frac{g_h}{\omega} \dot{h} \right) \delta h + \left(M_\alpha - C_\alpha \frac{g_\alpha}{\omega} \dot{\theta} \right) \delta\theta \right] dy'$$

$$= \int_0^{l'} \left(P - m\omega_h^2 \frac{g_h}{\omega} f_h \underline{\dot{h}} \right) f_h \, dy' \delta \underline{h} +$$

$$\int_0^{l'} \left(M_\alpha - I_\alpha \omega_\alpha^2 \frac{g_\alpha}{\omega} f_\theta \underline{\dot{\theta}} \right) f_\theta \, dy' \delta \underline{\theta} = Q_h \, \delta \underline{h} + Q_\theta \, \delta \underline{\theta} \qquad (17)$$

where

g_h structural damping coefficient for bending vibration

g_α structural damping coefficient for torsional vibration

In this expression the aerodynamic forces appropriate to sinusoidal oscillations are used. The application of the structural damping as in equation (17) (proportional to deflection and in phase with velocity) corresponds to the manner in which it is introduced in reference 5.

For the half-wing

$$Q_h = \int_0^{l'} \left(P - m\omega_h^2 \frac{g_h}{\omega} f_h \underline{\dot{h}} \right) f_h \, dy'$$

$$= -\pi \rho b_r^3 \omega^2 \int_0^{l'} \left(\frac{b}{b_r} \right)^3 \left[\frac{\underline{h}}{b} A_{ch} f_h^2 + \underline{h} \left(-i \frac{1}{k_n} \right) \left(\left[-1 \right] + A_{ch} \right) (\tan \Lambda) f_h \frac{df_h}{dy'} + \right.$$

$$- \left[\underline{h} \frac{1}{k_n^2} b (\tan^2 \Lambda) f_h \frac{d^2 f_h}{dy'^2} \right] + \underline{\theta} A_{c\alpha} f_\theta f_h + \underline{\theta} A_{c\tau} b (\tan \Lambda) f_h \frac{df_\theta}{dy'} +$$

$$\left. - \left[\underline{\theta} \left(-\frac{a}{k_n^2} \right) b^2 (\tan^2 \Lambda) f_h \frac{d^2 f_\theta}{dy'^2} \right] + \underline{h} \frac{1}{\kappa} i \left(\frac{\omega_h}{\omega} \right)^2 g_h f_h^2 \right] dy' \qquad (18)$$

where b_r is the semichord at some reference section. Performance of the operations indicated in equation (16) and collection of terms lead to the equation of equilibrium in the bending degree of freedom

$$\left(\underline{h}\left\{\left[1-\left(\frac{\omega_h}{\omega}\right)^2(1+ig_h)\right]\frac{1}{b_r}\int_0^{\eta'}\left(\frac{b}{b_r}\right)^2\frac{1}{\kappa}f_h^2d\eta'-\frac{1}{b_r}\int_0^{\eta'}\left(\frac{b}{b_r}\right)^2A_{ch}f_h^2d\eta'+\right.\right.$$

$$\int_0^{\eta'}\left(\frac{b}{b_r}\right)^3\tan\Lambda\left(i\,\frac{1}{k_n}\right)\left(\left[-1\right]+A_{ch}\right)f_h\frac{df_h}{d\eta'}\,d\eta'-$$

$$\left.\left.\left[b_r\int_0^{\eta'}\left(\frac{b}{b_r}\right)^4\tan^2\Lambda\left(\frac{1}{k_n^2}\right)f_h\frac{d^2f_h}{d\eta'^2}\,d\eta'\right]\right\}+\right.$$

$$\underline{\theta}\left\{\int_0^{\eta'}\left(\frac{b}{b_r}\right)^3\left(\frac{x_\alpha}{\kappa}-A_{c\alpha}\right)f_hf_\theta\,d\eta'-b_r\int_0^{\eta'}\left(\frac{b}{b_r}\right)^4A_{c\tau}(\tan\Lambda)f_h\frac{df_\theta}{d\eta'}\,d\eta'+\right.$$

$$\left.\left.\left[b_r^2\int_0^{\eta'}\left(\frac{b}{b_r}\right)^5\frac{a}{k_n^2}\tan^2\Lambda\,f_h\frac{d^2f_\theta}{d\eta'^2}\,d\eta'\right]\right\}\right)\pi\rho b_r^3\omega^2=0 \qquad (19)$$

where

$$\frac{1}{\kappa}=\frac{m}{\pi\rho b^2}$$

By a parallel development the equation of equilibrium for the torsional degree of freedom may also be obtained

$$\left(\underline{h}\left\{\left[\frac{1}{b_r}\int_0^{\eta'}\left(\frac{b}{b_r}\right)^3\left(\frac{x_\alpha}{\kappa}-A_{ah}\right)f_hf_\theta\,d\eta'+\int_0^{\eta'}\left(\frac{b}{b_r}\right)^4\tan\Lambda\left(i\,\frac{1}{k_n}\right)\left(\left[a\right]+\right.\right.\right.\right.$$

$$\left.\left.\left.\left.A_{ah}\right)f_\theta\frac{df_h}{d\eta'}\,d\eta'+\left[b_r\int_0^{\eta'}\left(\frac{b}{b_r}\right)^5\tan^2\Lambda\left(\frac{a}{k_n^2}\right)f_\theta\frac{d^2f_h}{d\eta'^2}\,d\eta'\right]\right]\right\}+\right.$$

$$\underline{\theta}\left\{\left[1-\left(\frac{\omega_\alpha}{\omega}\right)^2(1+ig_\alpha)\right]\int_0^{\eta'}\left(\frac{b}{b_r}\right)^4\frac{r_\alpha^2}{\kappa}f_\theta^2d\eta'-\int_0^{\eta'}\left(\frac{b}{b_r}\right)^4A_{a\alpha}f_\theta^2d\eta'-\right.$$

$$b_r\int_0^{\eta'}\left(\frac{b}{b_r}\right)^5\tan\Lambda(A_{a\tau})f_\theta\frac{df_\theta}{d\eta'}\,d\eta'-$$

$$\left.\left.\left.\left[b_r^2\int_0^{\eta'}\left(\frac{b}{b_r}\right)^6\tan^2\Lambda\left(\frac{1}{8}+a^2\right)\frac{1}{k_n^2}f_\theta\frac{d^2f_\theta}{d\eta'^2}\,d\eta'\right]\right\}\right)\pi\rho b_r^4\omega^2=0 \qquad (20)$$

where $r_\alpha = \sqrt{I_\alpha/mb^2}$, (radius of gyration of wing about the elastic axis).

Determinantal equation for flutter.— Equations (19) and (20) may be rewritten with the use of the nondimensional coordinate $\eta = \frac{y'}{l'}$. They then are in the form

$$(\underline{h}A_2 + \underline{\theta}B_2)\pi\rho b_r{}^3\omega^2 = 0 \tag{19a}$$

$$(\underline{h}D_2 + \underline{\theta}E_2)\pi\rho b_r{}^4\omega^2 = 0 \tag{20a}$$

where

$$A_2 = \left[1 - \left(\frac{\omega_h}{\omega}\right)^2(1 + ig_h)\right]\frac{l'}{b_r}\int_0^{1.0}\left(\frac{b}{b_r}\right)^2\frac{1}{\kappa}\left[F_h(\eta)\right]^2 d\eta -$$

$$\frac{l'}{b_r}\int_0^{1.0}\left(\frac{b}{b_r}\right)^2 A_{ch}\left[F_h(\eta)\right]^2 d\eta + \int_0^{1.0}\left(\frac{b}{b_r}\right)^3\tan\Lambda\left(i\,\frac{1}{k_n}\right)\left(\left[-1\right] +\right.$$

$$\left.A_{ch}\right)\left[F_h(\eta)\right]\frac{dF_h}{d\eta}\,d\eta - \left[\frac{b_r}{l'}\int_0^{1.0}\left(\frac{b}{b_r}\right)^4\tan^2\Lambda\left(\frac{1}{k_n}\right)^2\left[F_h(\eta)\right]\frac{d^2F_h}{d\eta^2}\,d\eta\right]$$

$$B_2 = l'\int_0^{1.0}\left(\frac{b}{b_r}\right)^3\left(\frac{x_\alpha}{\kappa} - A_{c\alpha}\right)\left[F_h(\eta)\right]\left[F_\theta(\eta)\right]d\eta -$$

$$b_r\int_0^{1.0}\left(\frac{b}{b_r}\right)^4\tan\Lambda\left(A_{c\tau}\right)\left[F_h(\eta)\right]\frac{dF_\theta}{d\eta}\,d\eta +$$

$$\left[\frac{b_r{}^2}{l'}\int_0^{1.0}\left(\frac{b}{b_r}\right)^5\tan^2\Lambda\left(\frac{a}{k_n{}^2}\right)\left[F_h(\eta)\right]\frac{d^2F_\theta}{d\eta^2}\,d\eta\right]$$

$$D_2 = \frac{l'}{b_r}\int_0^{1.0}\left(\frac{b}{b_r}\right)^3\left(\frac{x_\alpha}{\kappa} - A_{ah}\right)\left[F_\theta(\eta)\right]\left[F_h(\eta)\right]d\eta +$$

$$\int_0^{1.0}\left(\frac{b}{b_r}\right)^4 \tan\Lambda\left(i\,\frac{1}{k_n}\right)\left([a] + A_{ah}\right)\left[F_\theta(\eta)\right]\frac{dF_h}{d\eta}\,d\eta +$$

$$\left[\frac{b_r}{l'}\int_0^{1.0}\left(\frac{b}{b_r}\right)^5 \tan^2\Lambda\left(\frac{a}{k_n^2}\right)\left[F_\theta(\eta)\right]\frac{d^2F_h}{d\eta^2}\,d\eta\right]$$

$$E_2 = l'\left[1 - \left(\frac{\omega_\alpha}{\omega}\right)^2(1 + ig_\alpha)\right]\int_0^{1.0}\left(\frac{b}{b_r}\right)^4 \frac{r_\alpha^2}{\kappa}\left[F_\theta(\eta)\right]^2 d\eta -$$

$$l'\int_0^{1.0}\left(\frac{b}{b_r}\right)^4 A_{a\alpha}\left[F_\theta(\eta)\right]^2 d\eta - b_r\int_0^{1.0}\left(\frac{b}{b_r}\right)^5 \tan\Lambda(A_{aT})\left[F_\theta(\eta)\right]\frac{dF_\theta}{d\eta}\,d\eta -$$

$$\left[\frac{b_r^2}{l'}\int_0^{1.0}\left(\frac{b}{b_r}\right)^6 \tan^2\Lambda\left(\frac{1}{8} + a^2\right)\frac{1}{k_n^2}\left[F_\theta(\eta)\right]\frac{d^2F_\theta}{d\eta^2}\,d\eta\right]$$

in which $F_h(\eta) = f_h(l'\eta)$ and $F_\theta(\eta) = f_\theta(l'\eta)$.

The borderline condition of flutter, separating damped and undamped oscillations, is determined from the nontrivial solution of the simultaneous homogeneous equations (19a) and (20a). Such a solution corresponds to the fact that mechanical equilibrium exists for sinusoidal oscillations at a certain airspeed and with a certain frequency. The flutter condition thus is given by the vanishing of the determinant of the coefficients

$$\begin{vmatrix} A_2 & B_2 \\ D_2 & E_2 \end{vmatrix} = 0$$

Application to the case of uniform, cantilever, swept wings is made in the next section.

Application to Uniform Cantilever Swept Wings

The first step in the application of the theory is to assume or develop the deflection functions to be used. For the purpose of applying the analysis to the wing models employed in the experiments it appeared reasonable to use for the deflection functions, $F_h(\eta)$ and $F_\theta(\eta)$, the uncoupled first bending and first torsion mode shapes of an ideal uniform cantilever beam. Although approximations for these mode shapes could be used, the analysis utilized the exact expressions developed from equations (120) and (106d), respectively, of reference 8 by application of appropriate boundary conditions.

The bending-mode shape can be written

$$F_h(\eta) = C_1\left[\frac{\sinh \beta_1 + \sin \beta_1}{\cosh \beta_1 + \cos \beta_1}(\cos \beta_1\eta - \cosh \beta_1\eta) + \sinh \beta_1\eta - \sin \beta_1\eta\right]$$

where $\beta_1 = 0.5969\pi$ for first bending. The torsion mode shape can be written

$$F_\theta(\eta) = C_2 \sin \beta_2\eta$$

where $\beta_2 = \frac{\pi}{2}$ for first torsion and C_1 and C_2 are constants.

The integrals appearing in the determinant elements A_2, B_2, D_2, and E_2 are

$$\int_0^{1.0} F_h{}^2 d\eta = 1.8554C_1{}^2$$

$$\int_0^{1.0} F_\theta{}^2 d\eta = 0.5000C_2{}^2$$

$$\int_0^{1.0} F_h \frac{dF_h}{d\eta} d\eta = 3.7110C_1{}^2$$

$$\int_0^{1.0} F_\theta \frac{dF_\theta}{d\eta}\, d\eta = 0.3183C_2^2$$

$$\int_0^{1.0} F_h \frac{d^2F_h}{d\eta^2}\, d\eta = 1.5926C_1^2$$

$$\int_0^{1.0} F_\theta \frac{d^2F_\theta}{d\eta^2}\, d\eta = -1.2337C_2^2$$

$$\int_0^{1.0} F_hF_\theta\, d\eta = \int_0^{1.0} F_\theta F_h\, d\eta = -0.9233C_1C_2$$

$$\int_0^{1.0} F_h \frac{dF_\theta}{d\eta}\, d\eta = -1.4040C_1C_2$$

$$\int_0^{1.0} F_\theta \frac{dF_h}{d\eta}\, d\eta = -2.0669C_1C_2$$

$$\int_0^{1.0} F_h \frac{d^2F_\theta}{d\eta^2}\, d\eta = 2.2782C_1C_2$$

$$\int_0^{1.0} F_\theta \frac{d^2F_h}{d\eta^2}\, d\eta = -1.4722C_1C_2$$

The flutter determinant becomes

$$\begin{vmatrix} 1.8554c_1^2\frac{l'}{b_r}A + 3.7110c_1^2\left(1\frac{1}{k_n}\right)\left(\left[\frac{1}{l}\right] + A_{ch}\right)\tan\Lambda - \left[1.5986c_1^2\frac{\tan^2\Lambda}{l'/b_r}\frac{1}{k_n^2}\right] & -0.9233c_1c_2l'B - (-1.4040c_1c_2)b_rA_{c\alpha}\tan\Lambda + \left[2.2782c_1c_2\frac{\tan^2\Lambda}{l'/b_r}\frac{a}{k_n^2}\right] \\ -0.9233c_1c_2\frac{l'}{b_r}D - 2.0669c_1c_2\left(1\frac{1}{k_n}\right)\left(\left[a\right] + A_{ah}\right) + \left[1.4722c_1c_2\frac{\tan^2\Lambda}{l'/b_r}\frac{a}{k_n^2}\right] & 0.5000c_2^2l'E - 0.3183c_2^2b_rA_{a\alpha}\tan\Lambda - \left[1.2337c_2^2\frac{\tan^2\Lambda}{l'/b_r}\left(\frac{1}{8} + a^2\right)\frac{1}{k_n^2}\right] \end{vmatrix} = 0$$

or more conveniently, when columns and rows of the determinant are divided by appropriate terms

$$\begin{vmatrix} A + 2.0000\frac{\tan\Lambda}{l'/b_r}\left(1\frac{1}{k_n}\right)\left(\left[\frac{1}{l}\right] + A_{ch}\right) - \left[0.8583\left(\frac{\tan\Lambda}{l'/b_r}\right)^2\frac{1}{k_n^2}\right] & B - 1.5206\frac{\tan\Lambda}{l'/b_r}A_{c\alpha} - \left[2.4675\left(\frac{\tan\Lambda}{l'/b_r}\right)^2\frac{a}{k_n^2}\right] \\ 0.9189 + 2.0571\frac{\tan\Lambda}{l'/b_r}\left(1\frac{1}{k_n}\right)\left(\left[a\right] + A_{ah}\right) + \left[1.4652\left(\frac{\tan\Lambda}{l'/b_r}\right)^2\frac{a}{k_n^2}\right] & E - 0.6366\frac{\tan\Lambda}{l'/b_r}A_{a\alpha} + \left[2.4675\left(\frac{\tan\Lambda}{l'/b_r}\right)^2\left(\frac{1}{8} + a^2\right)\frac{1}{k_n^2}\right] \end{vmatrix} = 0$$

where

$$A = \frac{1}{\kappa}\left[1 - \left(\frac{\omega_h}{\omega}\right)^2(1 + ig_h)\right] - A_{ch}$$

$$B = \frac{x_\alpha}{\kappa} - A_{c\alpha}$$

$$D = \frac{x_\alpha}{\kappa} - A_{ah}$$

$$E = \frac{r_\alpha^2}{\kappa}\left[1 - \left(\frac{\omega_\alpha}{\omega}\right)^2(1 + ig_\alpha)\right] - A_{a\alpha}$$

It is interesting to note that the parameters Λ and l'/b_r appear only in the combination $\frac{\tan \Lambda}{l'/b_r}$ in the immediately preceding determinant. The solution of the determinant results in the flutter condition.

RESULTS AND DISCUSSION

Experimental Investigation

Presentation of experimental data.- Results of the experimental investigation are listed in detail in tables I to VII, and some significant experimental trends are illustrated in figures 5 to 10. As a basis for presenting and comparing the test results, the ratio of experimental tunnel stream conditions to the reference flutter conditions is employed so that the data indicate more clearly combined effects of aspect ratio, sweep, and Mach number. As previously mentioned, use of the reference flutter speed V_R serves to reduce variations in flutter characteristics which arise from changes in other parameters, such as density and section properties, which are not pertinent to this investigation. (See appendix B.)

Some effects on flutter speed.- A typical plot showing the effect of compressibility on the flutter speed of wings at various angles of sweepback is shown in figure 5. These data are from tests of the rectangular-plan-form models (type 30) that were swept back by use of the rotating mount, for which arrangement the reference flutter speed does not vary with either Mach number or sweep angle. Observe the large increase in speed ratio at the high sweep angles.

The data of reference 1 from tests of a rigid, flexibly mounted rectangular model having a rotating base are also plotted in figure 5. It can be seen that the data from the cantilever models of the present paper which had a similar method of sweep are in conformity with the data from the flexibly mounted model. This indicates that, for uniform wings having the range of parameters involved in these tests, the differences due to mode shape are not very great.

Figure 6 is a cross plot of the data from figure 5 plotted against Λ at a Mach number approximately equal to 0.65. The data of the swept wings of constant length-to-chord ratio and of the sheared swept wings are also included for comparison. The velocity ratio V_e/V_R is relatively constant at small sweep angles but rises noticeably at the large sweep angles. It is pointed out that the reference flutter speed V_R may be considered to correspond to a

horizontal line at $\frac{V_e}{V_R} = 1$ for the rotated and constant-length-chord-ratio wings, but for the sheared wings this reference speed corresponds to a curve decreasing somewhat less rapidly than $\sqrt{\cos \Lambda}$ as Λ increases. (See appendix B.)

The order of magnitude of some three-dimensional effects may be noted from the fact that the shorter wings $\left(\frac{l}{c} = 6.5, \text{ fig. } 6, \text{ series V}\right)$ have higher velocity ratios than the longer wings $\left(\frac{l}{c} = 8.5, \text{ series IV}\right)$. This increase may be due partly to differences in flutter modes as well as aerodynamic effects.

Some effects on flutter frequency.- Figure 7 is a representative plot of the flutter-frequency data given in table II. The figure shows the variation in flutter-frequency ratio with Mach number for different values of sweep angle for the models rotated back on the special mount. The ordinate is the ratio of the experimental flutter frequency to the reference flutter frequency f_e/f_R. It appears that there is a reduction in flutter frequency with increase in Mach number and also an increase in flutter frequency with increase in sweep. The data from reference 1 show the same trend with increase in sweep. Considerably more scatter may be noted in the frequency data than in the speed data (fig. 5) from the same tests.

The results of the tests for rotated wings with chordwise laminations (models 40A, B, C, D) are given in table II. At sweep angles up to 30° the values of the speed ratio V_e/V_R for wings of this construction were low (in the neighborhood of 0.9), and the flutter frequency ratios f_e/f_R were high (of the order of 1.4). As these results indicate and as visual observation showed, these models fluttered in a mode that apparently involved an appreciable proportion of the second bending mode. The models with spanwise laminations (models 30A, B, C, D) also showed indications of this higher flutter mode at low sweep angles; however, these models were able to pass through the small speed range of higher mode flutter without sufficiently violent oscillations to cause failure. At a still higher speed these models with spanwise laminations fluttered in a lower mode resembling a coupling of the torsion and first bending modes. This lower mode type of flutter characterized the flutter of both the sheared- and constant-length-chord-ratio models.

For those wing models having the sheared type of balsa construction (models 22', 23, 24, and 25), the results are more difficult to compare

with those of the other models. This difficulty arises chiefly because the lightness of the wood produced relatively high mass-density ratios κ and partly because of the nonhomogeneity of the mixed wood construction. For high values of κ the flutter-speed coefficient changes rather abruptly even for the unswept models (reference 5). The data are nevertheless included in table I.

Effect of shift in center-of-gravity position on the flutter speed of swept wings.- Results of the investigation of the effects of center-of-gravity shift on the flutter speed of swept wings are illustrated in figure 8. This figure is a cross plot of the experimental indicated air speeds as a function of sweep angle for various center-of-gravity positions. The ordinate is the experimental indicated air speed $V_e\sqrt{\frac{\rho}{0.00238}}$, which serves to reduce the scatter resulting from flutter tests at different densities of testing medium. The data were taken in the Mach number range between 0.14 and 0.44, so that compressibility effects are presumably negligible. As in the case of unswept wings, forward movement of the center of gravity increases the flutter speed. Again, the flutter speed increases with increase in the angle of sweep.

The models tested at zero sweep angle (models 91-1, 91-2, 91-3) were of different construction from and of larger size than the models tested at the higher sweep angles. Because of the manner of plotting the results, namely as experimental indicated airspeed (fig. 8), a comparison of the results of tests at $\Lambda = 0^\circ$ with the results of the tests of swept models is not particularly significant. The points at zero sweep angle are included, however, to show that the increase in flutter speed due to a shift in the center-of-gravity position for the swept models is of the same order of magnitude as for the unswept models. For the unswept models, the divergence speed V_D and the reference flutter speed V_R are fairly near each other, and although the models appeared to flutter, the proximity of the flutter speed to the divergence speed may have influenced the value of the critical speed.

The method used to vary the center of gravity (see fig. 1(g)) produced two bumps on the airfoil surface. At the low Mach numbers of these tests, however, the effect of this roughness on the flutter speed is considered negligible. For proper interpretation of figure 8 the fact must be kept in mind that the method of varying the location of the center of gravity changed the radius of gyration r_α and the torsional frequency f_α.

The effect of sweepforward on the critical speed.- An attempt was made to determine the variation in flutter speed with angle of sweepforward by testing wings on the mount that could be rotated both backward and forward. As expected, however, the model tended to diverge at

forward sweep angles in spite of the relatively forward position of the elastic axis in this D-spar wing.

Figure 9 shows a plot of the ratio of critical speed to the reference flutter speed V_R against sweep angle Λ. Note the different curves for the sweptback and for the sweptforward conditions and the sharp reduction in critical speed as the angle of sweepforward is increased. The different curves result from two different phenomena. When the wing was swept back it fluttered, whereas at forward sweep angles it diverged before the flutter speed was reached. Superposed on this plot for the negative values of sweep are the results of calculations based on an analytical study of divergence (reference 9). Reasonable agreement exists between theory and experiment at forward sweep angles. The small difference between the theoretical and experimental results may perhaps be due to an inaccuracy in determining either the position of the elastic axis of the model or the required slope of the lift curve or both.

The divergence speed V_D for the wing at zero sweep angle, as calculated by the simplified theory of reference 5, is also plotted in figure 9. This calculation is based on the assumption of a two-dimensional unswept wing in an incompressible medium. The values of the uncoupled torsion frequency and the density of the testing medium at time of flutter or divergence are employed. Reference 9 shows that a relatively small amount of sweepback raises the divergence speed sharply. For convenience, however, the numerical quantity V_D (based on the wing at zero sweep) is listed in table I for all the tests.

Effect of tip modifications.— Tests to investigate some of the over-all effects of tip shape were conducted and some results are shown in figure 10. Two sweep angles and two length-to-chord ratios were used in the experiments conducted at two Mach numbers. It is seen that, of the three tip shapes used, namely, tips perpendicular to the air stream, perpendicular to the wing leading edge, and parallel to the air stream, the wings with tips parallel to the air stream gave the highest flutter speeds.

Discussion and Comparison of Analytical and Experimental Results

Correlation of analytical and experimental results has been made for wings swept back in the two different manners; that is, (1) sheared back with a constant value of A_g, and (2) rotated back. The two types of sheared wings (series I) and two rotated wings (models 30B and 30D) have been analyzed.

Results of some solutions of the flutter determinant for a wing (model 30B) on a rotating base at several angles of sweepback are shown in figures 11 and 12. Figure 11 shows the flutter-speed coefficient as a function of the bending-to-torsion frequency ratio, and figure 12 shows the flutter frequency ratio as a function of the bending-to-torsion frequency ratio.

The calculated results (for those wings investigated analytically) are included in tables I and II. The ratios of experimental to analytical flutter speeds and flutter frequencies have been plotted against the angle of sweep in figures 13 to 16. If an experimental value coincides with the corresponding analytically predicted value, the ratio will fall at a value of 1.0 on the figures. Deviations of experimental results above or below the analytical results appear on the figures as ratios respectively greater than or less than 1.0. The flutter-speed ratios plotted in figure 13 for the two rotated wings show very good agreement between analysis and experiment over the range of sweep angle, 0° to 60°. Such good agreement in both the trends and in the numerical quantities is gratifying but probably should not be expected in general. In view of the discussion of the last term in equation (5a) it may be of interest to mention that failure to include the terms arising from the last term of equation (5a) in the calculations for model 30B would decrease the ratio V_e/V_Λ corresponding to $\Lambda = 60^\circ$ by about 3 percent. The flutter frequency ratios of figure 14 obtained from the same two rotated wings are in good agreement.

The flutter-speed ratios plotted in figure 15 for the two types of sheared wings do not show such good conformity at the low angles of sweep, whereas for sweep angles beyond 45° the ratios are considerably nearer to 1.0. The sheared wings are again observed to have a constant value of A_g of 2.0 (aspect ratio for the whole wing would be 4.0). For this small value of aspect ratio the finite-span correction is appreciable at zero angle of sweep and, if made, would bring better agreement at that point. Analysis of the corrections for finite-span effects on swept wings requires further consideration.

Figures 13 and 15 also afford a comparison of the behavior of wings swept back in two manners: (1) rotated back with constant length-to-chord ratio but decreasing aspect ratio (fig. 13), and (2) sheared back with constant aspect ratio and increasing length-to-chord ratio (fig. 15). A study of these two figures suggests that the length-to-chord ratio rather than the aspect ratio $\left(\frac{\text{Span}^2}{\text{Area}}\right)$ may be the relevant parameter in determining corrections for finite swept wings. (Admittedly, effects of tip shape and root condition are also involved and have not been precisely separated.)

Figure 16, which refers to the same sheared wings as figure 15, shows the ratios of experimental to predicted flutter frequencies. The trend is for the ratio to decrease as the angle of sweep increases. Table I shows that the flutter frequency f_R obtained with V_R and used as a reference in a previous section of the paper is not significantly different from the frequency f_Λ predicted by the present analysis.

A few remarks can be made on estimates of over-all trends of the flutter speed of swept wings. As a first consideration the conclusion may be made that if a rigid infinite yawed wing were mounted on springs which permitted it to move vertically as a unit and to rotate about an elastic axis, the flutter speed would be proportional to $\frac{1}{\cos \Lambda}$. A finite yawed wing mounted on similar springs would be expected to have a flutter speed lying above the curve of $\frac{1}{\cos \Lambda}$ because of finite-span effects. For a finite sweptback wing clamped at its root, however, the greater degree of coupling between bending and torsion adversely affects the flutter speed so as to bring the speed below the curve of $\frac{1}{\cos \Lambda}$ for an infinite wing. This statement is illustrated in figure 17 which refers to a wing (model 30B) on a rotating base. The ordinate is the ratio of flutter speed at a given angle of sweep to the flutter speed calculated at zero angle of sweep. A theoretical curve is shown, together with experimentally determined points. Curves of $\frac{1}{\cos \Lambda}$ and $\frac{1}{\sqrt{\cos \Lambda}}$ are shown for convenience of comparison. The curve for model 30D (not shown in fig. 17) also followed this trend quite closely. The foregoing remarks should prove useful for making estimates and discussing trends but are not intended to replace more complete calculation. In particular, mention may be made, for example, that a far-forward location of section center of gravity would lead to an entirely different trend. Moreover, as is apparent from the analysis, the bending stiffness can play an increasingly significant role with increase in the angle of sweep.

The experiments and calculations deal in general with wings having low ratios of natural first bending to first torsion frequencies. At high values of the ratio of bending frequency to torsion frequency, the position of the elastic axis becomes relatively more significant. Additional calculations to develop the theoretical trends are desirable.

CONCLUSIONS

In a discussion and comparison of the results of an investigation of the flutter of a group of swept wings, the manner of sweep is significant. This paper deals with two main groups of uniform, swept wings: rotated wings and sheared wings. In presenting the data, employment of a certain reference flutter speed was found convenient. The following conclusions seem to apply:

1. Comparison with experiment indicates that the analysis presented is satisfactory for giving the main effects of sweep, at least for nearly uniform cantilever wings of moderate length-to-chord ratios. Additional calculations are desirable to investigate various theoretical trends.

2. The coupling between bending and torsion adversely affects the flutter speed. The fact, however, that only a part of the forward velocity is aerodynamically effective increases the flutter speed. Certain approximate relations can be used to estimate some of the trends.

3. Although a precise separation of the effects of Mach number, aspect ratio, tip shape, and center-of-gravity position has not been accomplished, the order of magnitude of some of these combined effects has been experimentally determined. Experimental results indicated are

(a) The location of the section center of gravity is an important parameter and produces effects for swept wings similar to those for unswept wings over the range (30 percent to 70 percent chord) of locations tested.

(b) Appreciable differences in flutter speed have been found to be due to tip shape.

(c) The length-to-chord ratio of swept wings is a more relevant finite-span parameter than is the aspect ratio.

(d) Compressibility effects attributable to Mach number are fairly small, at least up to a Mach number of 0.8.

(e) The sweptforward wings could not be made to flutter but diverged before the flutter speed was reached.

Langley Aeronautical Laboratory
National Advisory Committee for Aeronautics
Langley Air Force Base, Va., September 9, 1948

APPENDIX A

THE EFFECT OF SWEEP ON THE FREQUENCIES OF A CANTILEVER BEAM

Early in the investigation it was decided to make an experimental vibration study of a simple beam at various sweep angles. The uniform, plate-like aluminum-alloy beam shown in figure 18 was used to make the study amenable to analysis. Length-to-chord ratios of 6, 3, and 1.5 were tested, the length l being defined as the length along the mid-chord. A single 60-inch beam was used throughout the investigation, the desired length and sweep angle being obtained by clamping the beam in the proper position with a $1\frac{1}{2}$- by $1\frac{1}{2}$- by 14-inch aluminum-alloy crossbar.

Figures 18 and 19 show the variation in modes and frequencies with sweep angle. In most cases, an increase in sweep angle increased the natural vibration frequencies. As expected, the effect of sweep was more pronounced at the smaller values of length-to-chord ratio. The fundamental mode was found by striking the beam and measuring the frequency with a self-generating vibration pick-up and paper recorder. The second and third modes were excited by light-weight electromagnetic shakers clamped to the beam. These shakers were attached as close to the root as possible to give a node either predominantly spanwise or chordwise. The mode with the spanwise node, designated second mode, was primarily torsional vibration, whereas the mode with the chordwise node, designated third mode, was primarily a second bending vibration.

The first two bending frequencies and the lowest torsion frequency, determined analytically for a straight uniform unswept beam, are plotted in figure 19. Good agreement exists with the experimental results for the length-to-chord ratios of 6 and 3, but for a ratio of 1.5 (length equal to 12 inches and chord equal to 8 inches) less favorable agreement exists. This discrepancy may be attributed to the fact that the beam at the short length-to-chord ratio of 1.5 resembled more a plate than a beam and did not meet the theoretical assumptions of a perfectly rigid base and of simple-beam stress distributions. The data are valid for use in comparing the experimental frequencies of the beam when swept with the frequencies at zero sweep, which was the purpose of the test.

APPENDIX B

DISCUSSION OF THE REFERENCE FLUTTER SPEED

For use in comparing data of swept and unswept wings, a reference flutter speed V_R is convenient. This reference flutter speed is the flutter speed determined from the simplified theory of reference 5. This theory deals with two-dimensional unswept wings in incompressible flow and depends upon a number of wing parameters. The calculations in this report utilize parameters of sections perpendicular to the leading edge, first bending frequency, uncoupled torsion frequency, density of testing medium at time of flutter, and zero damping. Symbolically,

$$V_R = b\omega_\alpha f\left(\kappa, x_{cg}, x_{ea}, r_\alpha^2, \frac{f_h}{f_\alpha}\right)$$

Variation in reference flutter speed with sweep angle for sheared swept wings.- The reference flutter speed is independent of sweep angle for a homogeneous rotated wing and for homogeneous wings swept back by keeping the length-to-chord ratio constant. For a series of homogeneous wings swept back by the method of shearing, however, a definite variation in reference flutter speed with sweep angle exists since sweeping a wing by shearing causes a reduction in chord perpendicular to the wing leading edge and an increase in length along the midchord as the angle of sweep is increased. The resulting reduction in the mass-density-ratio parameter and first bending frequency tends to raise the reference flutter speed, whereas the reduction in semichord tends to lower the reference flutter speed as the angle of sweep is increased. The final effect upon the reference flutter speed depends on the other properites of the wing. The purpose of this section is to show the effect of these changes on the magnitude of the reference flutter speed for a series of homogeneous sheared wings having properties similar to those of the sheared swept models used in this paper.

Let the subscript o refer to properties of the wing at zero sweep angle. The following parameters are then functions of the sweep angle:

$$b = b_o \cos \Lambda$$

$$l = \frac{l_o}{\cos \Lambda}$$

Since m is proportional to b,

$$\kappa = \frac{\pi\rho b^2}{m} = \kappa_o \cos \Lambda$$

Similarly, since I is proportional to b

$$f_{h_1} = \frac{0.56}{l^2}\sqrt{\frac{EI}{m}} = \left(f_{h_1}\right)_o (\cos \Lambda)^2$$

Also, because f_α is independent of Λ,

$$\frac{f_{h_1}}{f_\alpha} = \left(\frac{f_{h_1}}{f_\alpha}\right)_o (\cos \Lambda)^2$$

An estimate of the effect on the flutter speed of these changes in semichord and mass parameter with sweep angle may be obtained from the approximate formula given in reference 5.

$$V_R \approx b\omega_\alpha\sqrt{\frac{r_\alpha^2}{\kappa}\frac{0.5}{0.5 + a + x_\alpha}} = V_{R_o}\sqrt{\cos \Lambda}$$

This approximate analysis of the effect on the reference flutter speed does not depend upon the first bending frequency but assumes f_h/f_α to be small.

In order to include the effect of changes in bending–torsion frequency ratio, a more complete analysis must be carried out. Some results of a numerical analysis are presented in figure 20, based on a homogeneous wing with the following properties at zero sweep angle:

$x_{cg} = 50$ $\qquad b_o = 0.333$

$x_{ea} = 45$ $\qquad \left(\frac{1}{\kappa}\right)_o = 10$

$r_\alpha^2 = 0.25$

$f_\alpha = 100$ $\qquad \left(\frac{f_{h_1}}{f_\alpha}\right)_o = 0.4$

In figure 20 the curve showing the decrease in V_R with Λ is slightly above the $\sqrt{\cos \Lambda}$ factor indicated by the approximate formula.

Effect of elastic-axis position on reference flutter speed.- As pointed out in the definition of elastic axis, the measured locus of elastic centers x_{ea}' fell behind the "section" elastic axis for the swept models with bases parallel to the air stream. In order to get an idea of the effect of elastic-axis position on the chosen reference flutter speed, computations were made both of V_R and a second reference flutter speed V_R' similar to V_R except that x_{ea}' was used in place of x_{ea}. The maximum difference between these two values of reference flutter speed was of the order of 7 percent. This difference occurred at a sweep angle of 60° when the "wing" elastic axis was farthest behind the "section" elastic axis. Thus, for wings of this type, the reference flutter speed is not very sensitive to elastic-axis position. The reference flutter frequency f_R' was found in conjunction with V_R'. The maximum difference between f_R and f_R' was less than 10 percent. Thus, the convenient use of the reference flutter speed and reference frequency is not altered by these elastic-axis considerations.

REFERENCES

1. Kramer, Edward H.: The Effect of Sweepback on the Critical Flutter Speed of Wings. MR No. TSEAC5-4595-2-5, Eng. Div., Air Technical Service Command, Army Air Forces, March 15, 1946.

2. Broadbent, E. G.: Some Considerations of the Flutter Problems of High-Speed Aircraft. Sec. International Aero. Conference, N. Y., 1949, pp. 556-581.

3. Fettis, Henry E.: Calculations of the Flutter Characteristics of Swept Wings at Subsonic Speeds. MR No. TSEAC5-4595-2-9, Air Materiel Command, Army Air Forces, May 13, 1946.

4. Spielberg, Irvin, Fettis, H. E., and Toney, H. S.: Methods for Calculating the Flutter and Vibration Characteristics of Swept Wings. MR No. MCREXA5-4595-8-4, Air Materiel Command, U. S. Air Force, Aug. 3, 1948.

5. Theodorsen, Theodore, and Garrick, I. E.: Mechanism of Flutter - A Theoretical and Experimental Investigation of the Flutter Problem. NACA Rep. 685, 1940.

6. Theodorsen, Theodore: General Theory of Aerodynamic Instability and the Mechanism of Flutter. NACA Rep. 496, 1935.

7. Smilg, Benjamin, and Wasserman, Lee S.: Application of Three-Dimensional Flutter Theory to Aircraft Structures. ACTR No. 4798, Materiel Div., Army Air Corps, July 9, 1942.

8. Timoshenko, S.: Vibration Problems in Engineering. D. Van Nostrand Co., Inc., 1928.

9. Diederich, Franklin W., and Budiansky, Bernard: Divergence of Swept Wings. NACA TN 1680, 1948.

TABLE I.- DATA FOR SWEPT MODELS - SERIES I

Spruce wings																							
Model	Λ (deg)	A_R	f_{h_1} (cps)	f_{h_2} (cps)	f_t (cps)	f_α (cps)	GJ (lb-in.^{2})	EI (lb-in.^{2})	NACA airfoil section	M_{cr}	l (in.)	c (in.)	b (ft)	x_{cg} (percent chord)	x_{ea} (percent chord)	x_{ea}' (percent chord)	$a + x_\alpha$	a	r_α^2	$\frac{1}{\kappa}$	ρ $\left(\frac{\text{slugs}}{\text{cu ft}}\right)$	Percent Freon	f_e (cps)
11A	0	2	45	272	108	107	15,000	25,100	16-005	0.89	16.0	8.0	0.333	48.4	45	45	-0.032	-0.10	0.232	13.3	0.00287	95	66
11A'	0	2	26	-----	59	57	----------	----------	16-005	.89	16.0	8.0	.333	48.4	26.6	26.6	-.032	-.468	.396	17.6	.00217	0	42
11B'	0	2	29	-----	61	43	----------	----------	16-005	.89	16.0	8.0	.333	48.4	29.7	29.7	-.032	-.406	.371	40.5	.000943	88	38
12	15	2	43	-----	103	103	14,400	54,700	16-005.2	.88	16.6	7.72	.321	48.5	46.3	46	-.03	-.074	.23	9.69	.00725	96	64
12	15	2	42	-----	105	105	14,400	54,700	16-005.2	.88	16.6	7.72	.321	48.5	46.3	46	-.03	-.074	.23	8.47	.00486	98	62
12	15	2	42	-----	103	102	14,400	54,700	16-005.2	.88	16.6	7.72	.321	48.5	46.3	46	-.03	-.074	.23	11.2	.00367	97	55
13	30	2	33	196	94	93	11,100	53,500	16-005.8	.87	18.2	6.87	.284	48.8	46.0	49	-.024	-.080	.23	7.15	.00746	99	61
14	45	2	22	139	93	92	9,240	33,000	16-007.1	.85	22.6	5.62	.234	48.8	46.0	60	-.024	-.080	.23	7.78	.00720	85	54
14	45	2	21	136	92	91	9,240	33,000	16-007.1	.85	22.6	5.62	.234	48.8	46.0	60	-.024	-.080	.23	19.8	.00285	94	37
15	60	2	12	69	93	93	4,580	19,100	16-010	.81	32.0	4.0	.167	48.8	46.0	65	-.024	-.080	.23	9.10	.00757	92	37
15	60	2	12	67	93	93	4,580	19,100	16-010	.91	32.0	4.0	.167	48.8	46.0	65	-.024	-.080	.23	14.0	.00493	90	36

Model	f_B (cps)	f_A (cps)	$\frac{f_B}{f_\alpha}$	$\frac{f_e}{f_B}$	$\frac{f_e}{f_A}$	φ (deg)	$\left(\frac{q}{\text{sq ft}}\right)$	M	V_e (mph)	V_R (mph)	V_R' (mph)	V_A (mph)	$\frac{V_e}{bc_\alpha}$	$\frac{V_e}{V_B}$	$\frac{V_e}{V_A}$	V_D (mph)	Remarks
11A	70	-----	0.62	0.99	----	90	235	0.82	274	260	260	-----	1.80	1.05	----	314	Tunnel excitation frequency = 67 cps.
11A'	40	-----	1.12	1.03	----	90	85.0	.24	191	129	129	-----	3.53	1.48	----	583	Model failed. Slotted $4\frac{3}{4}$ inches from trailing edge.
11B'	42	-----	.97	.91	----	170	70.5	.74	262	197	197	-----	4.22	1.33	----	183	Model failed. Slots uncovered.
12	70	-----	.63	.92	----	70	375	.64	218	176	-----	-----	1.54	1.24	----	175	
12	71	71	.59	.87	0.87	50	320	.71	245	206	-----	205	1.70	1.19	1.20	217	Tunnel excitation frequency = 61 cps.
12	69	69	.54	.80	.80	50	307	.79	276	225	-----	220	1.95	1.23	1.25	245	
13	60	65	.66	1.01	.94	70	334	.68	202	154	-----	159	1.77	1.31	1.27	149	
14	56	61	.59	.97	.88	60	300	.56	196	134	-----	166	2.11	1.46	1.18	119	
14	51	53	.41	.78	.70	40	234	.51	275	191	-----	245	2.99	1.44	1.12	187	
15	53	58	.40	.70	.64	40	265	.51	179	103	107	184	2.71	1.73	.97	105	
15	51	55	.39	.71	.65	30	264	.62	222	124	127	222	3.35	1.79	1.00	122	

TABLE I.- DATA FOR SHEARED SWEPT MODELS - SERIES I - Concluded

Balsa wings																						
Model	Λ (deg)	A_s	f_{h_1} (cps)	f_{h_2} (cps)	f_t (cps)	f_α (cps)	GJ (lb-in.^{2})	EI (lb-in.^{2})	NACA airfoil section	M_{cr}	l (in.)	c (in.)	b (ft)	x_{cg} (percent chord)	x_{ea} (percent chord)	x_{ea}' (percent chord)	$a + x_\alpha$	a	r_α^2	$\frac{l}{c}$	ρ $\left(\frac{\text{slugs}}{\text{cu ft}}\right)$	Percent Freon	f_e (cps)
22'	15	2	31	155	63	61	---------	---------	16-005.2	0.88	16.6	7.72	0.321	48.8	42.4	42.4	-0.024	-0.152	0.292	2.19	0.00854	98	50
22'	15	2	31	154	64	62	---------	---------	16-005.2	.93	16.6	7.72	.321	48.8	42.4	42.4	-.024	-.152	.292	3.82	.00488	93	51
22'	15	2	31	154	64	62	---------	---------	16-005.2	.99	16.6	7.72	.321	48.8	42.4	42.4	-.024	-.152	.292	18.7	.00100	92	45
23	30	2	35	219	89	99	6230	27,900	16-005.8	.97	18.2	6.37	.884	48.0	48.0	52	-.04	-.04	.304	3.18	.00864	99	60
23	30	2	34	216	89	89	6230	27,900	16-005.8	.87	18.2	6.87	.234	48.0	48.0	52	-.04	-.04	.304	6.34	.00321	91	62
23	30	2	34	220	91	91	6230	27,900	16-005.8	.87	18.2	6.87	.284	48.0	48.0	52	-.04	-.04	.304	9.15	.00300	89	60
23	30	2	34	216	89	89	6230	27,900	16-005.8	.87	18.2	6.87	.284	48.0	48.0	52	-.04	-.04	.304	14.9	.00184	90	53
24	45	2	19	123	73	73	2810	10,800	16-007.1	.85	21.8	5.66	.236	47.0	49.0	57	-.06	-.02	.311	3.64	.00784	85	51
24	45	2	19	122	73	73	2810	10,900	16-007.1	.85	21.8	5.66	.236	47.0	49.0	57	-.06	-.02	.311	8.40	.00339	93	49
24	45	2	19	122	73	73	2810	10,800	16-007.1	.85	21.8	5.66	.236	47.0	49.0	57	-.06	-.02	.311	13.2	.00216	91	45
24	45	2	19	120	74	74	2810	10,800	16-007.1	.85	21.8	5.66	.236	47.0	49.0	57	-.06	-.02	.311	29.4	.000970	74	-----
24	45	2	19	120	73	73	2810	10,800	16-007.1	.85	21.8	5.66	.236	47.0	49.0	57	-.06	-.02	.311	30.6	.000933	89	34
25A	60	2	8.6	54	66	65	1950	6,470	16-010	.81	32.0	4.0	.167	46.9	40.0	71	-.062	-.20	.359	34.6	.000954	88	29
25B	60	2	8.6	48	70	68	---------	5,500	16-010	.81	32.0	4.0	.167	46.9	40.0	71	-.062	-.20	.359	9.36	.00353	91	-----

Model	f_R (cps)	f_A (cps)	$\frac{f_\alpha}{f_\alpha}$	$\frac{f_e}{f_R}$	$\frac{f_e}{f_A}$	φ (deg)	$\left(\frac{q}{\text{sq ft}}\right)$	M	V_e (mph)	V_R (mph)	V_R' (mph)	V_A (mph)	$\frac{V_e}{bw_\alpha}$	$\frac{V_\alpha}{V_R}$	$\frac{V_\alpha}{V_A}$	V_D (mph)	Remarks
22'	46	-----	0.82	1.07	----	70	101	0.30	104	97.3	-----	-----	1.25	1.07	----	79.9	Tunnel excitation frequency = 49 cps.
22'	48	48	.83	1.07	1.06	50	74.7	.34	119	95.0	-----	96	1.41	1.25	1.24	107	Slotted $2\frac{3}{16}$ inches from trailing edge.
22'	46	46	.72	.96	.98	50	54.2	.64	224	167	-----	168	2.64	1.34	1.33	238	
23	62	-----	.68	.96	----	130	159	.42	142	137	-----	-----	1.31	1.04	----	110	
23	62	65	.70	1.01	.95	70	152	.62	212	176	-----	175	1.95	1.21	1.21	180	Tunnel excitation frequency = 61 cps.
23	63	-----	.67	.96	----	60	171	.66	229	195	-----	-----	2.07	1.24	----	190	Tunnel excitation frequency = 61 cps.
23	60	65	.59	.87	.82	90	152	.81	275	221	-----	224	2.53	1.24	1.23	237	
24	49	-----	.71	1.06	----	90	125	.34	121	97.1	-----	-----	1.63	1.25	----	80.1	
24	49	58	.65	1.00	.84	40	120	.54	180	132	-----	145	2.35	1.37	1.24	127	
24	48	-----	.60	.95	----	40	108	.64	215	160	-----	-----	2.82	1.35	----	159	
24	44	-----	----	----	----	-----	83.5	.76	251	226	-----	-----	3.76	1.25	----	232	
24	43	45	.47	.79	.75	60	73.0	.81	277	226	-----	252	3.77	1.22	1.10	232	
25A	37	40	.44	.73	.72	10	76.8	.79	272	161	169	278	5.90	1.69	0.98	210	Model failed.
25B	45	48	----	----	----	-----	73.6	.41	139	93.5	97.5	161	2.85	1.49	0.86	115	Model failed.

TABLE II.- ROTATED WINGS - SERIES II

Model	Λ (deg)	A_g	f_{h_1} (cps)	f_{h_2} (cps)	f_t (cps)	f_α (cps)	GJ (lb-in.²)	EI (lb-in.²)	NACA airfoil section	M_{cr}	l (in.)	c (in.)	b (ft)	x_{cg} (percent chord)	x_{ea} (percent chord)	x_{ea}' (percent chord)	$a + x_\alpha$	a	r_α^2	$\frac{l}{x}$	ρ $\left(\frac{\text{slugs}}{\text{cu ft}}\right)$	Percent Freon	f_e (cps)
Lengthwise laminations																							
30A	0	6.20	11.9	76.0	90.4	83.0	3760	---------	16-010	0.81	24.8	4	0.167	46.0	35	35	−0.08	−0.30	0.311	36.8	0.00220	0	42
30B	0	6.20	12.0	72.6	90.0	88.0	3760	6920	16-010	.81	24.8	4	.167	46.0	40	40	−.08	−.20	.277	37.8	.00214	0	48
30B	30	4.65	12.1	73.0	91.0	88.8	3760	6920	16-010	.81	24.8	4	.167	46.0	40	40	−.08	−.20	.277	37.7	.00215	0	51
30B	30	4.65	12.0	73.0	90.0	88.0	3760	6920	16-010	.81	24.8	4	.167	46.0	40	40	−.08	−.20	.277	37.8	.00214	0	50
30B	45	3.10	12.1	73.0	91.0	88.8	3760	6920	16-010	.81	24.8	4	.167	46.0	40	40	−.08	−.20	.277	37.8	.00214	0	-----
30B	45	3.10	12.2	73.0	90.0	88.0	3760	6920	16-010	.81	24.8	4	.167	46.0	40	40	−.08	−.20	.277	37.8	.00214	0	55
30B	60	1.55	12.0	72.5	90.0	88.0	3760	6920	16-010	.81	24.8	4	.167	46.0	40	40	−.08	−.20	.277	39.8	.00204	0	-----
30C	0	6.20	12.2	69.0	86.0	75.8	4000	6950	16-010	.81	24.8	4	.167	48.5	39	39	−.03	−.22	.292	40.5	.00200	89	34
30C	0	6.20	12.2	69.0	86.0	75.8	4000	6950	16-010	.81	24.8	4	.167	48.5	39	39	−.03	−.22	.292	98.9	.000820	86	24
30C	0	6.20	13.3	70.0	84.0	74.2	4000	6950	16-010	.81	24.8	4	.167	48.5	39	39	−.03	−.22	.292	92.6	.000876	83	21
30C	15	5.78	12.2	69.0	86.0	75.8	4000	6950	16-010	.81	24.8	4	.167	48.5	39	39	−.03	−.22	.292	92.6	.000870	81	27
30C	30	4.65	12.2	69.0	86.0	75.8	4000	6950	16-010	.81	24.8	4	.167	48.5	39	39	−.03	−.22	.292	40.0	.00202	89	37
30C	30	4.65	12.2	70.0	86.5	76.2	4000	6950	16-010	.81	24.8	4	.167	48.5	39	39	−.03	−.22	.292	81.4	.000995	86	-----
30C	30	4.65	12.2	70.0	86.5	76.2	4000	6950	16-010	.81	24.8	4	.167	48.5	39	39	−.03	−.22	.292	80.0	.00100	85	31
30C	45	3.10	12.2	70.0	86.5	76.2	4000	6950	16-010	.81	24.8	4	.167	48.5	39	39	−.03	−.22	.292	45.2	.00179	87	40
30D	15	5.78	13.2	80.2	87.1	82.4	4350	---------	16-010	.81	24.8	4	.167	48	39.5	39.5	−.04	−.21	.280	8.70	.00933	99	50
30D	15	5.78	13.2	80.2	87.1	82.4	4350	---------	16-010	.81	24.8	4	.167	48	39.5	39.5	−.04	−.21	.280	8.72	.00930	99	51
30D	15	5.78	13.2	80.2	87.1	82.4	4350	---------	16-010	.81	24.8	4	.167	48	39.5	39.5	−.04	−.21	.280	8.76	.00927	99	51
30D	30	4.65	13.5	81.7	92.5	87.4	4350	---------	16-010	.81	24.8	4	.167	48	39.5	39.5	−.04	−.21	.280	8.90	.00910	99	53
30D	45	3.10	13.3	81.7	88.2	83.4	4350	---------	16-010	.81	24.8	4	.167	48	39.5	39.5	−.04	−.21	.280	8.85	.00905	99	56
30D	60	1.55	13.5	82.0	90.5	85.5	4350	---------	16-010	.81	24.8	4	.167	48	39.5	39.5	−.04	−.21	.280	9.54	.00852	99	65

Model	f_R (cps)	f_Λ (cps)	$\frac{f_e}{f_\alpha}$	$\frac{f_e}{f_R}$	$\frac{f_e}{f_\Lambda}$	φ (deg)	$\left(\frac{q}{\text{lb/sq ft}}\right)$	M	V_o (mph)	V_R (mph)	V_R' (mph)	V_Λ (mph)	$\frac{V_o}{bx_\alpha}$	$\frac{V_o}{V_R}$	$\frac{V_o}{V_\Lambda}$	V_D (mph)	Remarks
30A	45	-----	0.51	0.91	----	70	127	0.30	232	209	209	-----	3.91	1.11	----	318	Wing failed. Tunnel excitation frequency = 40.7 cps.
30B	44	46	.54	1.08	1.04	60	121	.29	229	212	212	215	3.64	1.08	1.06	263	
30B	47	47	.57	1.08	1.08	60	126	.30	235	214	214	229	3.74	1.10	1.03	266	
30B	44	47	.57	1.14	1.08	40	129	.30	237	212	212	229	3.77	1.12	1.04	263	
30B	44	47	----	----	----	-----	166	.34	269	214	214	265	4.28	1.26	1.01	266	
30B	44	47	.62	1.25	1.16	50	169	.35	272	212	212	265	4.32	1.28	1.02	263	
30B	46	48	----	----	----	-----	275	.45	350	219	219	353	5.59	1.60	.99	265	Wing failed.
30C	41	-----	.45	.83	----	30	104	.63	219	189	189	-----	4.05	1.16	----	249	
30C	37	-----	.32	.66	----	30	74.4	.81	286	290	290	-----	5.29	.986	----	393	
30C	36	-----	.29	.59	----	30	79.6	.82	288	270	270	-----	5.43	1.07	----	369	Wing failed.
30C	36	-----	.36	.74	----	30	72.5	.78	278	282	282	-----	5.13	.986	----	376	
30C	41	-----	.48	.89	----	50	113	.65	226	187	187	-----	4.18	1.21	----	248	
30C	41	-----	----	----	----	-----	88.1	.81	284	263	263	-----	5.22	1.08	----	355	
30C	38	-----	.40	.80	----	30	88.6	.81	289	260	260	-----	5.32	1.11	----	352	
30C	41	-----	.53	.98	----	40	147	.76	273	199	199	-----	5.02	1.37	----	265	
30D	51	51	.61	.98	.98	50	110	.31	104	100	100	100	1.77	1.05	1.04	119	
30D	52	52	.61	.98	.98	50	115	.32	107	100	100	101	1.82	1.08	1.06	119	
30D	52	52	.61	.98	.98	50	121	.33	109	100	100	101	1.85	1.10	1.08	119	
30D	54	56	.61	.98	.95	40	150	.38	123	106	106	116	1.97	1.16	1.06	129	
30D	52	55	.67	1.08	1.02	60	178	.41	135	101	101	130	2.86	1.34	1.04	122	
30D	53	57	.77	1.24	1.14	90	307	.55	182	107	107	182	2.98	1.70	1.00	130	

TABLE II.- ROTATED WINGS - SERIES II - Concluded

Chordwise laminations																							
Model	Λ (deg)	A_g	f_{h_1} (cps)	f_{h_2} (cps)	f_t (cps)	f_α (cps)	GJ (lb-in.^{2})	EI (lb-in.^{2})	NACA airfoil section	M_{cr}	l (in.)	c (in.)	b (ft)	x_{cg} - (percent chord)	x_{ea} (percent chord)	x_{ea}' (percent chord)	$a + x_\alpha$	a	r_α^2	$\frac{l}{r}$	ρ $\left(\frac{\text{slugs}}{\text{cu ft}}\right)$	Percent Freon	f_e (cps)
40A	0	6.20	9.4	57.4	90.0	88.4	3540	5250	16-010	0.81	24.8	4	0.167	46	40	40	-0.08	-0.20	0.277	36.5	0.00222	0	62
40A	0	6.20	9.6	57.1	91.0	88.5	3540	5250	16-010	.81	24.8	4	.167	46	40	40	-.08	-.20	.277	24.2	.00334	90	56
40A	0	6.20	9.6	57.1	91.0	88.5	3540	5250	16-010	.81	24.8	4	.167	46	40	40	-.08	-.20	.277	37.7	.00215	89	61
40A	0	6.20	9.6	57.1	91.0	88.5	3540	5250	16-010	.81	24.8	4	.167	46	40	40	-.08	-.20	.277	75.0	.00108	82	61
40A	15	5.78	9.3	55.8	90.6	88.2	3540	5250	16-010	.81	24.8	4	.167	46	40	40	-.08	-.20	.277	35.1	.00231	0	61
40A	30	4.65	9.3	55.8	90.6	88.2	3540	5250	16-010	.81	24.8	4	.167	46	40	40	-.08	-.20	.277	37.5	.00216	0	----
40B	0	6.20	9.5	55.0	90.5	85.5	3710	5020	16-010	.81	24.8	4	.167	49	40	40	-.02	-.20	.297	35.5	.00228	0	61
40C	0	6.20	9.0	54.4	61.0	58.2	2280	4350	16-010	.81	24.8	4	.167	46	38.5	38.5	-.08	-.23	.297	8.74	.00928	100	29
40D	0	6.20	9.4	58.0	88.9	84.0	3330	5050	16-010	.81	24.8	4	.167	48	39.5	39.5	-.04	-.21	.280	79.0	.000969	84	62
40D	15	5.78	9.6	58.3	88.9	84.0	3330	5050	16-010	.81	24.8	4	.167	48	39.5	39.5	-.04	-.21	.280	36.2	.00212	89	62
40D	15	5.78	9.5	57.9	87.5	82.6	3330	5050	16-010	.81	24.8	4	.167	48	39.5	39.5	-.04	-.21	.280	80.0	.000956	87	61
40D	30	4.65	9.5	57.5	89.0	84.1	3330	5050	16-010	.81	24.8	4	.167	48	39.5	39.5	-.04	-.21	.280	88.2	.000867	85	65
40D	45	3.10	9.6	58.3	88.9	84.0	3330	5050	16-010	.81	24.8	4	.167	48	39.5	39.5	-.04	-.21	.280	39.1	.00196	86	32

Model	f_R (cps)	f_A (cps)	$\frac{f_e}{f_\alpha}$	$\frac{f_e}{f_R}$	$\frac{f_e}{f_A}$	φ (deg)	$\left(\frac{q}{\text{sq ft}}\right)$	M	V_e (mph)	V_R (mph)	V_R' (mph)	V_A (mph)	$\frac{V_e}{bf_\alpha}$	$\frac{V_e}{V_R}$	$\frac{V_e}{V_A}$	V_D (mph)	Remarks
40A	47	-----	0.70	1.33	--	140	82.0	0.24	188	211	211	-----	2.98	0.892	--	260	
40A	49	-----	.63	1.15	--	60	86.7	.45	155	184	184	-----	2.45	.843	--	212	Tunnel excitation frequency = 57 cps.
40A	46	-----	.69	1.33	--	70	69.2	.50	172	215	215	-----	2.72	.800	--	265	
40A	43	-----	.69	1.44	--	70	63.6	.65	234	299	299	-----	3.70	.784	--	373	
40A	46	-----	.68	1.30	--	90	93.9	.26	201	208	208	-----	3.19	.967	--	254	
40A	46	-----	----	----	--	-----	127	.30	235	213	213	-----	3.73	1.10	--	263	Wing failed.
40B	45	-----	.71	1.37	--	10	77.7	.23	178	191	191	-----	2.91	.932	--	247	Wing failed.
40C	36	-----	.51	.83	--	80	57.6	.23	75.3	74.5	74.5	-----	1.81	1.01	--	90.4	Wing failed.
40D	40	-----	.73	1.54	--	30	52.3	.62	221	261	261	-----	3.69	.787	--	370	Tunnel excitation frequency = 61 cps.
40D	44	-----	.74	1.41	--	70	72.7	.51	177	194	194	-----	2.95	.913	--	251	
40D	40	-----	.74	1.54	--	30	57.9	.67	236	279	279	-----	3.99	.846	--	367	
40D	40	-----	.77	1.63	--	60	79.4	.82	290	298	298	-----	4.83	.973	--	392	
40D	44	-----	.38	.73	--	80	158	.73	254	200	200	-----	4.24	1.27	--	261	Wing failed.

TABLE III.- DATA FOR MODELS USED IN SWEEPFORWARD TESTS - SERIES III

Model	Λ (deg)	A_R	f_{h_1} (cps)	f_{h_2} (cps)	f_t (cps)	f_α (cps)	GJ (lb-in.^{2})	EI (lb-in.^{2})	NACA airfoil section	M_{cr}	l (in.)	c (in.)	b (ft)	x_{cg} (percent chord)	x_{ea} (percent chord)	x_{ea}' (percent chord)	$a + x_\alpha$	a	r_α^2	$\frac{l}{c}$	ρ $\left(\frac{\text{slugs}}{\text{cu ft}}\right)$	Percent Freon	f_e (cps)
50A	-30	4.65	15	87	168	137	10,100	14,100	16-010	0.81	24.8	4	0.167	50	33	33	0.0	-0.34	0.352	7.98	0.00895	96	-----
50A	-15	5.78	15	87	168	137	10,100	14,100	16-010	.81	24.8	4	.167	50	33	33	.0	-.34	.352	8.00	.00892	96	-----
50A	0	6.20	15	87	163	133	10,100	14,100	16-010	.81	24.8	4	.167	50	33	33	.0	-.34	.352	33.1	.00216	0	102
50B	0	6.20	14	82	166	116	11,400	11,900	16-010	.81	24.8	4	.167	50	26	26	.0	-.48	.456	8.66	.00823	99	91
50B	15	5.78	14	80	166	116	11,400	11,900	16-010	.81	24.8	4	.167	50	26	26	.0	-.48	.456	8.58	.00831	99	84
50B	30	4.65	14	80	166	116	11,400	11,900	16-010	.81	24.8	4	.167	50	26	26	.0	-.48	.456	9.04	.00787	99	74
50B	45	3.10	14	80	166	116	11,400	11,900	16-010	.81	24.8	4	.167	50	26	26	.0	-.48	.456	9.45	.00756	99	98

Model	f_R (cps)	f_Λ (cps)	$\frac{f_e}{f_\alpha}$	$\frac{f_e}{f_R}$	$\frac{f_e}{f_\Lambda}$	φ (deg)	$\left(\frac{q}{\frac{\text{lb}}{\text{sq ft}}}\right)$	M	V_e (mph)	V_R (mph)	V_R' (mph)	V_Λ (mph)	$\frac{V_e}{b\omega_\alpha}$	$\frac{V_e}{V_R}$	$\frac{V_e}{V_\Lambda}$	V_D (mph)	Remarks
50A	98	-----	----	----	--	-----	73.4	0.26	86.9	174	174	-----	0.888	0.498	--	294	Model diverged.
50A	98	-----	----	----	--	-----	107	.31	105	174	174	-----	1.075	.603	--	294	Model diverged.
50A	79	-----	0.77	1.29	--	40	211	.40	303	319	319	-----	3.18	.949	--	579	
50B	94	-----	.78	.97	--	100	260	.52	170	172	172	-----	2.05	.989	--	704	
50B	94	-----	.72	.90	--	70	257	.51	169	172	172	-----	2.04	.982	--	700	Model failed.
50B	93	-----	.63	.80	--	180	352	.61	202	179	179	-----	2.44	1.125	--	720	
50B	93	-----	.84	1.05	--	100	423	.68	226	179	179	-----	2.73	1.265	--	736	

TABLE IV.- SWEPT MODELS OF A CONSTANT LENGTH-TO-CHORD RATIO OF 8.5 - SERIES IV

Model	Λ (deg)	A_s	f_{h_1} (cps)	f_{h_2} (cps)	f_t (cps)	f_α (cps)	GJ (lb-in.^{2})	EI (lb-in.^{2})	NACA airfoil section	M_{cr}	l (in.)	a (in.)	b (ft)	x_{ag} (percent chord)	x_{ea} (percent chord)	x_{ea}' (percent chord)	$a + x_\alpha$	a	r_α^2	$\frac{l}{\kappa}$	ρ $\left(\frac{\text{slugs}}{\text{cu ft}}\right)$	Percent Freon	f_e (cps)
62	15	7.95	4.9	29.1	72.5	71.8	3730	7,820	16-010	0.81	3¼	4	0.167	41	44	46	-0.18	-0.12	0.175	13.5	0.00925	99	22
62	15	7.95	4.9	29.1	73.4	72.5	3730	7,820	16-010	.81	3¼	4	.167	41	44	46	-.18	-.12	.175	37.6	.00333	88	20
62	15	7.95	4.9	29.1	73.4	72.5	3730	7,820	16-010	.81	3¼	4	.167	41	44	46	-.18	-.12	.175	59.5	.00210	87	19
62	15	7.95	4.9	29.6	73.5	72.7	3730	7,820	16-010	.81	3¼	4	.167	41	44	46	-.18	-.12	.175	130.0	.000964	85	16
63	30	6.38	4.6	25.8	73.5	73.0	5450	5,870	16-010	.81	3¼	4	.167	41	44	47	-.18	-.12	.175	15.2	.00745	73	19
63	30	6.38	3.9	24.0	73.0	72.4	5450	5,870	16-010	.81	3¼	4	.167	41	44	47	-.18	-.12	.175	26.8	.00424	98	18
63	30	6.38	4.6	25.8	73.5	73.0	5450	5,870	16-010	.81	3¼	4	.167	41	44	47	-.18	-.12	.175	46.0	.00246	50	22
63	30	6.38	4.0	24.0	73.0	72.4	5450	5,870	16-010	.81	3¼	4	.167	41	44	47	-.18	-.12	.175	53.0	.00214	94	19
63	30	6.38	4.0	24.0	73.0	72.4	5450	5,870	16-010	.81	3¼	4	.167	41	44	47	-.18	-.12	.175	98.2	.00116	92	15
64	45	4.75	4.4	29.0	66.0	65.5	3500	6,080	16-010	.81	3¼	4	.167	41	44	57	-.18	-.12	.175	50.9	.00217	0	19
64	45	4.75	4.2	27.0	66.0	65.5	3500	6,080	16-010	.81	3¼	4	.167	41	44	57	-.18	-.12	.175	12.1	.00914	97	-----
64	45	4.75	4.2	27.0	66.0	65.5	3500	6,080	16-010	.81	3¼	4	.167	41	44	57	-.18	-.12	.175	41.9	.00263	54	18
64	45	4.75	4.1	27.0	65.0	64.4	3500	6,080	16-010	.81	3¼	4	.167	41	44	57	-.18	-.12	.175	51.3	.00215	92	17
64	45	4.75	4.1	27.0	65.0	64.4	3500	6,080	16-010	.81	3¼	4	.167	41	44	57	-.18	-.12	.175	116.0	.000953	86	16
65	60	2.12	5.7	33.4	77.0	76.2	4650	11,980	16-010	.81	3¼	4	.167	41	44	71	-.18	-.12	.175	44.1	.00297	94	17

Model	f_R (cps)	$\frac{f_e}{f_\alpha}$	$\frac{f_e}{f_R}$	φ (deg)	q $\left(\frac{\text{lb}}{\text{sq ft}}\right)$	M	V_e (mph)	V_R (mph)	V_R' (mph)	$\frac{V_e}{bw_\alpha}$	$\frac{V_e}{V_R}$	V_D (mph)	Remarks
62	35	0.28	0.59	30	91.8	0.29	95.4	105	104	1.85	0.905	91.6	
62	32	.28	.64	20	73.7	.41	143	167	171	2.76	.856	153	
62	31	.26	.60	20	69.7	.49	175	206	-----	3.37	.850	192	
62	29	.22	.55	20	57.5	.66	234	300	-----	4.50	.780	264	
63	35	.27	.56	180	98.8	.29	111	111	-----	2.12	1.000	97.6	
63	33	.25	.56	110	78.0	.38	129	142	-----	2.49	.908	128	
63	32	.30	.69	180	82.1	.40	176	183	-----	3.37	.962	170	
63	31	.26	.61	140	74.0	.52	179	195	-----	3.46	.918	180	
63	29	.20	.50	120	62.2	.64	222	262	-----	4.30	.848	246	
64	28	.29	.67	30	69.6	.22	173	174	176	3.69	.995	166	
64	32	----	----	-----	70.6	.24	83.9	91	90	1.80	.923	81.3	No record.
64	29	.27	.61	0	68.3	.36	155	160	160	3.31	.968	132	
64	27	.26	.62	30	63.5	.47	165	172	171	3.59	.960	173	Record shown in figure 3.
64	25	.23	.65	0	57.5	.66	235	248	-----	5.10	.948	260	
65	33	.22	.51	0	172	.67	234	186	-----.	4.29	1.258	176	

TABLE V.- DATA FOR SWEPT MODELS OF A CONSTANT LENGTH-CHORD RATIO OF 6.5 - SERIES V

Model	Λ (deg)	A_g	f_{h_1} (cps)	f_{h_2} (cps)	f_t (cps)	f_α (cps)	GJ (lb-in.^{2})	EI (lb-in.^{2})	NACA airfoil section	M_{cr}	l (in.)	c (in.)	b (ft)	x_{cg} (percent chord)	x_{ea} (percent chord)	x_{ea}' (percent chord)	$a + x_\alpha$	a	r_α^2	$\frac{1}{\mu}$	ρ $\left(\frac{\text{slugs}}{\text{cu ft}}\right)$	Percent Freon	f_e (cps)
72	15	6.09	7.6	54	97.3	96.3	3730	7,820	16-010	0.81	26	4	0.167	41	44	46	-0.18	-0.12	0.175	37.2	0.00336	94	30
72	15	6.09	7.6	54	97.3	96.3	3730	7,820	16-010	.81	26	4	.167	41	44	46	-.18	-.12	.175	81.5	.00153	89	22
73	30	4.88	6.4	40.0	98.0	97.0	5450	5,870	16-010	.81	26	4	.167	41	44	47	-.18	-.12	.175	34.7	.00327	96	29
73	30	4.88	6.4	40.0	98.0	97.0	5450	5,870	16-010	.81	26	4	.167	41	44	47	-.18	-.12	.175	57.4	.00198	95	24
73	30	4.88	6.4	40.0	98.0	97.0	5450	5,870	16-010	.81	26	4	.167	41	44	47	-.18	-.12	.175	108	.00105	93	22
74	45	3.25	6.5	40.0	79.0	78.2	3500	6,080	16-010	.81	26	4	.167	41	44	57	-.18	-.12	.175	14.2	.00779	98	29
74	45	3.25	6.7	39.5	78.5	77.7	3500	6,080	16-010	.81	26	4	.167	41	44	57	-.18	-.12	.175	56.0	.00197	93	26
74	45	3.25	6.7	39.5	78.5	77.7	3500	6,080	16-010	.81	26	4	.167	41	44	57	-.18	-.12	.175	120	.000923	90	21
75	60	1.65	7.2	51.8	82.4	81.6	4650	11,980	16-010	.81	26	4	.167	41	44	71	-.18	-.12	.175	15.8	.00829	95	39
75	60	1.65	7.2	51.8	84.6	83.8	4650	11,980	16-010	.81	26	4	.167	41	44	71	-.18	-.12	.175	16.7	.00783	100	39

Model	f_B (cps)	$\frac{f_e}{f_\alpha}$	$\frac{f_e}{f_B}$	φ (deg)	$\left(\frac{q}{\text{sq ft}}\right)$	M	V_e (mph)	V_B (mph)	V_B' (mph)	$\frac{V_e}{b\omega_\alpha}$	$\frac{V_e}{V_B}$	V_D (mph)	Remarks
72	43	0.31	0.71	10	143	0.59	197	220	221	2.88	0.895	201	
72	40	.23	.55	0	109	.74	255	318	319	3.73	.804	297	
73	43	.30	.67	-----	133	.57	193	216	214	2.78	.893	196	
73	41	.24	.57	80	118	.69	234	273	-----	3.38	.853	252	
73	39	.22	.55	-----	90.8	.82	280	363	-----	4.05	.770	345	
74	37	.37	.77	0	118	.35	118	115	-----	2.11	1.025	111	Wing failed.
74	33	.33	.77	0	104	.64	219	214	-----	3.95	1.023	218	
74	31	.28	.69	0	85.5	.83	291	308	-----	5.24	.945	320	
75	39	.47	.99	30	294	.54	181	127	128	3.11	1.425	113	Model damaged at root
75	38	.46	.97	0	295	.56	186	134	136	3.05	1.386	122	Rear half separated from base.

TABLE VI.- DATA FOR TIP-EFFECT MODELS - SERIES VI

Model	Λ (deg)	A_g	f_{h_1} (cps)	f_{h_2} (cps)	f_t (cps)	f_α (cps)	GJ (lb-in.^{2})	EI (lb-in.^{2})	NACA airfoil section	M_{cr}	l (in.)	c (in.)	b (ft)	x_{cg} (percent chord)	x_{ea} (percent chord)	x_{ea}' (percent chord)	$a + x_\alpha$	a	r_α^2	$\frac{l}{k}$	ρ $\left(\frac{\text{slugs}}{\text{cu ft}}\right)$	Percent Freon	f_θ (cps)
84-1	45	3.63	10	60	133	104	---	---	16-010	0.81	29	4	0.167	51	32	44	0.02	-0.36	0.378	9.15	0.00781	99	75
84-2	45	3.63	10	61	135	107	---	---	16-010	.81	29	4	.167	51	32	44	.02	-.36	.378	9.25	.00764	99	60
84-3	45	3.63	9.6	58	118	93	---	---	16-010	.81	29	4	.167	51.5	32	44	.03	-.36	.378	9.55	.00778	99	-----
85-1	60	2.75	5.0	32	92	72	10,800	13,400	16-010	.81	44	4	.167	50	32	58	0.0	-.36	.378	34.6	.00205	0	35
85-2	60	2.75	5.0	31	95	75	9,850	12,400	16-010	.81	44	4	.167	50	32	58	.0	-.36	.378	34.1	.00208	0	27
85-3	60	2.75	5.0	30	80	63	11,200	16,600	16-010	.81	44	4	.167	51	32	58	.02	-.36	.378	34.5	.00207	0	22

Model	f_R (cps)	$\frac{f_\theta}{f_\alpha}$	$\frac{f_\theta}{f_R}$	φ (deg)	$\left(\frac{q}{\text{sq ft}}\right)$ lb	M	V_θ (mph)	V_R (mph)	V_R' (mph)	$\frac{V_\theta}{bw_\alpha}$	$\frac{V_\theta}{V_R}$	V_D (mph)	Remarks
84-1	76	0.65	0.89	50	339	0.60	199	142	----	2.65	1.40	253	Tip perpendicular to air stream. Model failed.
84-2	78	.51	.70	0	382	.63	213	146	-----	2.80	1.47	259	Tip perpendicular to leading edge. Model failed.
84-3	68	----	----	-----	346	.60	201	127	-----	3.02	1.58	229	Tip parallel to air stream. Model failed.
85-1	43	.44	.72	-----	225	.41	322	185	189	6.24	1.74	341	Tip perpendicular to air stream. Model failed.
85-2	46	.33	.54	-----	173	.35	278	189	196	5.21	1.47	348	Tip perpendicular to leading edge. Model failed.
85-3	38	.32	.53	0	203	.39	304	159	159	6.77	1.91	295	Tip parallel to air stream. Model failed.

TABLE VII.- DATA FOR MODELS USED TO DETERMINE EFFECT OF CENTER-OF-GRAVITY SHIFT - SERIES VII

Model	A (deg)	A_g	f_{h_1} (cps)	f_{h_2} (cps)	f_t (cps)	f_α (cps)	GJ (lb-in.^{2})	EI (lb-in.^{2})	NACA airfoil section	l (in.)	c (in.)	b (ft)	x_{cg} (percent chord)	x_{ea} (percent chord)	x_{ea}' (percent chord)	$a + x_\alpha$	a	r_α^2	$\frac{I}{K}$	ρ $\left(\frac{\text{slugs}}{\text{cu ft}}\right)$	Percent Freon	f_e (cps)
91-1	0	6	4.2	24	31	23	34,100	128,000	16-010	48	8	0.333	39.9	48	48	-0.402	-0.04	0.307	17.3	0.00871	95	12.5
91-2	0	6	5.5	36	43	43	41,200	108,300	16-010	48	8	.333	41.0	43.8	43.8	-.18	-.124	.179	41.7	.00239	0	16
91-2	0	6	5.5	36	43	43	41,200	108,300	16-010	48	8	.333	41.0	43.8	43.8	-.18	-.124	.179	56.4	.00177	0	16
91-2	0	6	5.3	33	42	42	41,200	108,300	16-010	48	8	.333	41.0	43.8	43.8	-.18	-.124	.179	12.8	.00783	81	20
91-2	0	6	5.5	36	43	43	41,200	108,300	16-010	48	8	.333	41.0	43.8	43.8	-.18	-.124	.179	95.5	.00105	0	15
91-3	0	6	5.0	30	40	40	28,500	83,700	16-010	48	8	.333	49.0	48.4	48.4	-.02	-.032	.160	44.3	.00226	0	18
91-3	0	6	4.7	29	39	39	28,500	83,700	16-010	48	8	.333	49.0	48.4	48.4	-.02	-.032	.160	36.4	.00274	76	15
91-3	0	6	4.7	29	39	39	28,500	83,700	16-010	48	8	.333	49.0	48.4	48.4	-.02	-.032	.160	48.4	.00207	73	14
92-1	15	6.09	8.3	48	70	62	3,730	7,820	Modified 16-010	26	4	.167	31.2	44	46	-.376	-.12	.298	77.9	.00214	0	26
92-2	15	6.09	8.3	49	95	93	3,730	7,820	Modified 16-010	26	4	.167	42.9	44	46	-.142	-.12	.136	76.0	.00219	0	22
92-3	15	6.09	8.1	47	53	52	3,730	7,820	Modified 16-010	26	4	.167	54.5	44	46	.090	-.12	.411	74.5	.00224	0	26
93-1	30	4.42	6.3	40	78	68	5,450	5,870	Modified 16-010	23.6	4	.167	30	44	47	-.40	-.12	.310	76.0	.00199	0	26
93-2	30	4.42	6.8	44	99	99	5,450	5,870	Modified 16-010	23.6	4	.167	43	44	47	-.16	-.12	.134	74.0	.00210	0	23
93-3	30	4.42	6.3	51	54	50	5,450	5,870	Modified 16-010	23.6	4	.167	56	44	47	.12	-.12	.428	73.2	.00212	0	23
94-1	-(-45)	3.81	4.5	26	38	35	2,120	4,520	Modified 16-010	30.5	4	.167	44.5	56	----	-.11	.12	.427	68.2	.00223	0	18
94-2	-(-45)	3.81	4.8	28	70	70	2,120	4,520	Modified 16-010	30.5	4	.167	57.0	56	----	.14	.12	.134	68.2	.00223	0	18
94-3	-(-45)	3.81	4.6	28	40	38	2,120	4,520	Modified 16-010	30.5	4	.167	69.3	56	----	.386	.12	.307	68.2	.00223	0	17
95'-1	60	1.65	5.6	-----	54	50	1,900	4,560	Modified 16-010	26.4	4	.167	31.4	22	41	-.372	-.56	.267	75.8	.00201	0	24
95'-2	60	1.65	5.9	-----	71	47	1,900	4,560	Modified 16-010	26.4	4	.167	42.8	22	41	-.144	-.56	.308	73.0	.00209	0	23
95'-3	60	1.65	5.8	35	40	27	1,900	4,560	Modified 16-010	26.4	4	.167	54.3	22	41	.086	-.56	.779	69.0	.00218	0	23

Model	f_β (cps)	$\frac{f_\beta}{f_\alpha}$	$\frac{f_\beta}{f_t}$	φ (deg)	$\left(\frac{q}{\text{lb/sq ft}}\right)$	M	V_e (mph)	V_R (mph)	V_R' (mph)	$\frac{V_R}{bw_\alpha}$	$\frac{V_R}{V_R}$	V_D (mph)	Remarks
91-1	15	0.54	0.82	-----	153	0.37	127	231	231	3.83	0.548	79.9	Model failed.
91-2	19	.37	.81	40	109	.28	208	207	207	3.40	1.000	192	
91-2	19	.38	.86	20	105	.32	239	239	239	3.93	1.000	224	
91-2	21	.47	.94	40	128	.33	122	120	120	2.05	1.02	104	
91-2	18	.35	.83	30	106	.40	303	308	308	4.97	.985	291	
91-3	17	.45	1.09	100	61.5	.20	159	158	158	2.78	1.01	157	
91-3	17	.39	.91	10	58.4	.39	142	141	141	2.54	1.01	139	
91-3	16	.37	.89	0	57.2	.44	163	161	161	2.92	1.01	161	
92-1	36	.42	.72	0	195	.38	293	415	422	6.60	.706	245	
92-2	26	.23	.66	20	151	.33	255	258	257	3.76	.990	251	
92-3	28	.49	.93	20	87.5	.25	191	176	177	5.12	1.09	237	
93-1	26	.39	.65	-----	229	.41	324	503	-----	6.73	.645	267	
93-2	37	.23	.64	70	156	.34	264	265	-----	3.72	.997	257	
93-3	27	.45	.85	20	77.2	.23	185	170	-----	5.15	1.09	231	
94-1	20	.51	.88	20	61.0	.20	160	160	-----	6.38	1.00	122	Section reversed.
94-2	23	.26	.78	-----	62.2	.21	162	139	-----	3.24	1.17	136	Section reversed.
94-3	16	.44	1.04	40	39.5	.17	129	93.2	-----	4.78	1.39	110	Section reversed.
95'-1	27	.49	.89	30	258	.44	345	279	300	5.20	1.24	∞	Slotted $2\frac{1}{16}$ inches from trailing edge.
95'-2	26	.48	.86	20	212	.40	307	186	189	9.15	1.66	∞	Slotted $2\frac{1}{16}$ inches from trailing edge.
95'-3	20	.84	1.03	30	125	.30	234	121	123	12.1	1.94	∞	Slotted $2\frac{1}{16}$ inches from trailing edge.

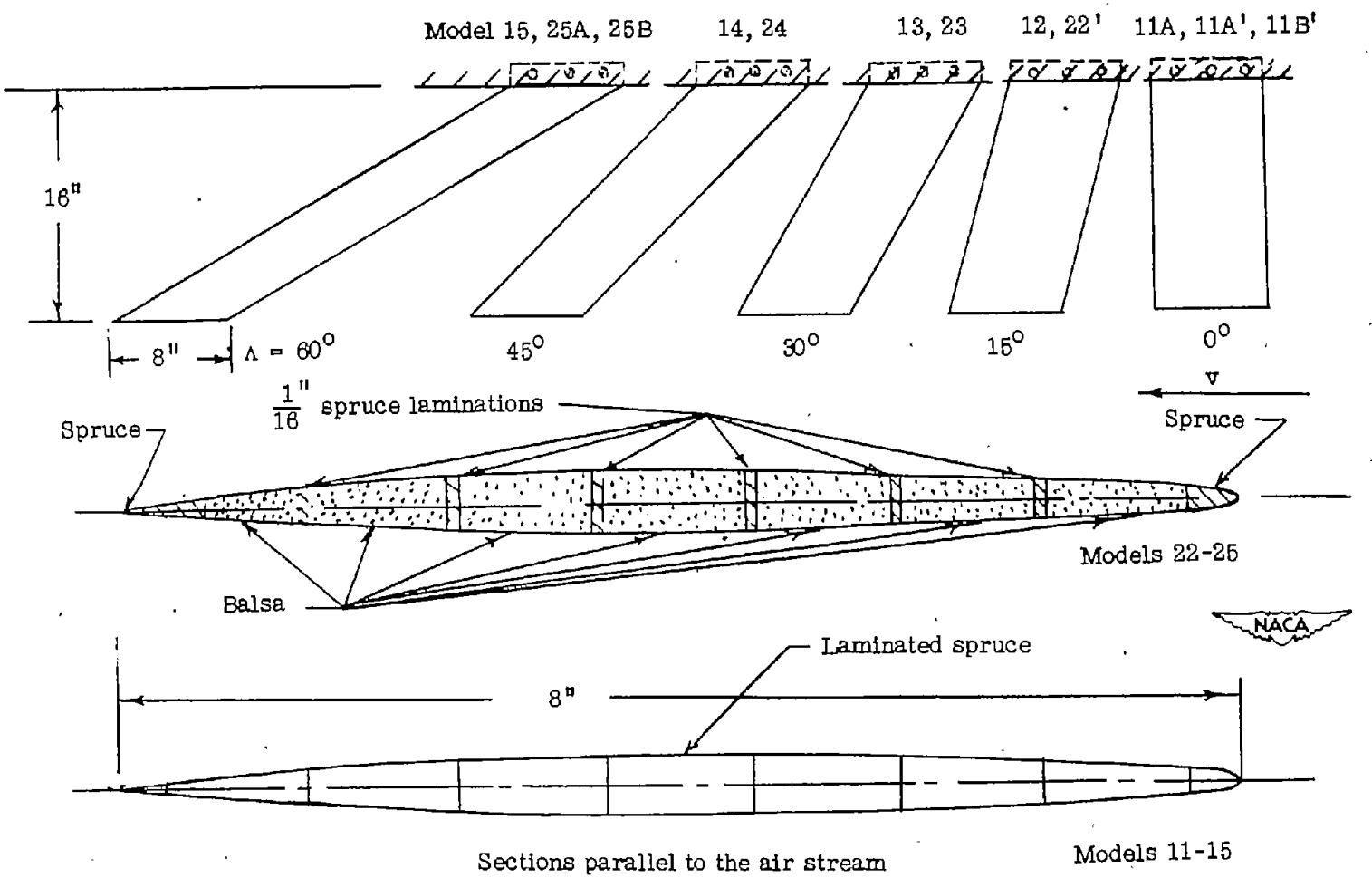

(a) Sheared swept models with a constant geometric aspect ratio of 2. Series I.

Figure 1.- Model plan form and cross-sectional construction.

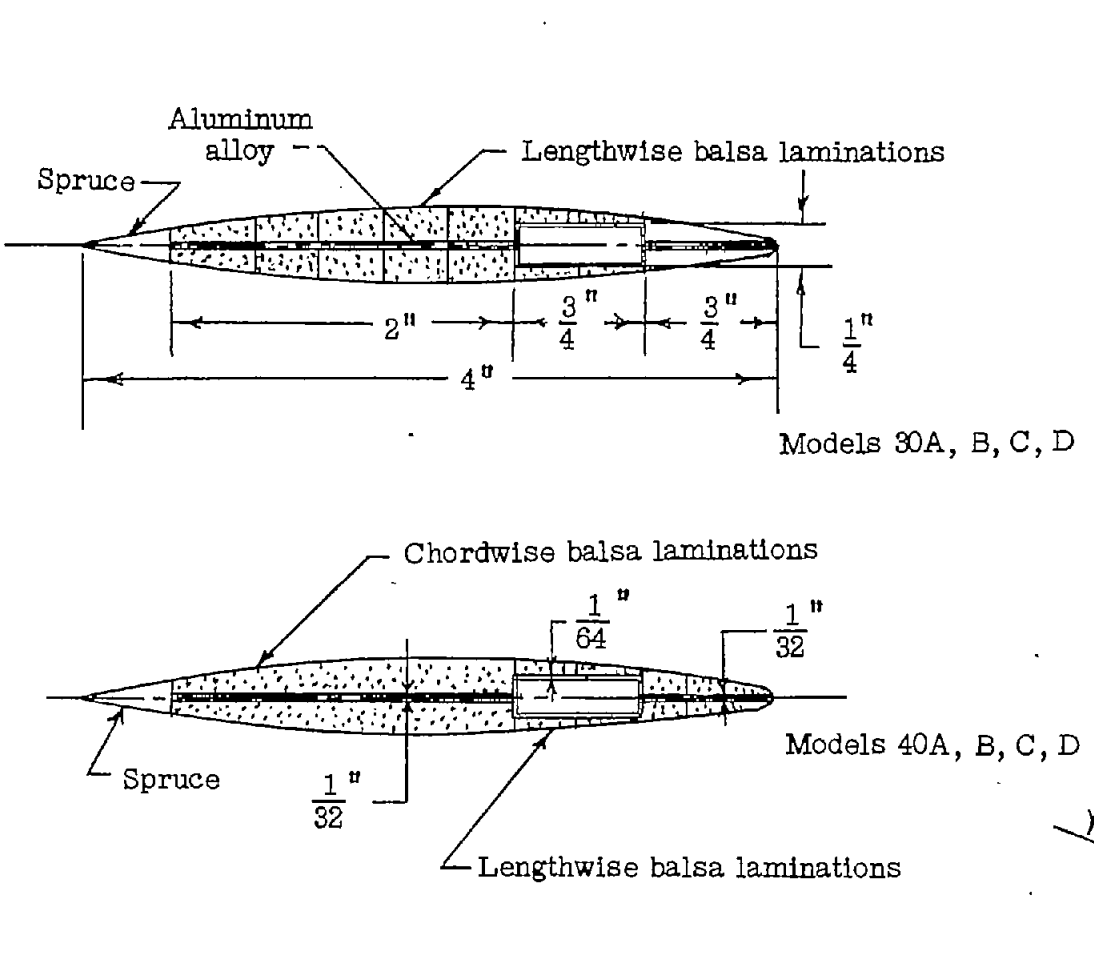

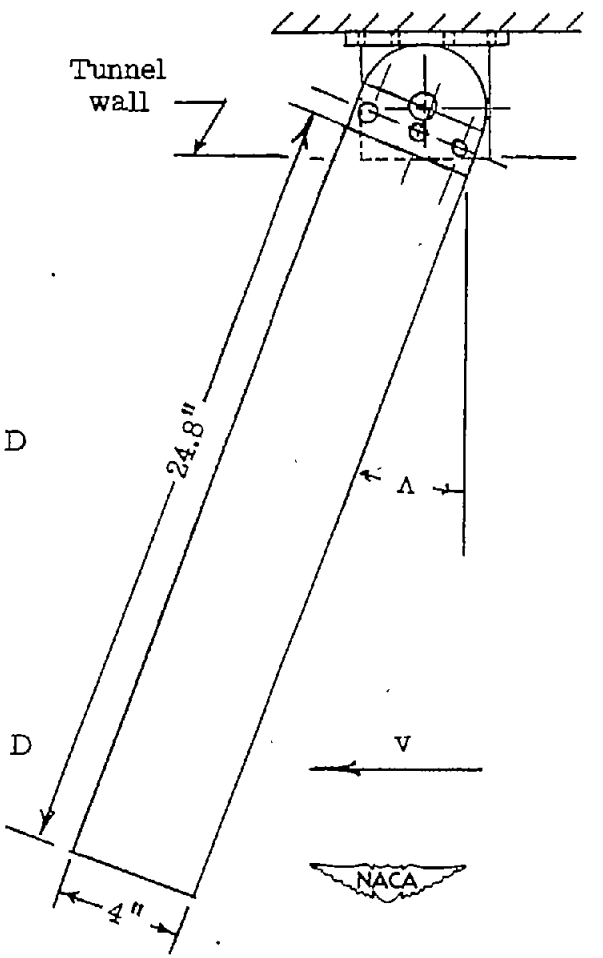

(b) Models swept back by use of a rotating mount. Series II.

Figure 1.- Continued.

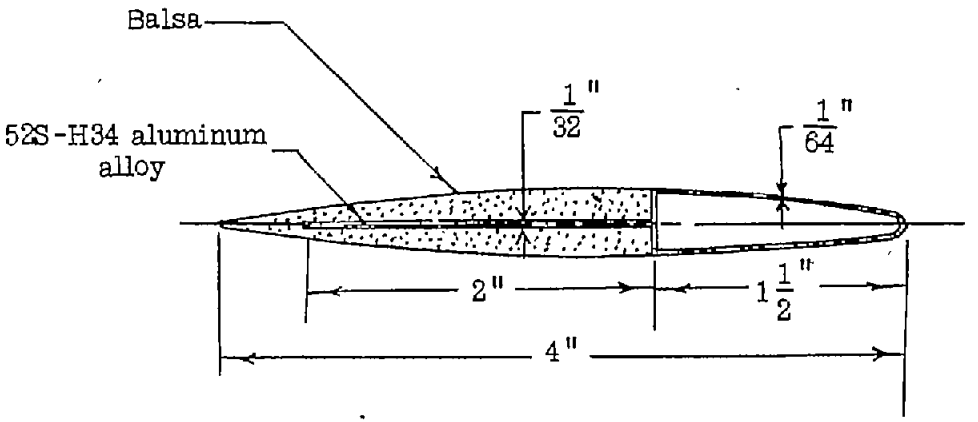

Models 50A, B

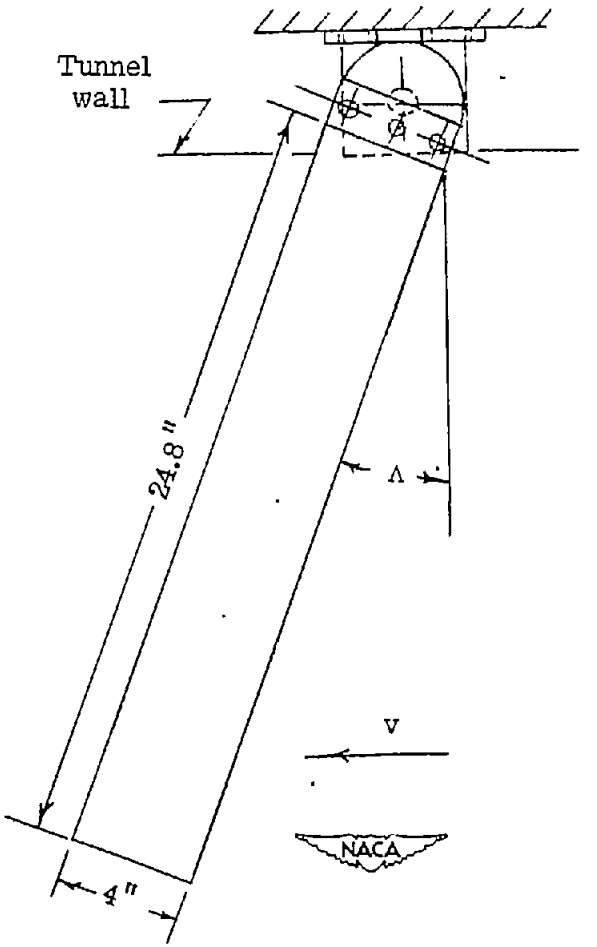

(c) Models in which a rotating mount is used to determine the effect of sweepback and sweepforward on the critical velocity. Series III.

Figure 1.- Continued.

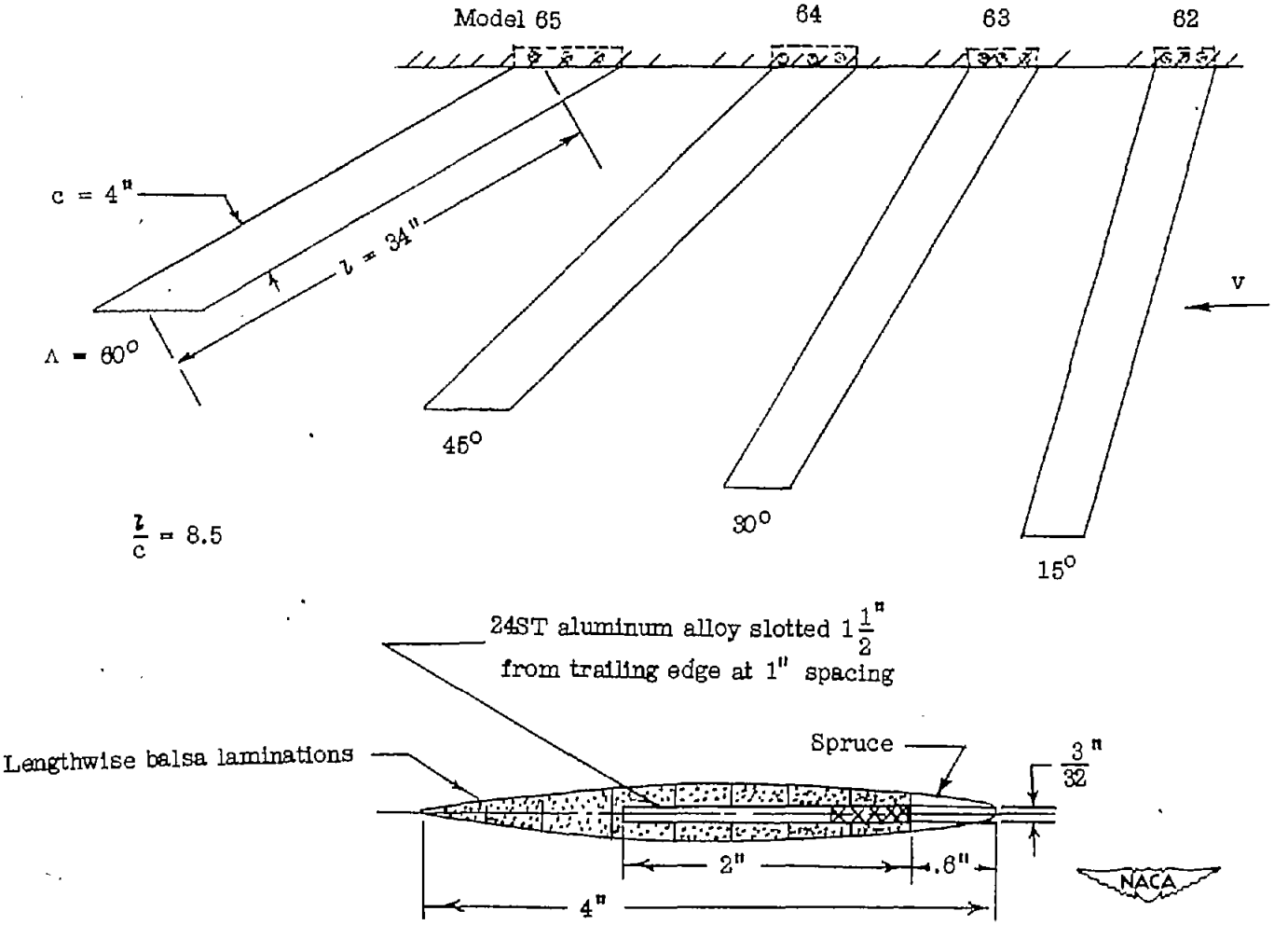

(d) Swept models having a length-chord ratio of 8.5. Series IV.

Figure 1.- Continued.

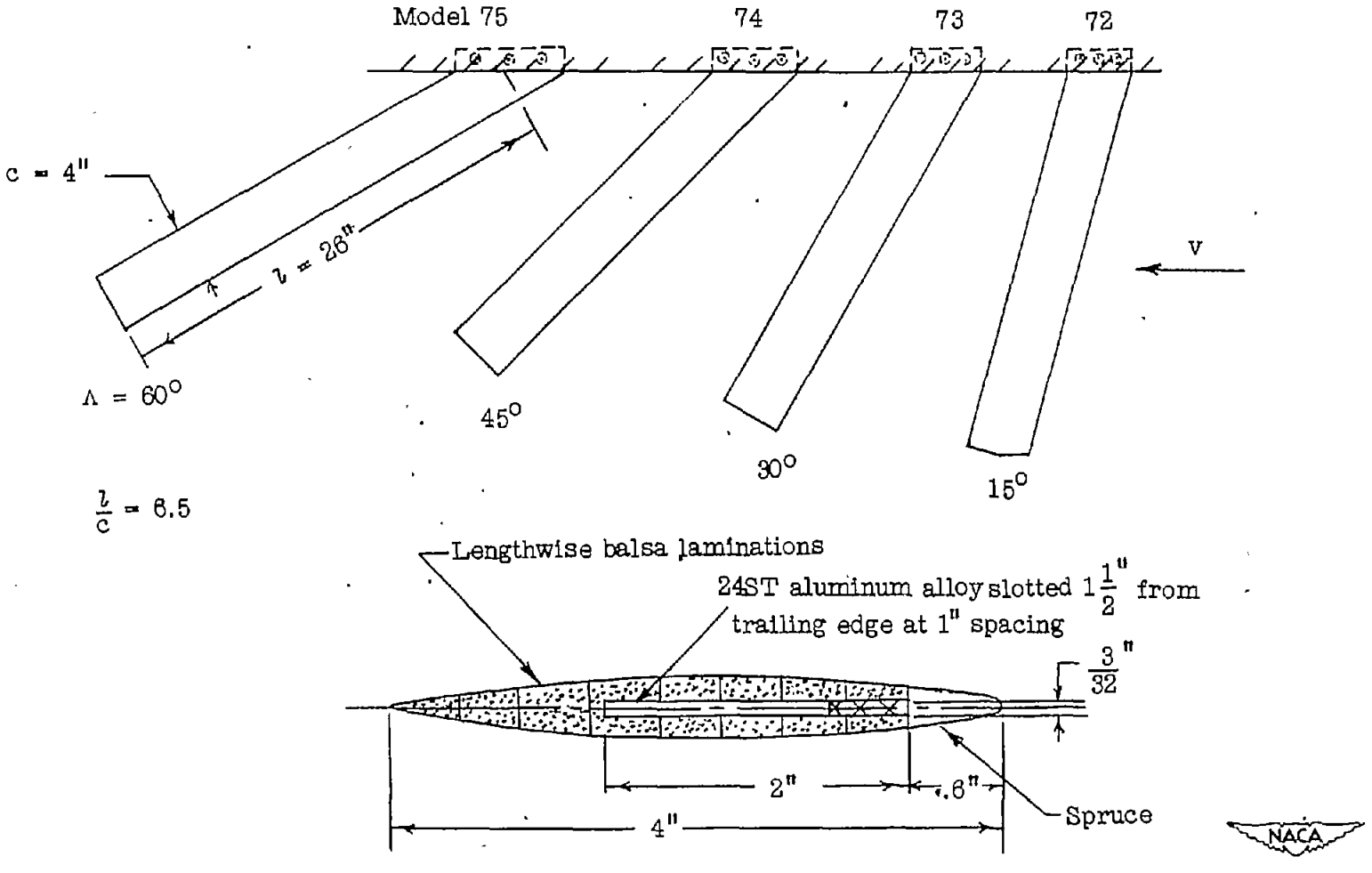

(e) Swept models having a length-chord ratio of 6.5. Series V.

Figure 1.- Continued.

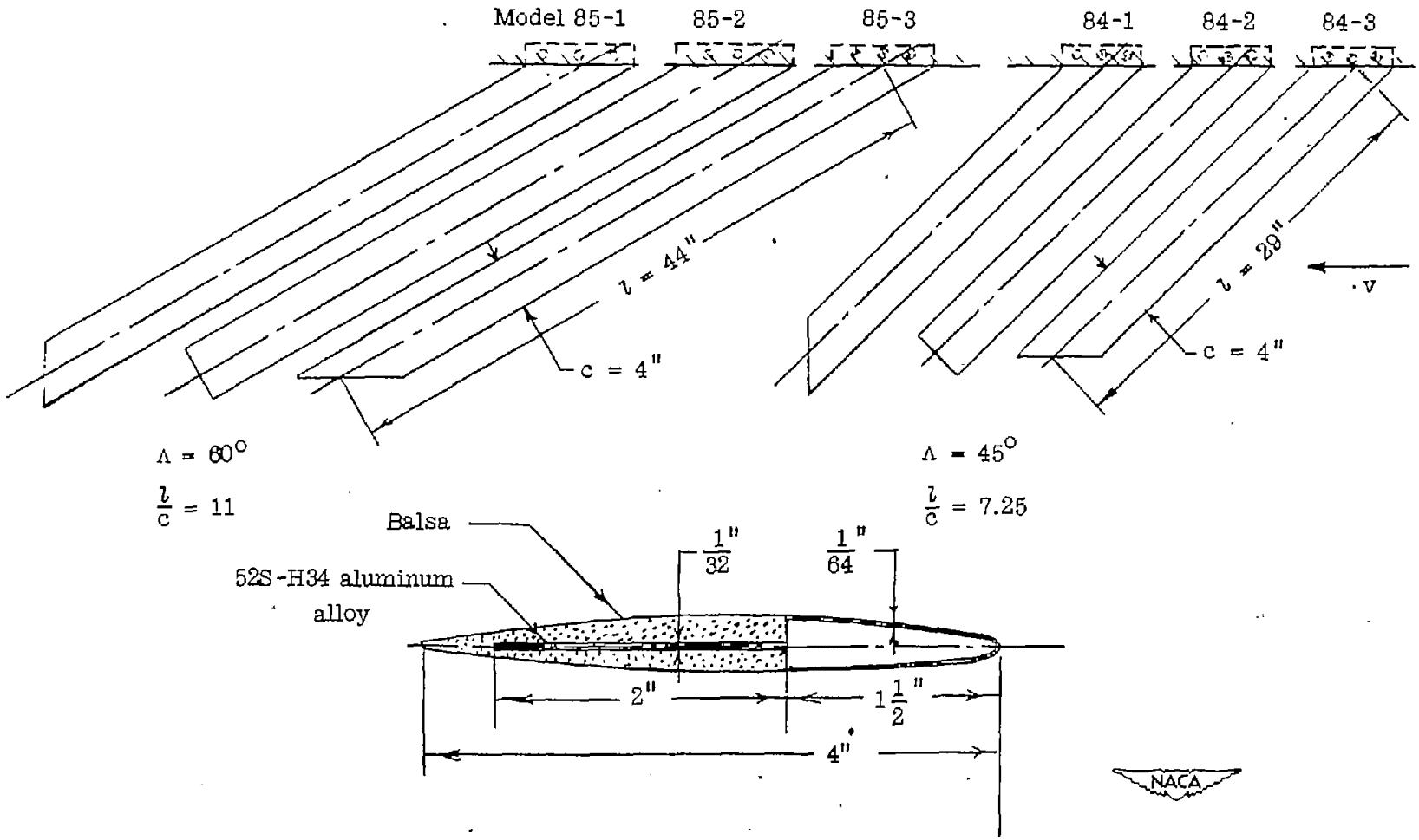

(f) Models used to investigate the effect of tip shape on the flutter velocity. Series VI.

Figure 1.- Continued.

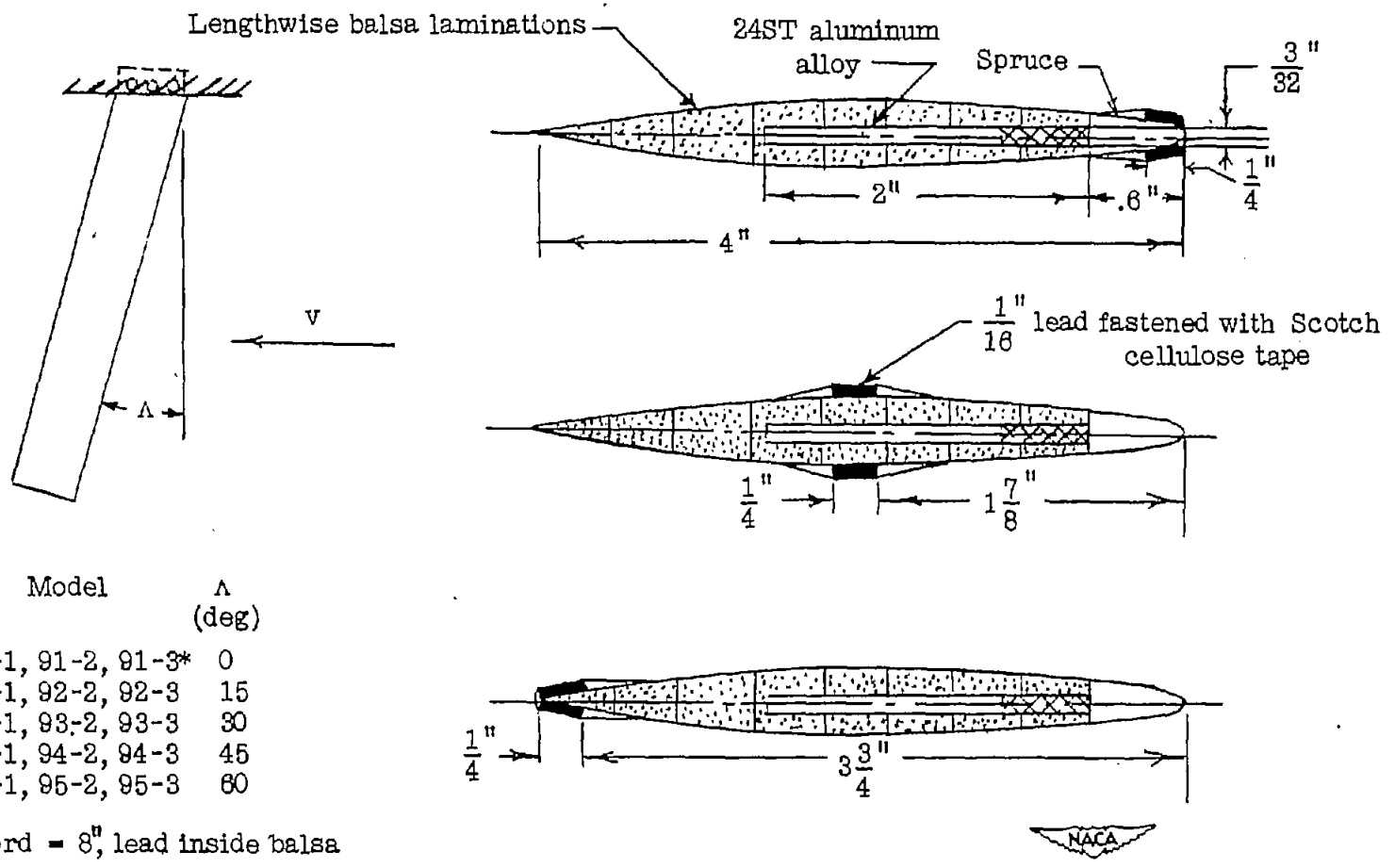

Model	Λ (deg)
91-1, 91-2, 91-3*	0
92-1, 92-2, 92-3	15
93-1, 93-2, 93-3	30
94-1, 94-2, 94-3	45
95-1, 95-2, 95-3	60

*Chord = 8", lead inside balsa

(g) Models used to determine the effect of center-of-gravity shift on the flutter velocity of swept wings. Series VII.

Figure 1.- Concluded.

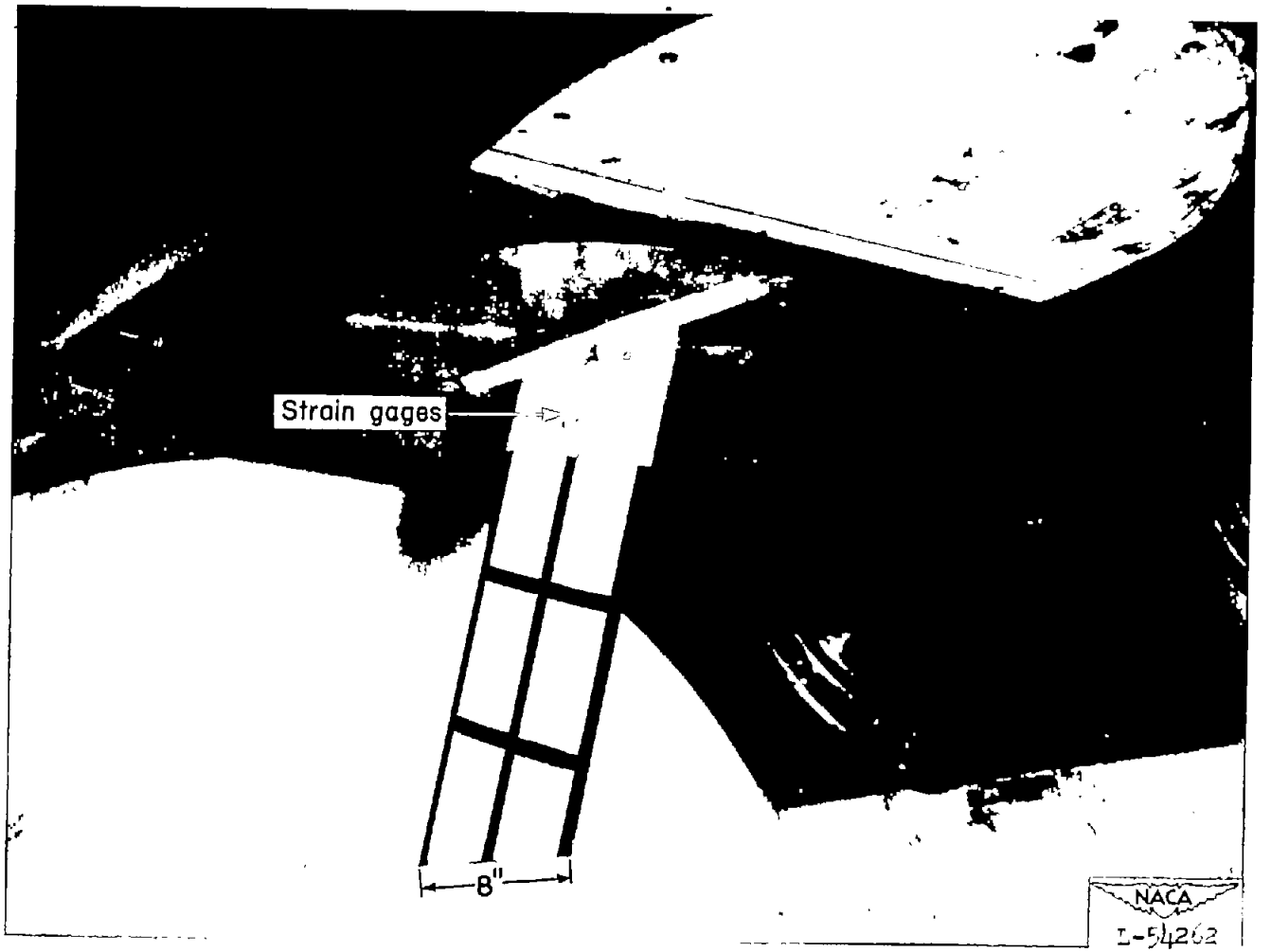

Figure 2.- Model 12 in the tunnel test section.

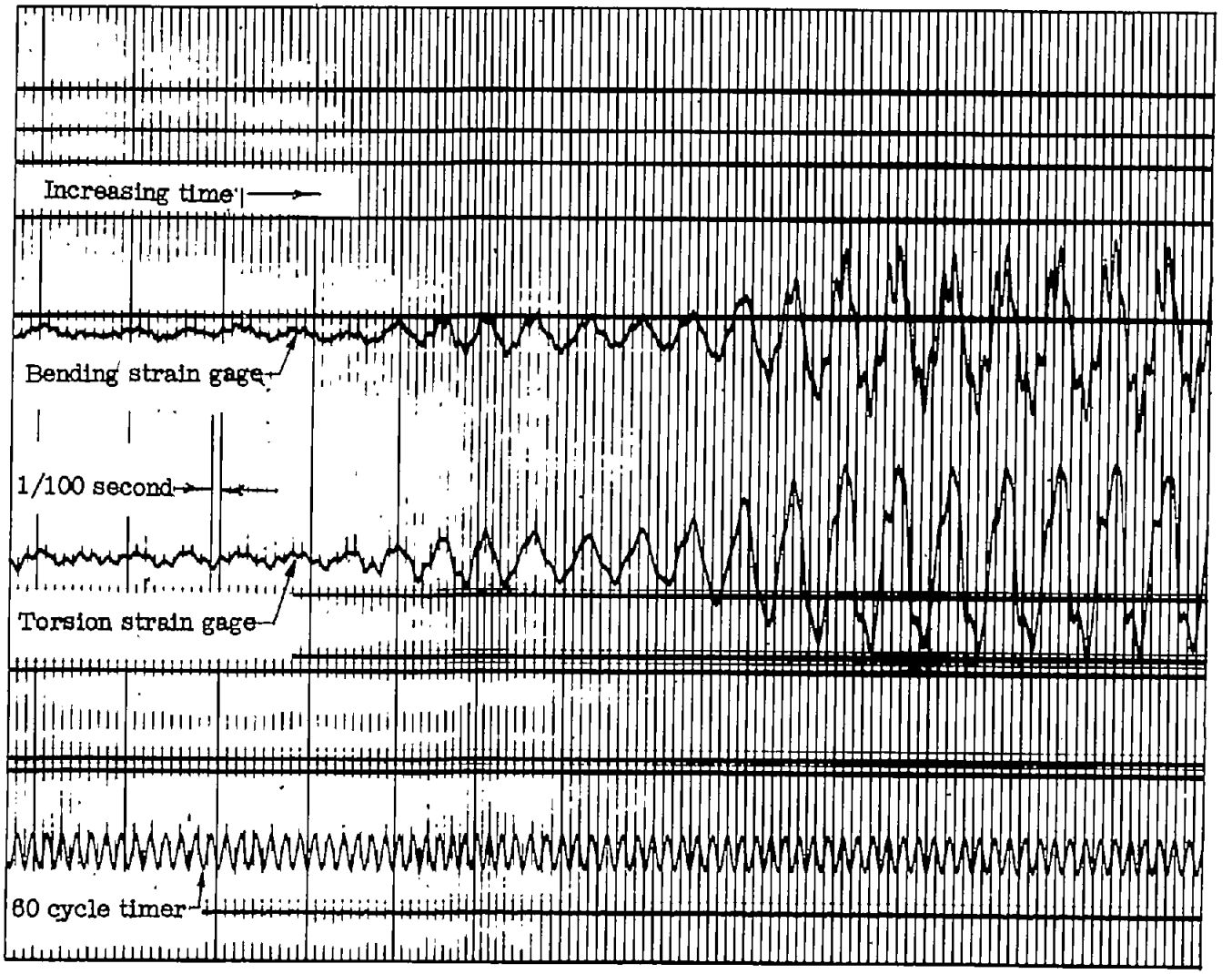

Figure 3.- Oscillograph record of model at flutter.

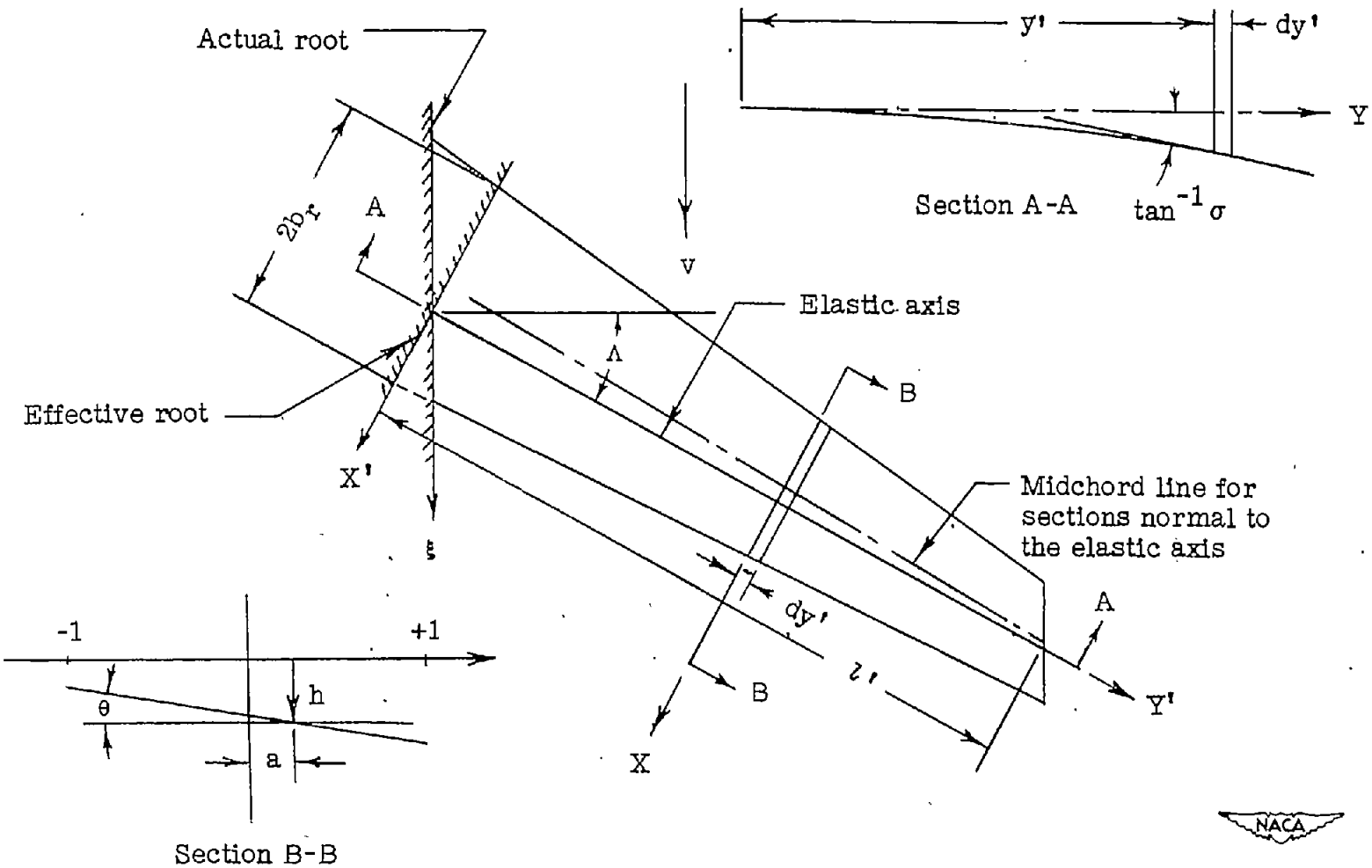

Figure 4.- Nonuniform swept wing treated in the present analysis.

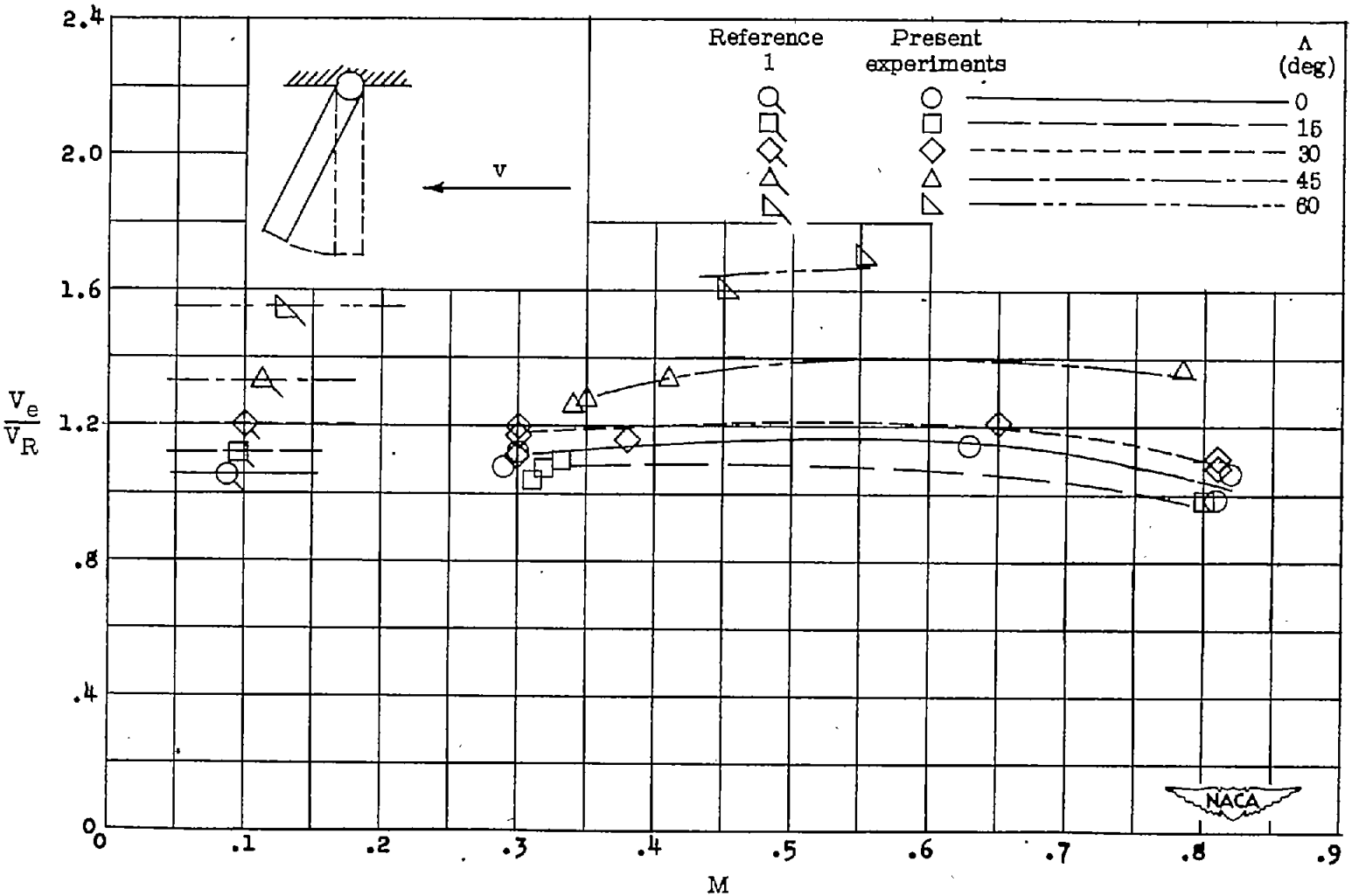

Figure 5.- Ratio of experimental to reference flutter speed as a function of Mach number for various sweep angles for series II models (fig. 1(b)) on the rotating mount.

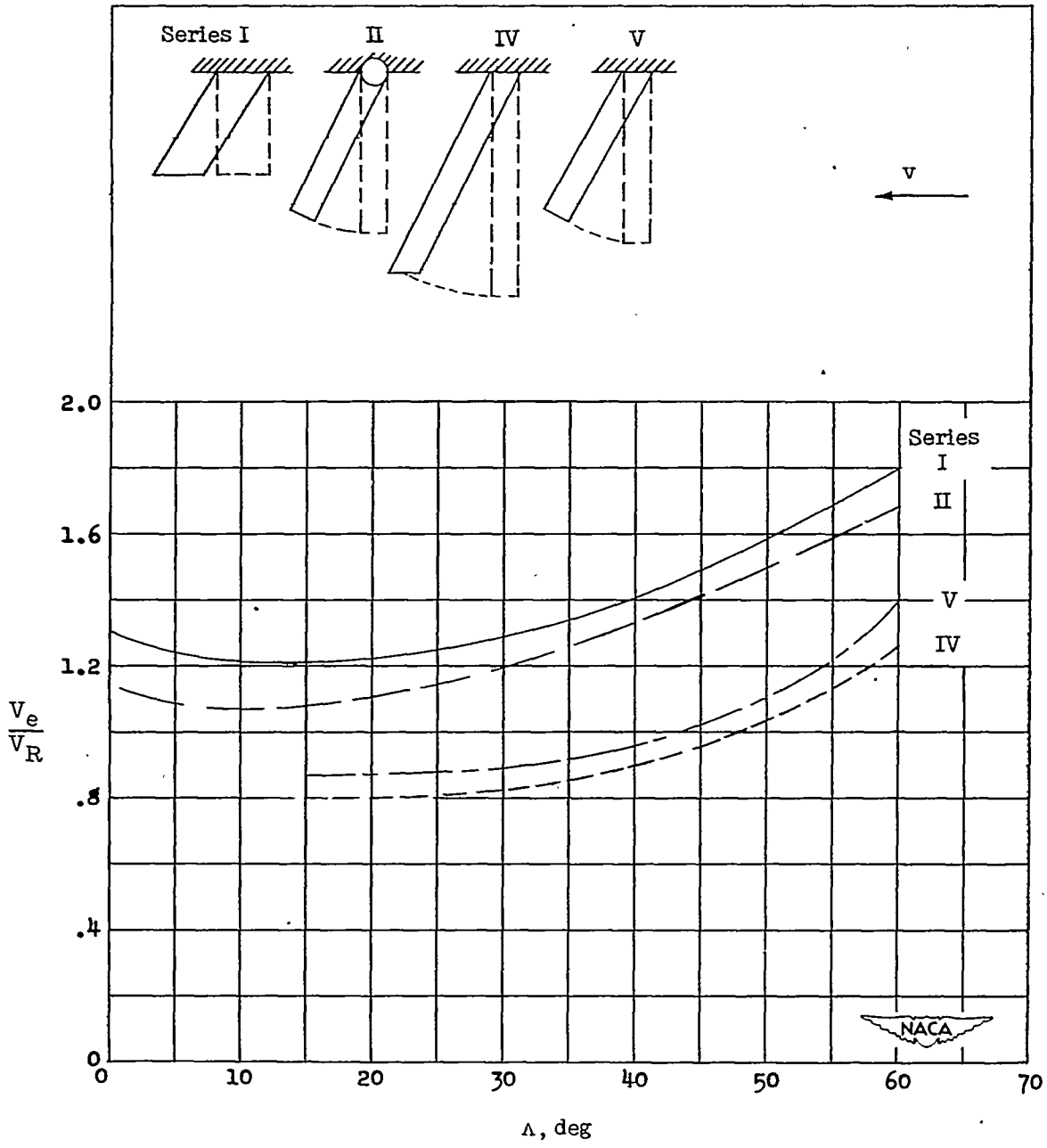

Figure 6.- Cross plot of ratio of experimental to reference flutter velocity as a function of sweep angle for various wings. Mach number is approximately 0.65.

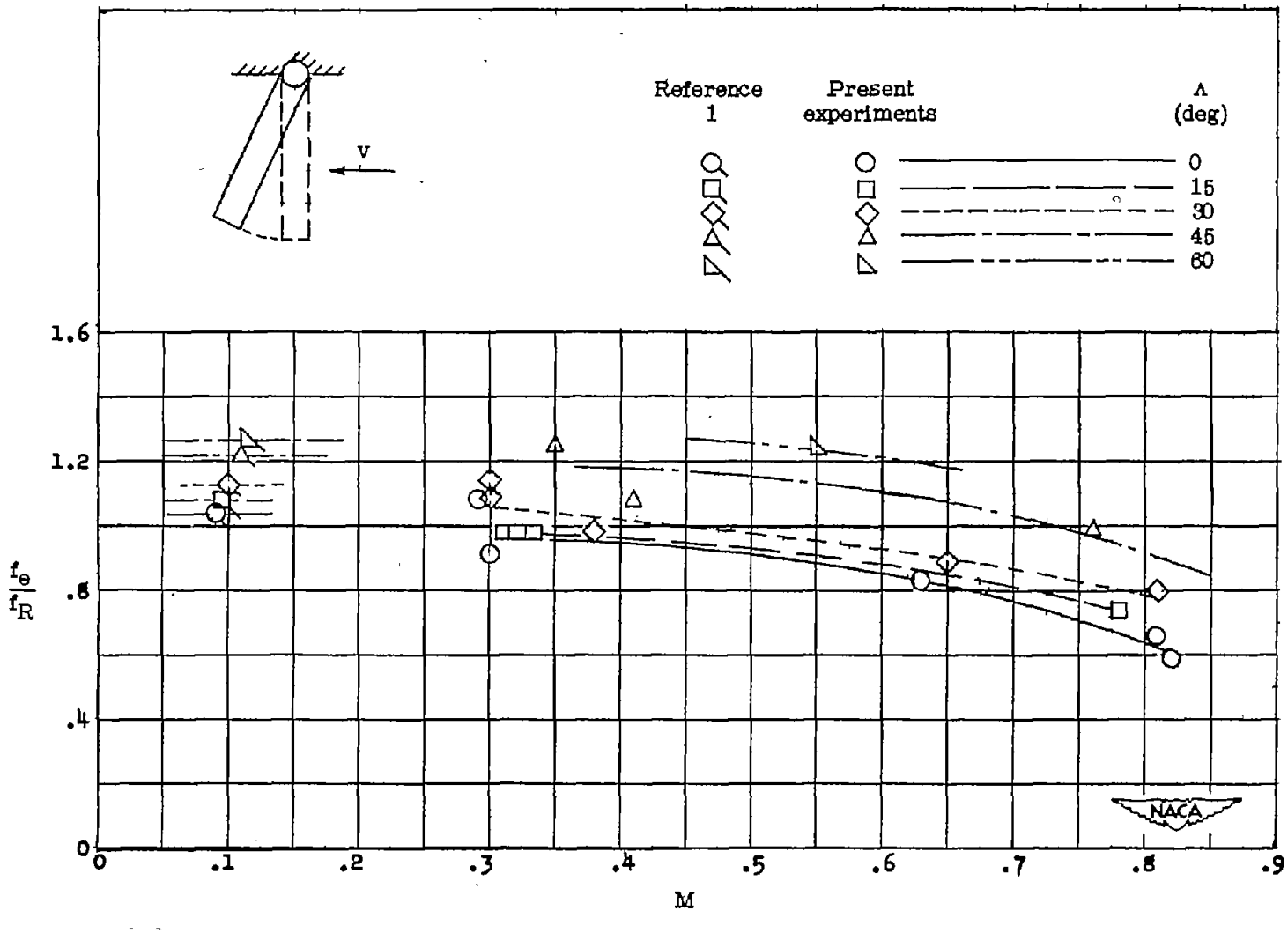

Figure 7.- Ratio of experimental to reference flutter frequency as a function of Mach number for various sweep angles for series II models (fig. 1(b)) on the rotating mount.

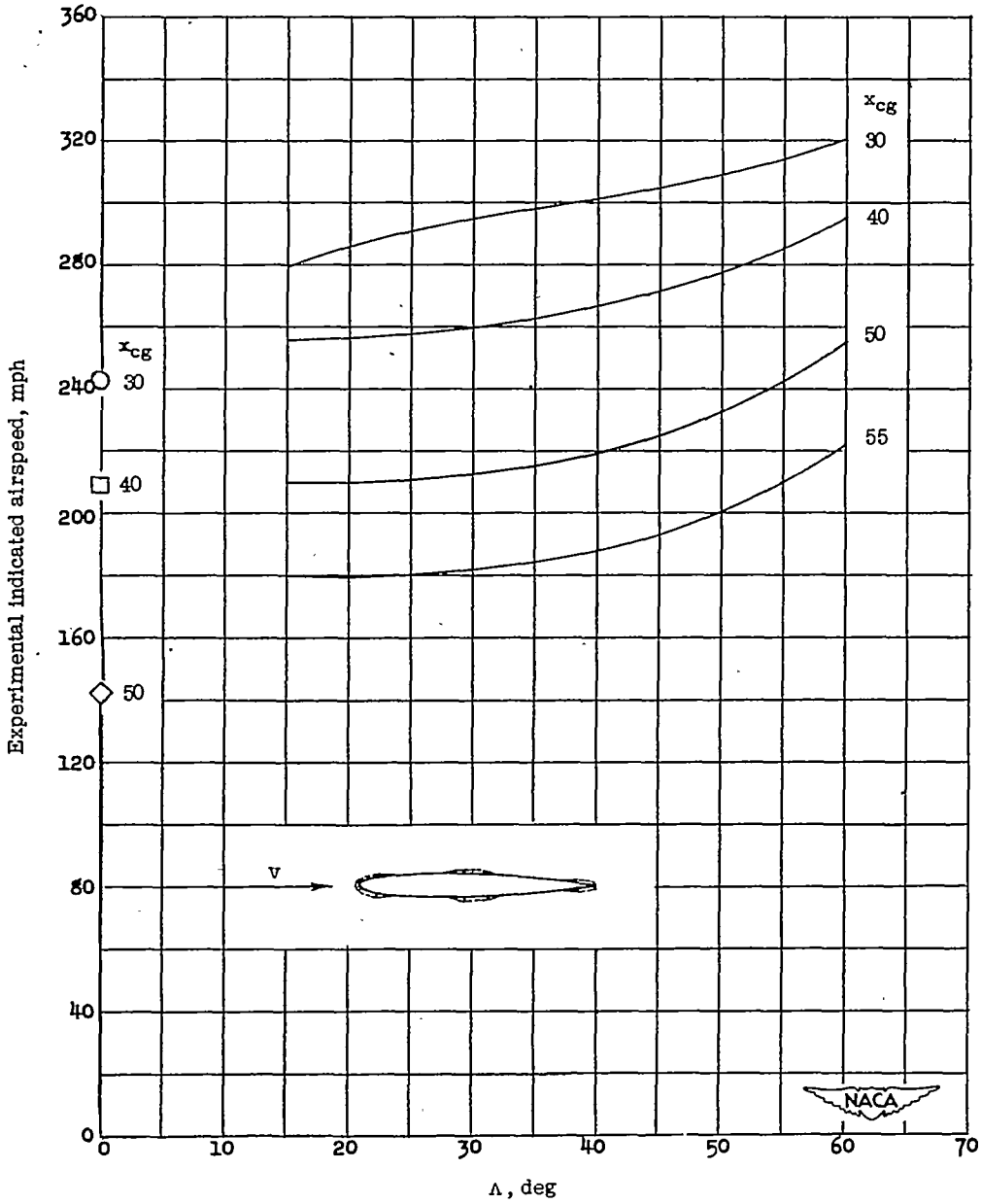

Figure 8.- Cross plot of flutter speed as a function of sweep angle for several center-of-gravity positions. Series VII models (fig. 1(g)). Length-chord ratio is approximately 6.

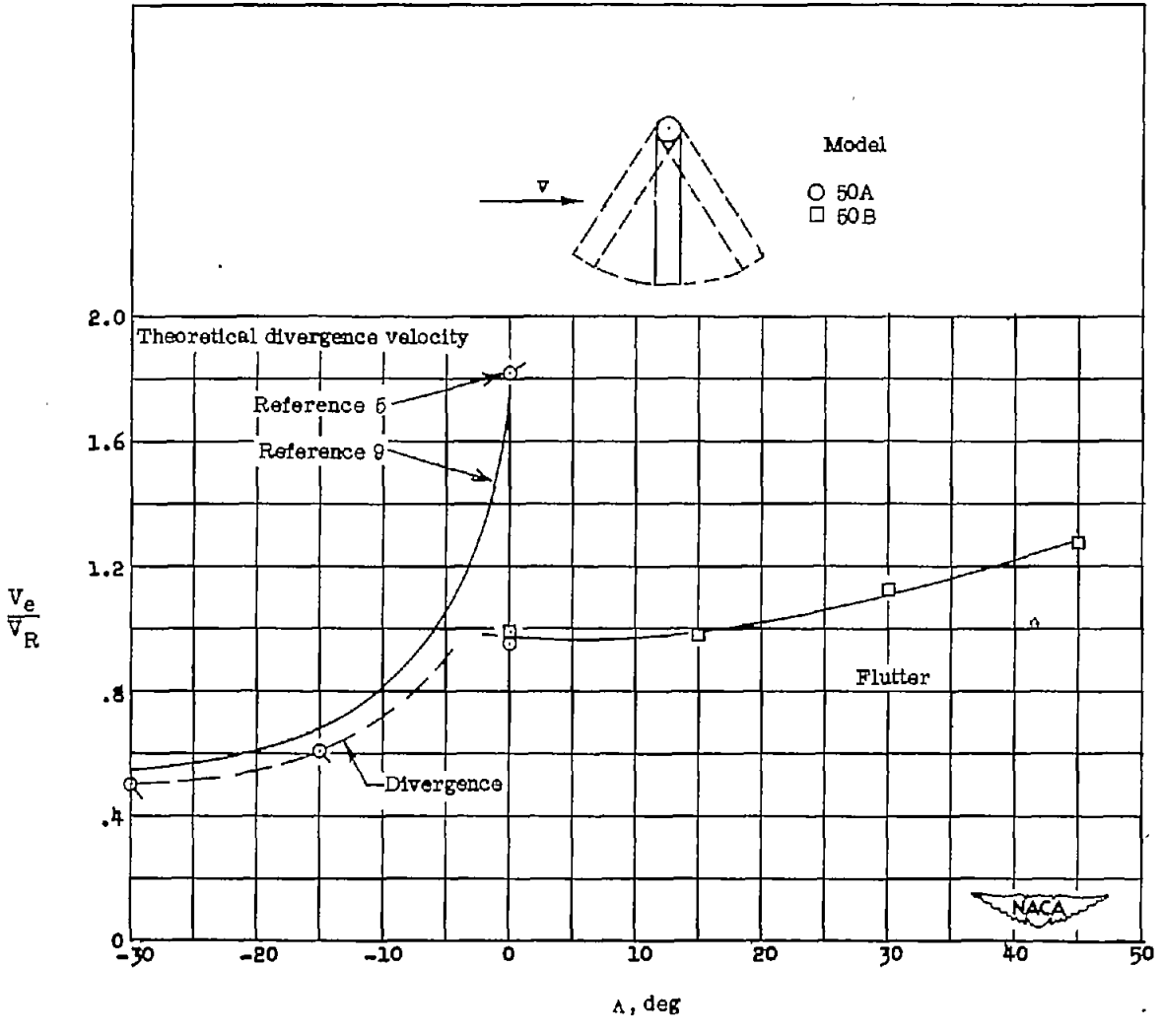

Figure 9.- Comparison of sweepforward and sweepback tests on wings tested on a rotating mount. Series III models (fig. 1(c)).

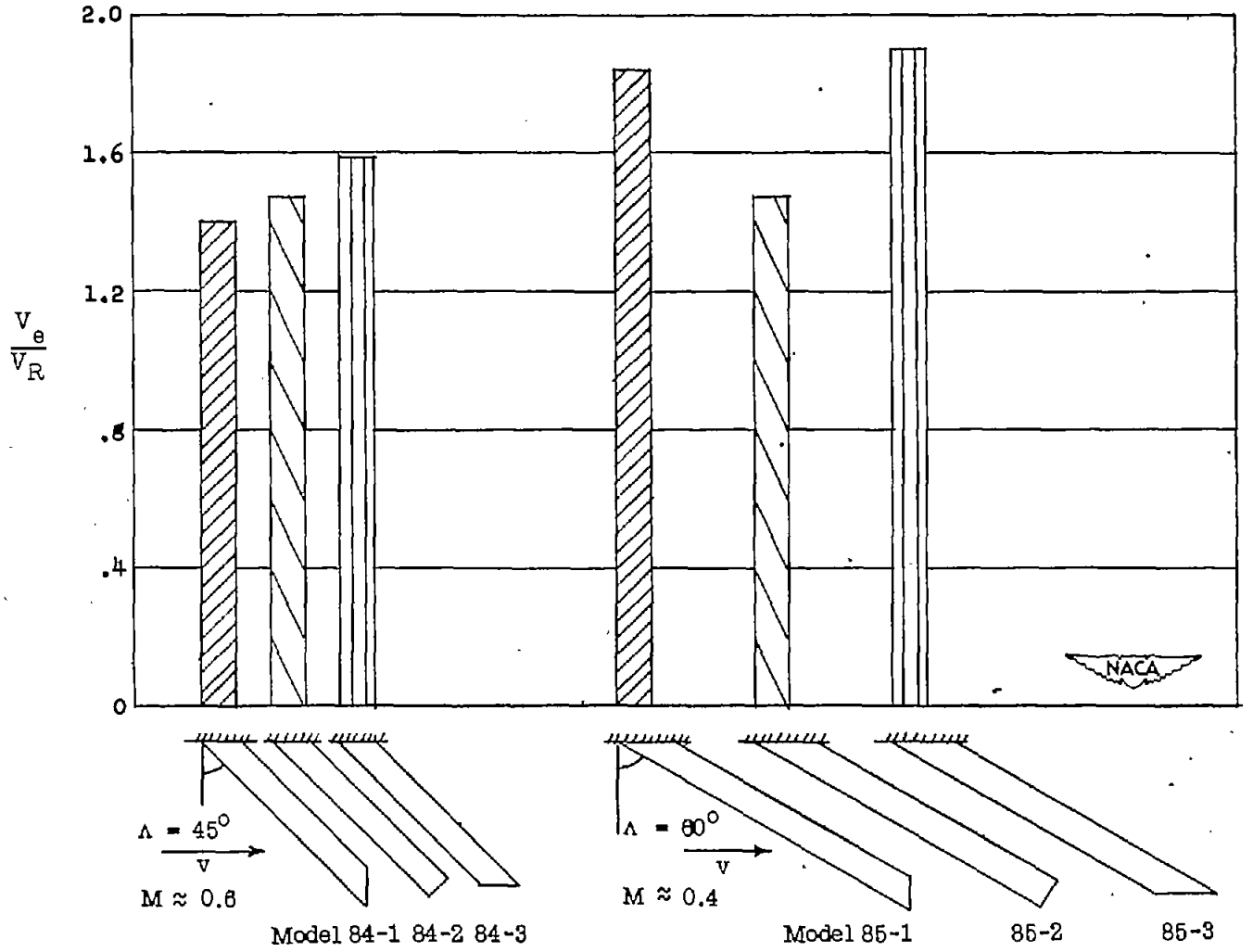

Figure 10.- Effect of tip shape on the flutter speed of swept wings. Wings of length-chord ratios of 7.25 and 11 (fig. 1(f)). Series VI models.

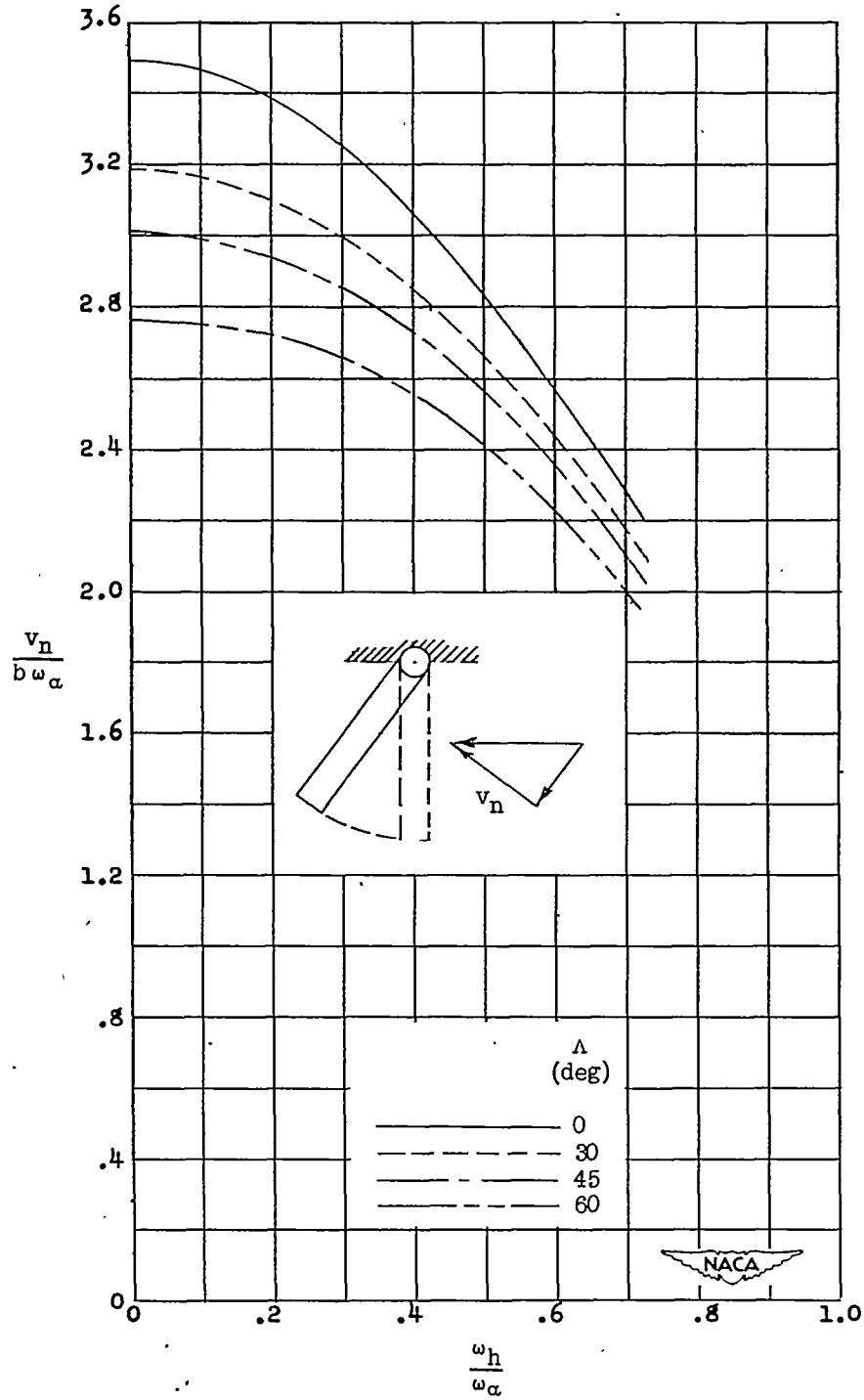

Figure 11.- Theoretical flutter-speed coefficient as a function of the ratio of bending to torsion frequency for the rotated model 30B at four angles of sweep and with a constant mass-density ratio $\left(\frac{1}{\kappa} = 37.8\right)$.

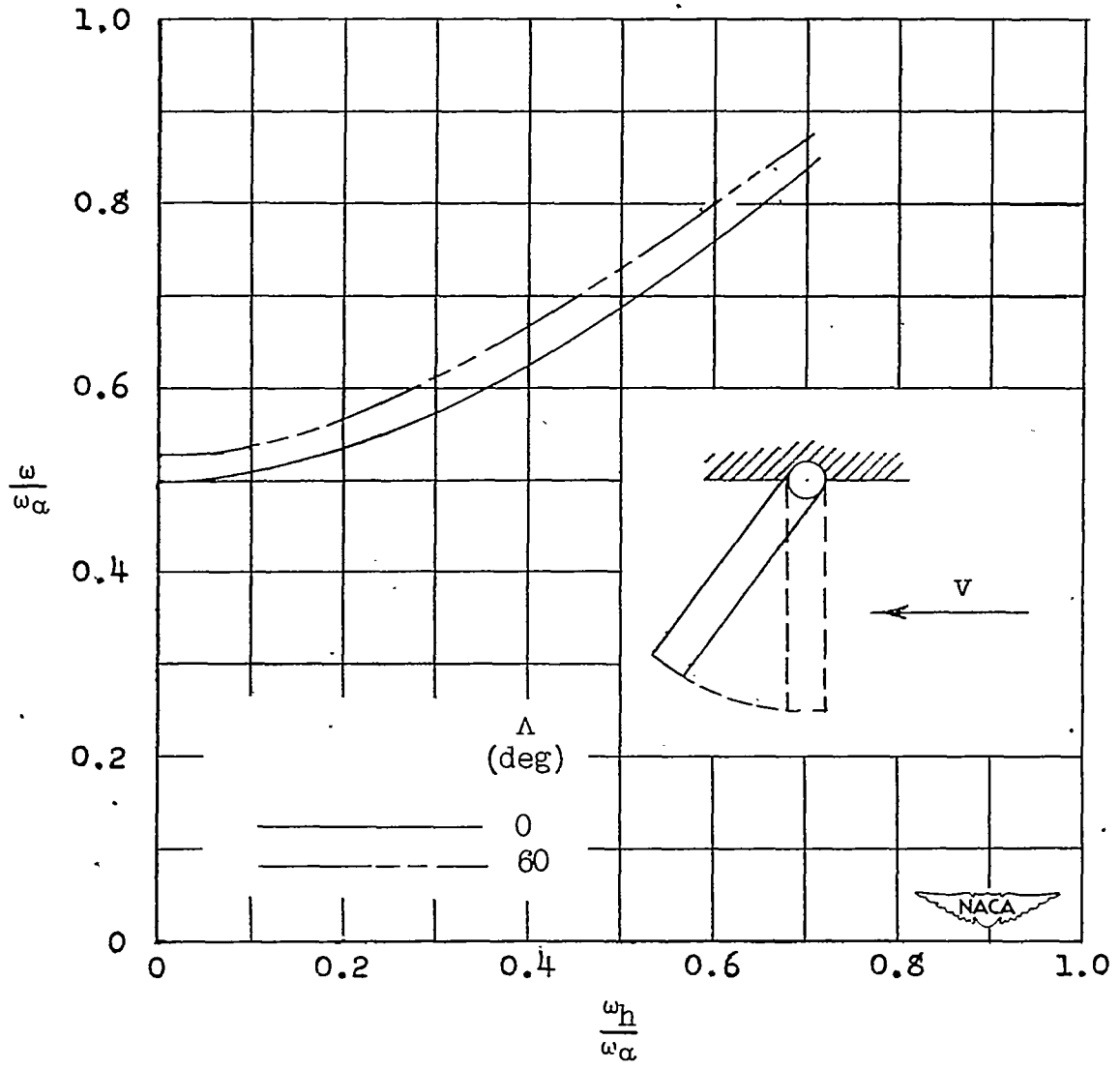

Figure 12.- Ratio of theoretical flutter frequency to torsional frequency as a function of the ratio of bending to torsion frequency for the rotated model 30B at two angles of sweep and with a constant mass-density ratio $\left(\frac{1}{\mu} = 37.8\right)$.

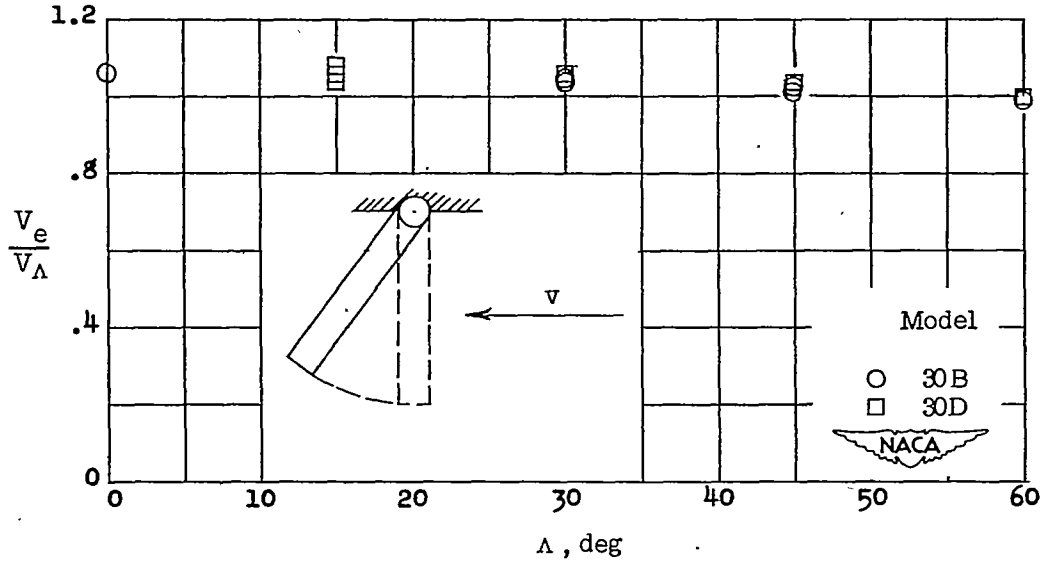

Figure 13.- Ratio of experimental to theoretically predicted flutter speed as a function of sweep angle for two rotated models.

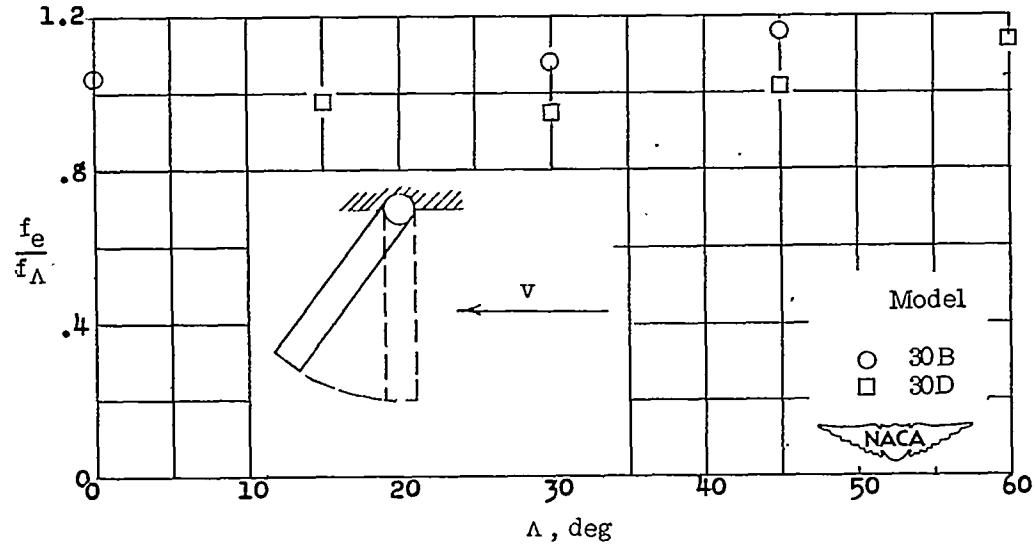

Figure 14.- Ratio of experimental to theoretically predicted flutter frequency as a function of sweep angle for two rotated models.

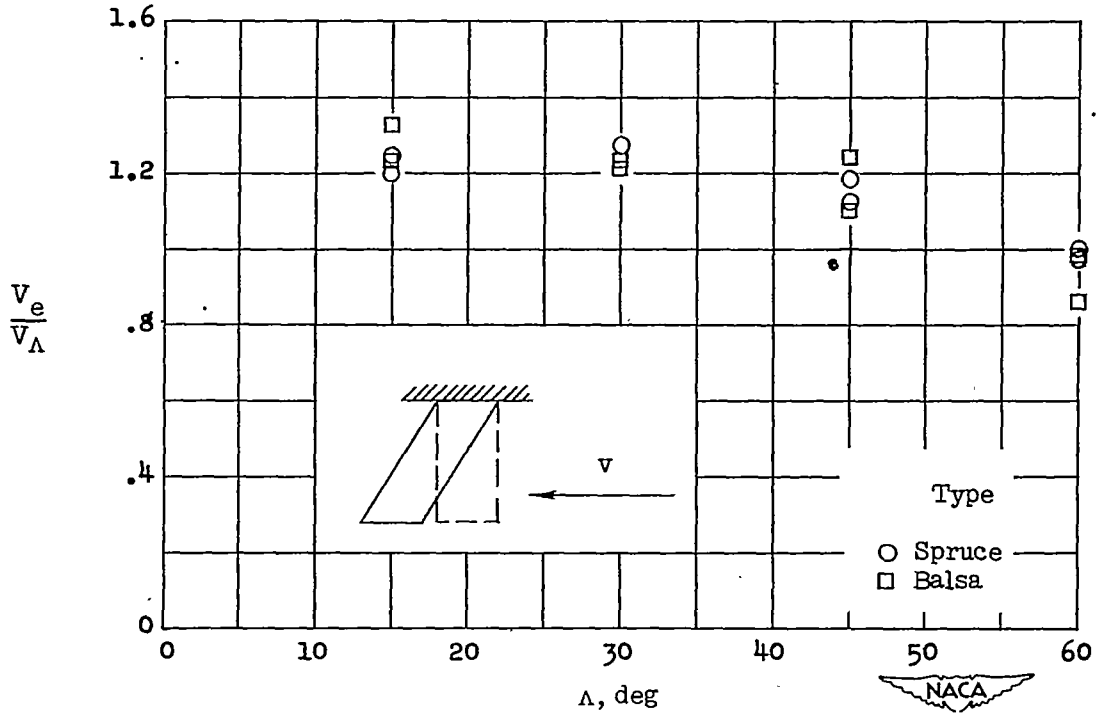

Figure 15.- Ratio of experimental to theoretically predicted flutter speed as a function of sweep angle for two types of sheared models.

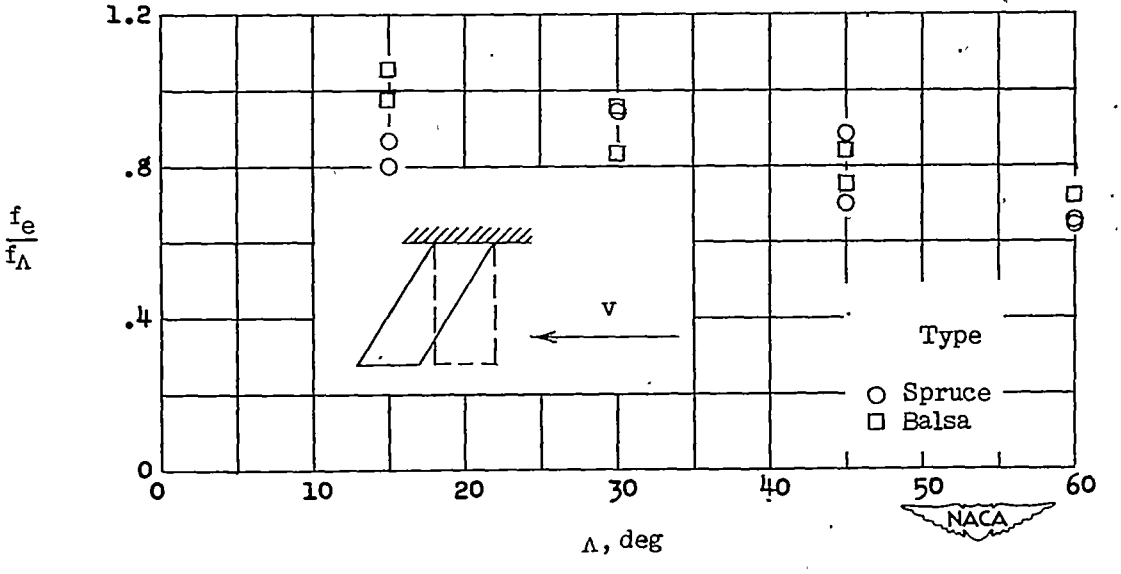

Figure 16.- Ratio of experimental to theoretically predicted flutter frequency as a function of sweep angle for two types of sheared wings.

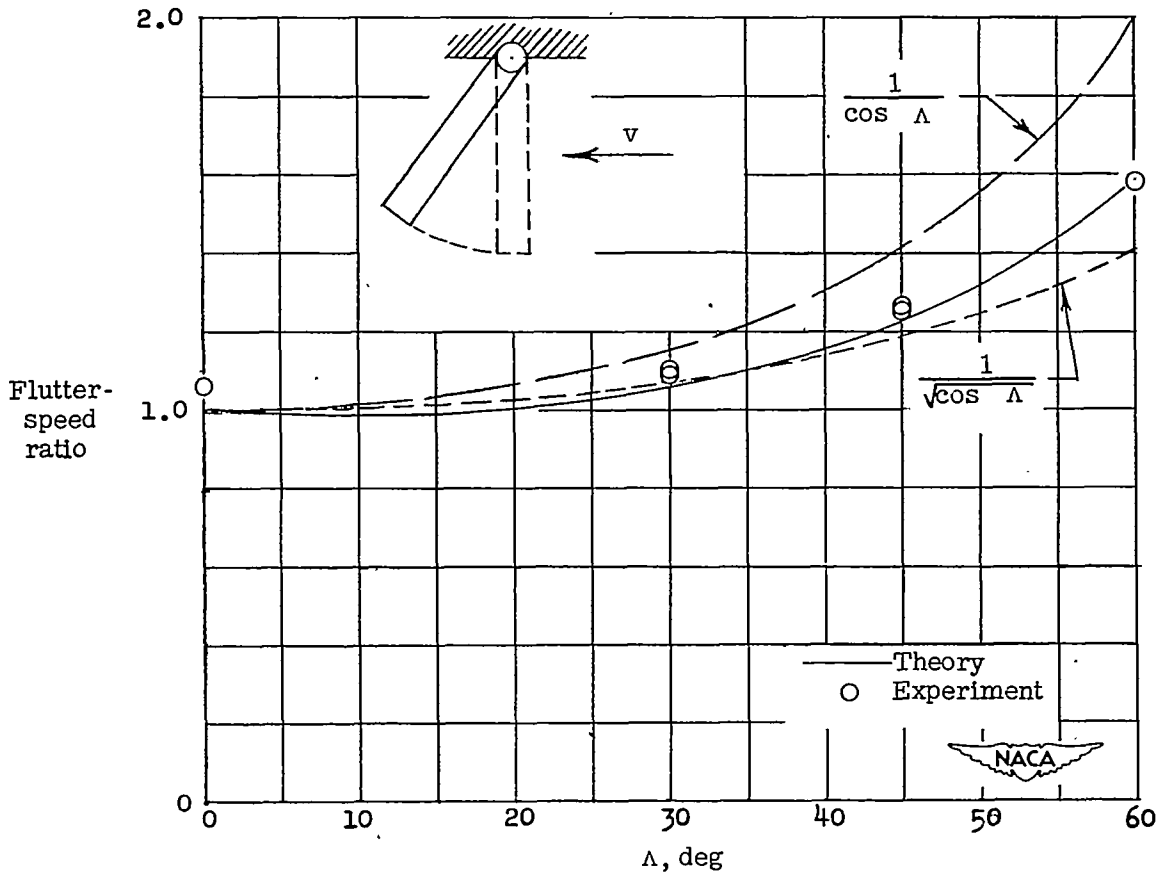

Figure 17.- Flutter-speed ratio as a function of sweep angle for model 30B at a constant mass-density ratio $\left(\frac{1}{\kappa} = 37.8\right)$, showing analytical and experimental results.

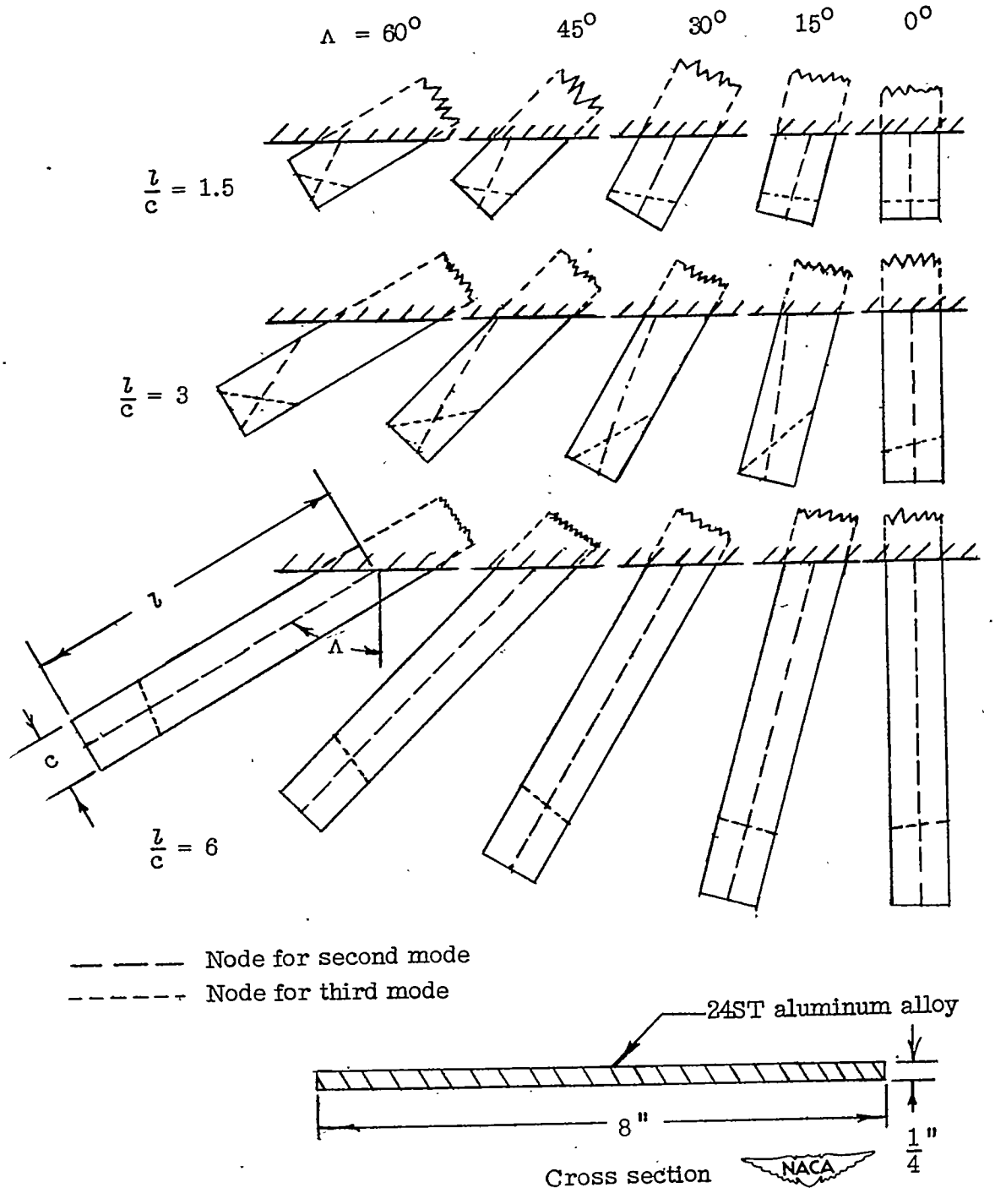

Figure 18.- Change in nodal lines with sweep and length-chord ratio for the vibration of a dural beam.

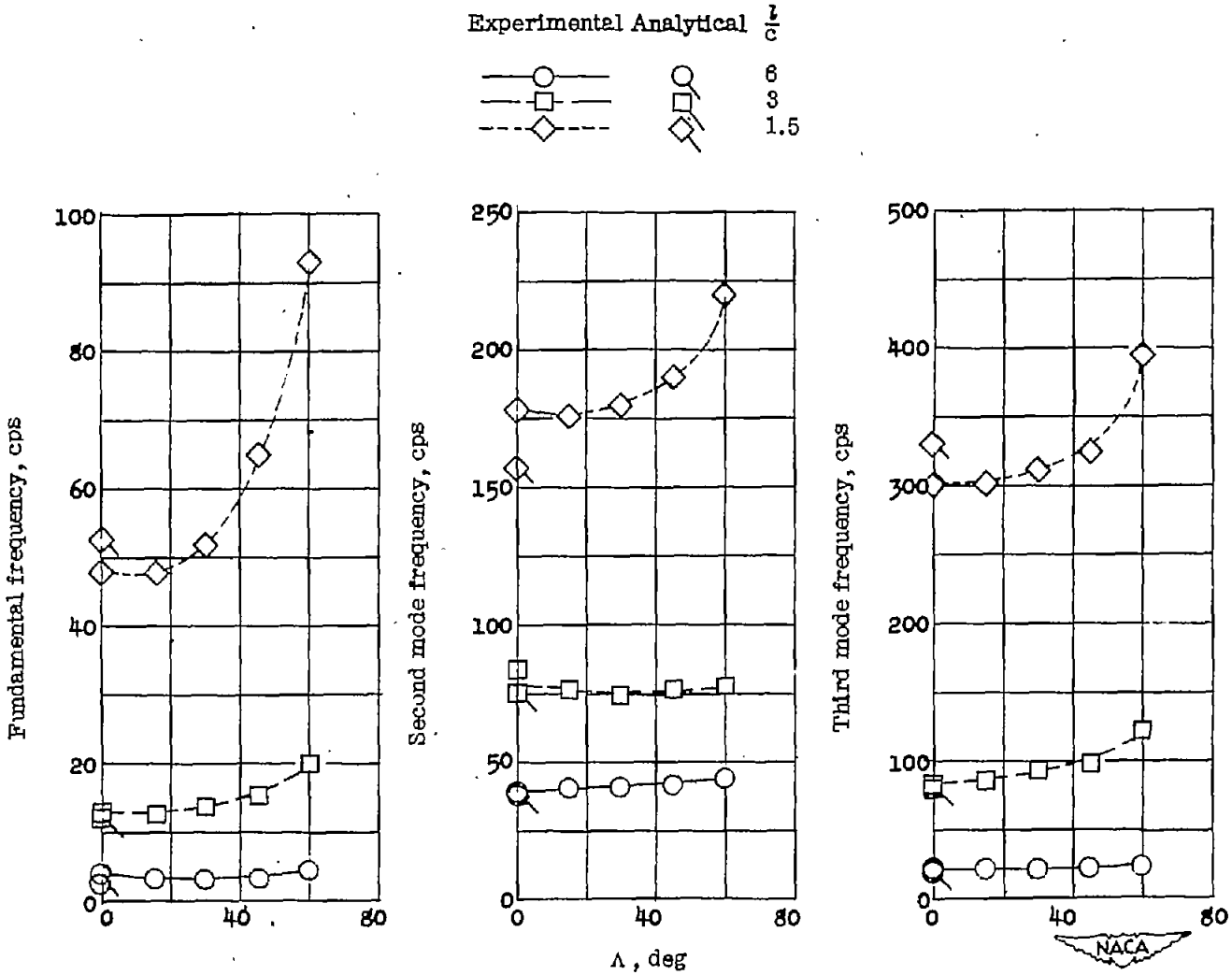

Figure 19.- Variation of frequencies with sweep and length-chord ratio for the vibration of an aluminum-alloy beam.

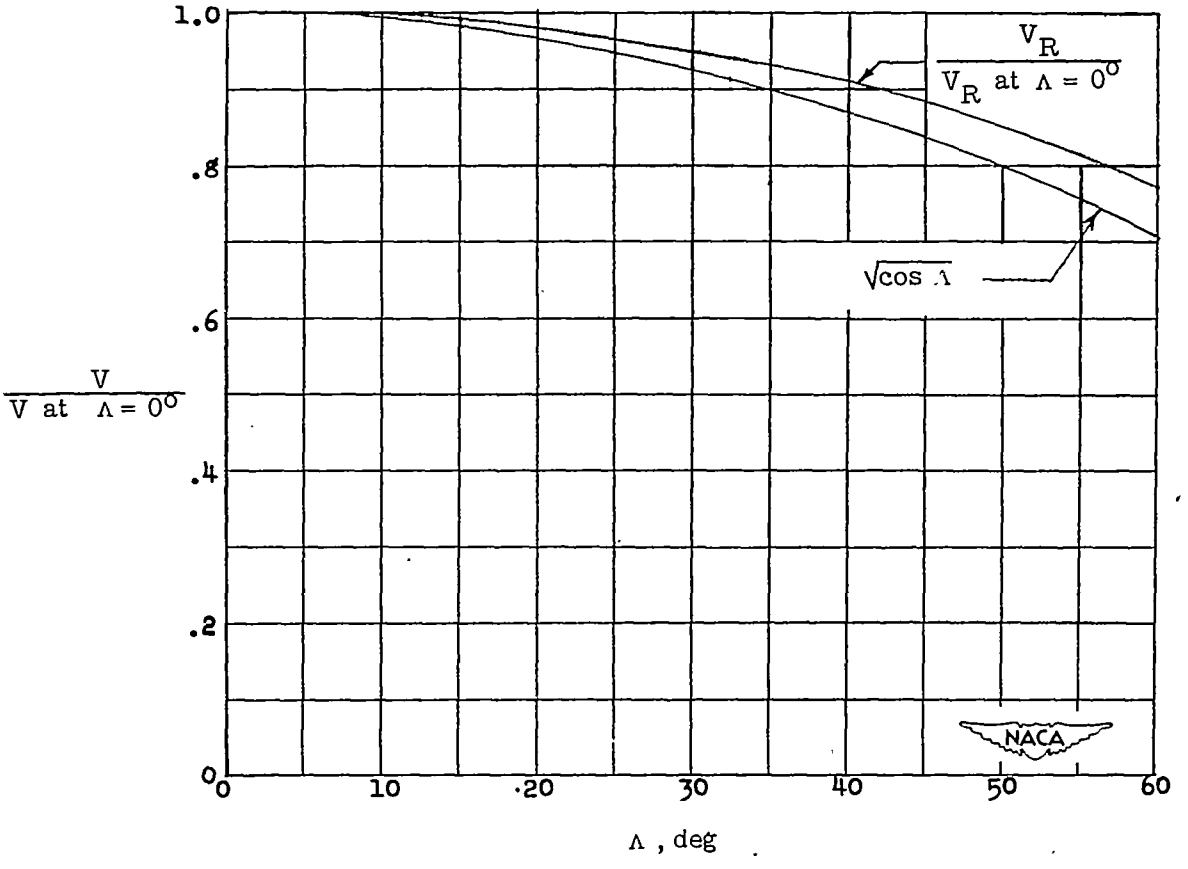

Figure 20.- Variation in reference flutter speed with sweep for sheared wings.

NACA-Langley - 6-19-50 -1000